

## **37. MAGNETOSTRATIGRAPHY OF SEDIMENT DRIFTS ON THE CONTINENTAL RISE OF WEST ANTARCTICA (ODP LEG 178, SITES 1095, 1096, AND 1101)<sup>1</sup>**

Gary D. Acton,<sup>2</sup> Yohan Guyodo,<sup>3</sup> and Stefanie A. Brachfeld<sup>4</sup>

### **ABSTRACT**

We present revised magnetostratigraphic interpretations for Ocean Drilling Program Sites 1095, 1096, and 1101, cored in sediment drifts located off the Pacific margin of the Antarctic Peninsula. The revised interpretations incorporate a variety of observations and results obtained since the end of Leg 178, of which the most significant are new paleomagnetic measurements from U-channel samples, composite depth scales that allow stratigraphic correlation between multiple holes cored at a site, and revised biostratigraphic interpretations. The U-channel data, which include more than 102,000 paleomagnetic observations from more than 13,400 intervals along U-channel samples, are included as electronic files. The magnetostratigraphic records at all three sites are consistent with sedimentation being continuous over the intervals cored, although the data resolution does not preclude short hiatuses less than a few hundred thousand years in duration. The magnetostratigraphic records start at the termination of Subchron C4Ar.2n (9.580 Ma) at ~515 meters composite depth (mcd) for Site 1095, at the onset of Subchron C3n.2n (4.620 Ma) at ~489.68 mcd for Site 1096, and at the onset of Subchron C2An.1n (3.040 Ma) at 209.38 meters below seafloor for Site 1101. All three sites provide paleomagnetic records that extend upward through the Brunhes Chron.

<sup>1</sup>Acton, G.D., Guyodo, Y., and Brachfeld, S.A., 2002. Magnetostratigraphy of sediment drifts on the continental rise of West Antarctica (ODP Leg 178, Sites 1095, 1096, and 1101). In Barker, P.F., Camerlenghi, A., Acton, G.D., and Ramsay, A.T.S. (Eds.) *Proc. ODP, Sci. Results*, 178, 1-61 [Online]. Available from World Wide Web: <[http://www-odp.tamu.edu/publications/178\\_SR/VOLUME/CHAPTERS/SR178\\_37.PDF](http://www-odp.tamu.edu/publications/178_SR/VOLUME/CHAPTERS/SR178_37.PDF)>. [Cited YYYY-MM-DD]  
<sup>2</sup>Ocean Drilling Program, Texas A&M University, 1000 Discovery Drive, College Station TX 77845-9547, USA. [acton@odpemail.tamu.edu](mailto:acton@odpemail.tamu.edu)  
<sup>3</sup>Department of Geological Sciences, University of Florida, 241 Williamson Hall, PO Box 112120, Gainesville FL 32611-2120, USA. Present address: Institute for Rock Magnetism and Department of Geology and Geophysics, University of Minnesota, 108 Pillsbury Hall, Minneapolis MN 55455, USA.  
<sup>4</sup>Byrd Polar Research Center, Ohio State University, 108 Scott Hall, 1090 Carmack Road, Columbus OH 43210, USA.

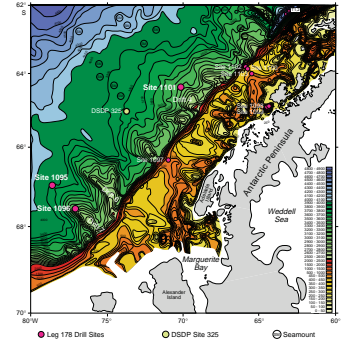
## INTRODUCTION

Magnetostratigraphic interpretations for Sites 1095, 1096, and 1101 (Fig. F1) presented here are similar to, though supercede, those in the Leg 178 *Initial Reports* volume (Barker, Camerlenghi, Acton, et al., 1999). The most significant changes are based on (1) assessment of postcruise paleomagnetic measurements made on U-channel samples; (2) reinterpretation of paleomagnetic data collected during Leg 178 from archive-half core sections and from discrete samples (~7 cm<sup>3</sup> of sediment in plastic cubes) taken from working-half core sections (Barker, Camerlenghi, Acton, et al., 1999); (3) additional processing and interpretation of the magnetic logging data (Williams et al., Chap. 31, this volume); (4) use of the meters composite depth (mcd) scale of Barker (Chap. 6, this volume), which has allowed us to place paleomagnetic data from multiple cored intervals into a common depth scale; and (5) incorporation of revised biostratigraphic events as summarized by Iwai et al. (Chap. 36, this volume).

We discuss the changes below and present complete revised magnetostratigraphies for Sites 1095, 1096, and 1101 (Tables T1, T2, T3). The pattern of polarity zones at these sites can be correlated with polarity chrons of the geomagnetic polarity timescale (GPTS) without requiring abrupt large changes in sedimentation rates or hiatuses. Hence, much of the interpretation is accomplished by fairly straightforward matching of the polarity zonation to the GPTS. The pattern matching is further facilitated by using the most complete stratigraphic sections available, which is accomplished through stratigraphic correlation between multiple holes cored at a site. Through such correlation, the data from all holes at a site are placed within a common stratigraphic framework and in a common depth scale, referred to as the meters composite depth (mcd) scale (see Acton et al., Chap. 5, and Barker, Chap. 6, both this volume). Without this, the relationship of reversals recorded in one hole relative those in other holes at the same site is often difficult to establish. Without independent age constraints, such as those provided by the biostratigraphic events that have known correlations to the GPTS, uncertainty in the pattern matching would exist in several intervals. The biostratigraphic data generally support our magnetostratigraphic interpretations built on pattern matching and together provide consistent ages for the Neogene sedimentary sections. Throughout this paper, we use the polarity chron ages and nomenclature of Cande and Kent (1995).

We do not present magnetostratigraphic interpretations for other Leg 178 sites. As discussed in "Paleomagnetism" in the "Site 1097" and "Shelf Transect" chapters of Barker, Camerlenghi, Acton, et al. (1999), only a few polarity zones can be discerned in the paleomagnetic data from the continental shelf (Sites 1097, 1100, 1102, and 1103) and these yield no independent age constraints. In contrast, Palmer Deep Sites 1098 and 1099, located within the inner shelf basin, give a detailed paleosecular variation (PSV) record of the Holocene and latest Pleistocene (Brachfeld et al., 2000), all of which falls within the uppermost portion of the Brunhes polarity chron. Currently, there are no comparable well-dated PSV records from the high latitudes of the Southern Hemisphere to correlate with the detailed directional changes observed in the Palmer Deep records. Instead, the chronology for the Palmer Deep sediments are constrained directly by <sup>14</sup>C ages (Domack et al., 2001), making the Palmer Deep PSV records a tool for dating Holocene

F1. Location map of Leg 178 drill sites, p. 20.



T1. Magnetostratigraphy, Site 1095, p. 42.

T2. Magnetostratigraphy, Site 1096, p. 46.

T3. Magnetostratigraphy, Site 1101, p. 48.

sedimentary sections that are being and will be cored elsewhere around Antarctica.

Similarly, more detailed chronologies than those provided by magnetic polarity stratigraphy can be obtained for Pleistocene sediments at the continental rise sites through correlation of the Leg 178 relative paleointensity records with global mean paleointensity records, such as Sint-800 (Guyodo and Valet, 1999), or with single high-quality records such as those recovered during Leg 162 in the North Atlantic (Channell et al., 1997; Channell, 1999). Additional independent chronologies can be obtained by using rock magnetic proxies, such as variations in magnetic susceptibility, that appear to correlate with oxygen isotope records. Guyodo et al. (2001) used both susceptibility and relative paleointensity to build a chronology for the interval recording the Jaramillo Subchron (C2r.1n) at ODP Site 1101. The importance of the magnetostratigraphy is evident even in that study, as it is the magnetostratigraphy that provides the key tie points, particularly the reversal boundaries for the Jaramillo Subchron.

## **PALEOMAGNETIC DATA**

Paleomagnetic analyses conducted during Leg 178 are described in the Leg 178 *Initial Reports* volume (Barker, Camerlenghi, Acton, et al., 1999). The shipboard paleomagnetic data from discrete and split-core sections are presented in tables in that volume or can be obtained via the World Wide Web from the Ocean Drilling Program (ODP). U-channel samples, which are strips of sediment, each 2 cm × 2 cm in cross section and up to 1.5 m long (Tauxe et al., 1983, Nagy and Valet, 1993; Weeks et al., 1993), were collected and measured postcruise. U-channel samples from Cores 178-1101A-1H through 10H were measured at the Institut de Physique du Globe de Paris, and all other U-channel samples were measured at the University of Florida. The U-channel magnetometers in both laboratories are Model 755R systems from 2-G Enterprises.

U-channel data have several advantages over split-core data. First, U-channel samples are collected from the center of split-core sections, which is the region least affected by coring disturbance and magnetic overprints related to coring with the advanced hydraulic piston corer (APC). In contrast, split-core sections from APC cores may contain a significant fraction of sediment by volume that is affected by core deformation. The deformation is most severe near the periphery of the core where the sediment is bent downward owing to friction as the piston corer cuts through the sediment and as the sediment slides into the core liner. This deformation can result in significant biases in paleomagnetic directions amounting to several degrees (Acton et al., 2002), though such deflections are insignificant for determination of polarity for the high-latitude sites cored during Leg 178. Second, relative to the shipboard magnetometer, U-channel magnetometers have smaller diameter sensor coils that are nearer the sample as the sample passes through the sensor region, which results in this magnetometer having greater sensitivity and higher spatial resolution (<7 cm) than the shipboard magnetometer (<10 cm). The sensitivity is further improved for the U-channel magnetometers used in this study because they reside in magnetically shielded rooms, whereas the shipboard magnetometer is on a metal ship that is constantly moving in the geomagnetic field. Because the resolution for the U-channel magnetometers is higher and be-

cause more time is available for measurement postcruise, we measured the U-channel samples at 1- to 2-cm intervals compared with 4- to 5-cm intervals for the split-core sections. Third, unlike the split-core sections, which were generally measured after alternating-field (AF) demagnetization of 0, 10, 20, and 25 or 30 mT, U-channel samples were subjected to progressive demagnetization up to 70–80 mT in steps of 5 or 10 mT. This allows principal component analysis (PCA) (Kirschvink, 1980) to be used to estimate the remanent magnetization direction from multiple demagnetization steps at peak AFs above the 10- to 25-mT fields needed to remove drilling overprints. The higher-quality U-channel data, along with the mcd scale, allow us to resolve conflicting results between holes at a site, as well as to identify intervals that are strongly affected by drilling overprints.

U-channel data from Holes 1095A, 1095B, 1095D, 1096A, 1096B, and 1101A are available in Tables T4, T5, T6, T7, T8, T9, respectively. Given the high latitude of the sites, the inclination is sufficient to assess the polarity of an interval. Declination and intensity information is, however, included in the paleomagnetism data tables of Barker, Camerlenghi, Acton, et al. (1999) and for the U-channel data from this study in Tables T4, T5, T6, T7, T8, T9.

Large fluctuations in the intensity over intervals comparable to or narrower than the sensor region for the long-core magnetometers can result in measurement artifacts (e.g., Nagy and Valet, 1993; Roberts et al., 1996). Although it is not practical to present the intensity data on a scale to compare with all directional changes, we have used the intensity data in our interpretation to avoid interpreting artifacts as reversals. Because we have archived the data, other investigators can also further evaluate the details of the paleomagnetic signal in intervals of interest.

For the tables giving the paleomagnetic results from U-channel samples (this study) and split-core samples (Shipboard Scientific Party, 1999a, 1999b, 1999c), data from intervals highly disturbed by drilling where such deformation was visually obvious were removed. In addition, data obtained within 5 cm of the ends of the U-channel or split-core samples were removed because these are biased by magnetic edge effects. These potentially erroneous data are not used in this study. U-channel samples from Cores 178-1095A-1H through 3H and from Cores 178-1096B-1H through 7H were taken from archive-half core sections. During Leg 178, these archive-half core sections were subjected to peak demagnetizing fields of 20 mT. In some cases, we remeasured these U-channel samples prior to beginning progressive demagnetization. In the tables, we retain these data as the 0-mT step because they contain information about the acquisition of viscous magnetization components (Fig. F2), although the user should be aware that any sample taken from the archive halves has been previously subjected to some level of demagnetization. All other U-channel samples are from working-half core sections, which were not subjected to any demagnetization prior to sampling.

As illustrated with a number of orthogonal vector demagnetization plots from AF and thermal demagnetization of discrete samples, which are shown in the “Paleomagnetism” sections of the “Site 1095,” “Site 1096,” and “Site 1101” chapters in the Leg 178 *Initial Reports* volume (Shipboard Scientific Party, 1999a, 1999b, 1999c) of Barker, Camerlenghi, Acton, et al. (1999), the sediments from the continental rise sites generally give stable univectorial directions after removal of a drilling overprint with 5- to 25-mT demagnetization. Similar behavior was

---

T4. Paleomagnetic data from U-channel samples, Hole 1095A, p. 49.

---



---

T5. Paleomagnetic data from U-channel samples, Hole 1095B, p. 50.

---



---

T6. Paleomagnetic data from U-channel samples, Hole 1095D, p. 51.

---



---

T7. Paleomagnetic data from U-channel samples, Hole 1096A, p. 52.

---



---

T8. Paleomagnetic data from U-channel samples, Hole 1096B, p. 53.

---

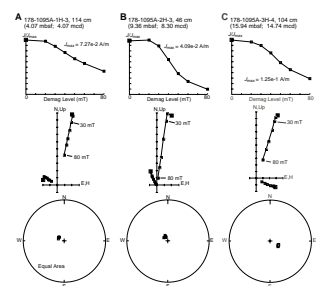


---

T9. Paleomagnetic data from U-channel samples, Hole 1101A, p. 54.

---

F2. Demagnetization of U-channel samples, Site 1095, p. 21.



seen on AF demagnetization of U-channel samples, as shown in Figures F2, F3, and F4.

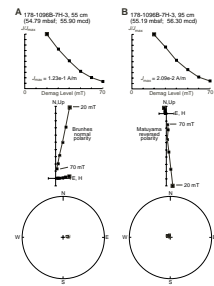
The PCA results for each interval along the U-channel samples are available for each hole in Tables T10, T11, T12, T13, T14, and T15. For the PCA direction, we find the best-fit line that passes through the vector demagnetization data without the constraint that the line pass through the origin of vector demagnetization plots. To avoid contamination by drilling overprints, we do not use demagnetization steps <20 mT in the PCA. We also use an iterative search program to find and delete data from demagnetization steps that are outliers, where an outlier is defined as a datum that degrades the fit of the line relative to all other demagnetization data used. We require that data from at least three steps are used and on average use directions from five or more steps to find the best estimate of the PCA direction.

The PCA results give precise directions and a clear indication of polarity in all but a few intervals, as discussed below for each site. A measure of how well the observations fit a line is provided by the maximum angular deviation (MAD), which is generated as part of PCA (Kirschvink, 1980). MAD values <10° are typically considered to provide lines that fit the observations well. Of the 13,439 intervals measured, 13,359 intervals (99.4%) have MAD values <10°, with 12,565 intervals (93.5%) having MAD values <3°.

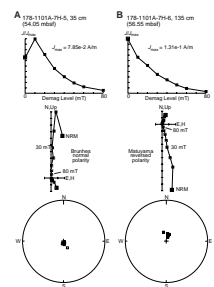
For comparison, we also compute a Fisherian mean (Fisher, 1953) of the highest three or four demagnetization steps for each interval from a U-channel sample. This is referred to as the stable end point direction. Typically only data from the highest three demagnetization steps are used in the average, unless the mean of these three directions has a dispersion (precision) parameter <200, in which case the data from the fourth highest demagnetization step is included. When the dispersion parameter is <200, we also use an iterative search to find and remove the direction that is the largest outlier. Comparison of the stable end joint with the PCA direction can be useful for indicating where unrecovered or partially unrecovered magnetization components exist or where progressive demagnetization has been ineffective in revealing linear demagnetization paths. For the Leg 178 sediments, the stable end point and PCA directions are virtually identical (Fig. F5), which indicates that a single magnetization component exists after removal of the drilling overprint and that this component can be isolated and accurately estimated using PCA or stable end points. The paleomagnetic direction obtained from a single demagnetization step at 20 or 30 mT from split-core sections similarly agrees well with the PCA direction or stable end point direction obtained from detailed progressive AF demagnetization of U-channel samples for most intervals (Fig. F5), with the few exceptions discussed below.

We interpret the component that is equally well resolved by PCA or by single-step demagnetization at 20 mT or higher as the characteristic remanent magnetization acquired by the sediment during deposition or shortly thereafter. The inclinations are therefore representative of the paleomagnetic field inclination at the time of deposition. Owing to the steepness of the paleomagnetic field vector at these high-latitude sites, the inclination gives a clear indication of polarity, with negative inclinations during normal polarity intervals and positive inclinations during reversed polarity intervals.

F3. AF demagnetization from U-channel samples, Site 1096, p. 24.



F4. AF demagnetization from U-channel samples, Site 1101, p. 25.



T10. PCA from U-channel paleomagnetic data, Hole 1095A, p. 55.

T11. PCA from U-channel paleomagnetic data, Hole 1095B, p. 56.

T12. PCA from U-channel paleomagnetic data, Hole 1095D, p. 57.

T13. PCA from U-channel paleomagnetic data, Hole 1096A, p. 58.

T14. PCA from U-channel paleomagnetic data, Hole 1096B, p. 59.

T15. PCA from U-channel paleomagnetic data, Hole 1101A, p. 60.

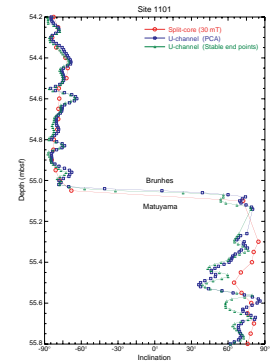
## ROCK MAGNETIC DATA

The median magnetizations for the three sites range from 0.01 to 0.07 A/m after 20-mT demagnetization, which is several orders of magnitude greater than the noise level of the magnetometers used in this study. Low-temperature rock magnetic analyses indicate that the main remanence-carrying mineral has a Verwey transition of 103–120 K, consistent with the presence of magnetite, slightly oxidized magnetite, or magnetite with some degree of cation (Ti, Al, or Mn) substitution (Brachfeld et al., [Chap. 14](#), this volume; Guyodo et al., 2001). Thermal demagnetization experiments reveal a high unblocking temperature component that unblocks from 500° to 600°C, although they also show that more than one-half the magnetization unblocks between 280° and 420°C (e.g., fig. F26 from Shipboard Scientific Party, 1999a). Both the medium and high unblocking temperature components record the same paleomagnetic direction. Hysteresis analyses indicate the sediments have coercivities of remanence generally between 20 and 40 mT, except for the upper 10–20 m of all three sites, where values are generally 30–90 mT (Brachfeld et al., [Chap. 14](#), this volume; Guyodo et al., 2001, unpubl. data). Furthermore, the samples from all three sites plot dominantly in the pseudo-single-domain region of Day plots (Day et al., 1977), with fewer samples falling in the multidomain region.

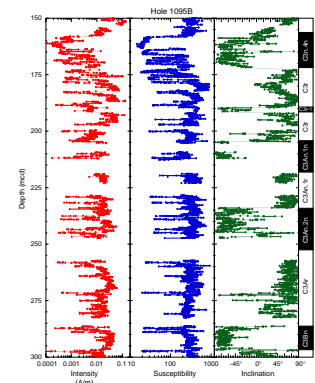
Together, these above observations suggest that most of the paleomagnetic signal is carried by magnetite and titanomagnetite, although we cannot preclude the presence of other carriers like pyrrhotite, greigite, maghemite, and hematite, particularly in the upper 10–20 m of sediment at all three sites. Most importantly, the magnetic minerals with medium to high coercivities and medium to high unblocking temperatures all appear to record a characteristic magnetization consistent with a depositional remanent magnetization (DRM) or postdepositional remanent magnetization (pDRM) that is acquired shortly after deposition.

In some relatively narrow intervals, the susceptibility drops by roughly an order of magnitude below that typical of the surrounding sediment (Fig. F6). These intervals are commonly <0.5 m thick but can be several meters thick. They are present at all three sites and can be correlated between holes at a site (Barker, [Chap. 6](#), this volume). The susceptibility lows are not associated with any obvious changes in lithology. As can also be seen in Figure F6, intervals of low intensity coincide with the susceptibility lows (Shipboard Scientific Party, 1999b). These lows are obviously associated with changes in the composition or concentration of the magnetic minerals, probably both. We do not know if they are primary (deposition) or secondary (alteration) features. Most importantly, the lows do not appear to affect the polarity for most intervals (Fig. F6). In some low-susceptibility and low-intensity intervals, however, the paleomagnetic inclination is shallower than would be expected for a high-latitude site. This may occur if the paleomagnetic signal decreases to near the noise level of the magnetometer ( $\sim 10^{-4}$  A/m) because the x-axis sensor is slightly less sensitive than that of the z-axis. Such a scenario may explain some of the difficulty in interpreting the magnetostratigraphy from 60 to 200 mcd at Site 1096, which contains an abundance of susceptibility lows. More commonly, there is little or no notable variation in the paleomagnetic direction across the susceptibility lows and therefore these lows do not adversely affect the magnetostratigraphic interpretation.

F5. Demagnetization of split-core sections, PCA of U-channel samples, and stable end points, p. 26.



F6. Notable susceptibility lows, Hole 1095B, p. 27.



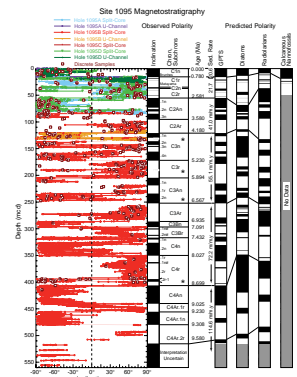
## SITE 1095

Paleomagnetic results from Site 1095 provide a magnetostratigraphy that correlates well with the GPTS from the termination of Subchron C4Ar.2n (9.580 Ma) at ~515 mcd upward through the Brunhes Chron (Figs. F7, F8, F9, F10). Exceptions occur in a few intervals where core deformation, dropstones, overprints, or low recovery bias or obscure the paleomagnetic signal.

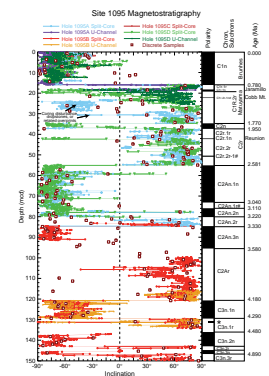
Differences between U-channel and split-core results, such as those in the upper 5 m of Hole 1095A (Fig. F11) and the interval from 18 to 25 mcd in Hole 1095D (Fig. F12), can be partly attributed to unremoved overprints in the split-core data. Other differences can be attributed to core deformation, such as that evident in core photos (see Barker, Camerlenghi, Acton, et al., 1999) in the interval from 178-1095D-3H-2, 80 cm, to 3H-4, 70 cm (18.48–21.38 mcd), which corresponds directly to where the split-core and U-channel data have their largest differences (Fig. F12). Other biases are also apparent in the split-core data. Dropstones, which are the coarse fraction of ice-rafted debris (IRD), appear to be a problem in a few intervals. Stones larger than 2 cm in diameter, which do not fit within a U-channel sample, along with other IRD may strongly bias the split-core results. In splitting whole cores, these stones may also be dragged several centimeters, resulting in additional core deformation. IRD or deformation probably explains the two shallow-inclination spikes in the split-core data at 4–7 mcd in Hole 1095D (Fig. F12). A large dropstone is evident in the core photo at Section 178-1095D-1H-4, 55 cm (5.05 mcd), and others may be present below the surface of the split cores.

Discrete samples were collected to better assess the magnetic signal and help refine the magnetostratigraphy. For most intervals, the inclinations from the discrete samples agree to within ~10° with those from U-channel samples, though some spurious discrete-sample results occur directly above 120 mcd (Fig. F7). For unknown reasons, ~20 of the discrete samples in this region of the core give shallow inclinations that differ significantly from the steep inclinations expected and observed from the U-channel samples and split-core sections. Given that the upper 120 m is soft sediment, it could be that some systematic deformation occurred as the discrete samples were collected or that the discrete samples have magnetizations that are near the resolution of the magnetometer, resulting in noise-dominated signals. Perhaps even a couple samples were misoriented, but errors during collection or operator errors during measurement are highly unlikely for so many samples in this interval. None of these are particularly appealing explanations for what are clearly anomalous results. Noise seems particularly unlikely because linear demagnetization paths are generally obtained for the samples with anomalous directions. In a few cases, the paths are planar rather than linear, which could indicate that some form of viscous magnetization has been acquired by the discrete samples, which were not measured in a magnetically shielded room, in contrast to the U-channel samples. Similar viscous components are absent from the split-core sections, so even that explanation has little appeal. Below 120 mcd, the agreement between results from discrete, U-channel, and split-core samples indicates that biases are negligible regardless of sample type. Thus, even in the absence of discrete or U-channel data, the split-core data accurately record the paleomagnetic field, with exceptions for intervals with IRD and core deformation as noted above.

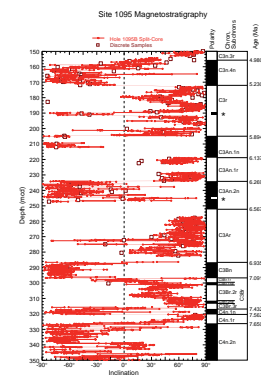
F7. Magnetostratigraphy, Site 1095, p. 28.



F8. Magnetostratigraphy and paleomagnetic inclinations, upper Site 1095, p. 29.



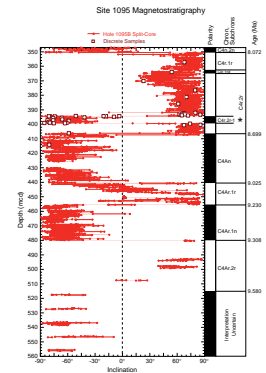
F9. Magnetostratigraphy and paleomagnetic inclinations, middle Site 1095, p. 30.



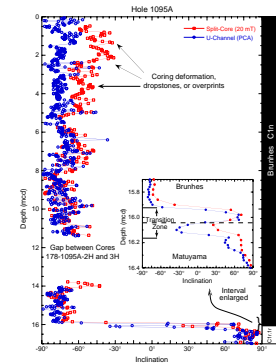
In Table T1, we provide a depth range within which each reversal occurs along with the best estimate of the depth of the reversal boundary. The size of the depth range is generally dependent on core recovery and coring gaps, although the length of time for the reversal to complete and the complexity of directional changes during the reversal are also factors. For example, the field direction over the Brunhes/Matuyama reversal shows a change from steep positive inclinations of the Matuyama Chron to shallow negative inclinations and then steep positive inclinations within the transition zone, before finally reaching steep negative inclinations of the Brunhes normal polarity chron (Fig. F11). The transition spans ~24 cm (15.92–16.16 mcd), which corresponds to ~12 k.y. A similar swing in inclination has been noted for the Brunhes–Matuyama transition in sediments from Leg 172 Sites 1060 and 1063 in the northwest Atlantic and from Leg 162 Site 983 in the North Atlantic, where again the transition for all three sites spanned ~5 to 12 k.y. (pp. 318–320 of Keigwin, Rio, Acton, et al., 1998; Channell and Kleiven, 2000). Other reversals appear to be virtually instantaneous within the resolution provided by the sedimentary record, such as the reversal at 84.56 mcd, which we interpret as the termination of Subchron C2An.2n. The best estimate of the reversal depth is generally the midpoint within the depth range. Exceptions to this, as noted in Table T1 and discussed further below, are restricted to reversals that fall within wide or uncertain polarity transition zones. Placement of the reversal to one side of the transition zone may be preferred because less erratic changes in the calculated sedimentation rates may result. Also, when core recovery is poor, magnetic logging data may narrow the region in which the reversal should be placed.

Original interpretation of the shipboard data was difficult for the upper 100 m of the section owing to conflicting results from Holes 1095A, 1095B, and 1095D. Part of the conflict results from inaccuracy in the meters below seafloor (mbsf) depth scale, which produces artificial vertical offsets between laterally continuous, coeval features (Fig. F13). Shipboard identification of Subchrons C1r.1n (Jaramillo) through C2An.2r was particularly difficult for this reason. Also, the split-core samples gave anomalous or somewhat biased paleomagnetic directions in a few intervals that we subsequently recognized when U-channel data were obtained (Fig. F12). Specifically, the region from ~17 to 55 mcd is more complexly magnetized (possibly caused by larger drilling overprints, core deformation, or a greater influence by IRD) than intervals above or below (Figs. F8, F12). These difficulties, in association with an interpreted seismic discontinuity and lithostratigraphic boundary, led us to propose a hiatus at ~52–55 mcd in Holes 1095A and 1095D during Leg 178. When the new paleomagnetic observations from U-channel samples along with the split-core data are plotted on the mcd scale, it appears unlikely that extended hiatuses occur here or elsewhere within the sedimentary section, at least within the resolution of the magnetostratigraphic observations. A hiatus of <200 k.y. would, however, be difficult to observe paleomagnetically within this interval given the relatively slow sedimentation rate, the resolution of the paleomagnetic data, and the age constraints provided by magnetostratigraphic reversals or biostratigraphic events. For example, placing a 200-k.y. hiatus at ~52–55 mcd does not produce abnormally fast or slow sedimentation rates in the sedimentary section above or below the hiatus. Thus, we cannot preclude the occurrence of a relatively short hiatus, such as might be caused by an erosional event that could produce a dis-

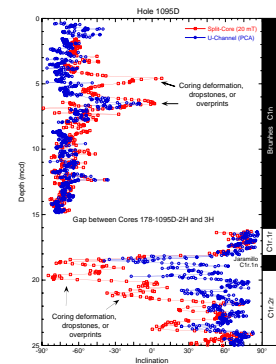
F10. Magnetostratigraphy and paleomagnetic inclinations, lower Site 1095, p. 31.



F11. U-channel and split-core inclinations, Hole 1095A, p. 32.



F12. U-channel and split-core inclinations, Hole 1095D, p. 33.

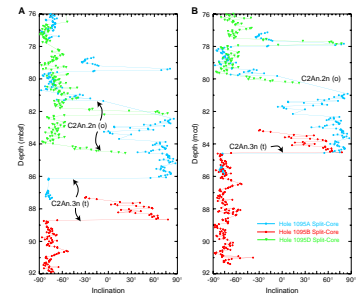


continuity in seismic reflection profiles and a subtle lithostratigraphic boundary.

Our magnetostratigraphic interpretation agrees well with biostratigraphic constraints in most intervals as illustrated in Figure F7, which shows the polarity zones predicted using the age constraints provided by the diatom, the radiolarian, and the calcareous nannofossil events given in Iwai et al. (Chap. 36, this volume). In constructing these predicted magnetostratigraphies, we averaged some diatom events with similar ages, some of which gave conflicting relative depths for their relative ages. For example, the top of the *Thalassiosira complicata* Zone has an age of 3.4 Ma and occurs at a depth of 62.48 mcd, whereas the top of the *Thalassiosira inura* Zone has an age of 1.75 Ma and occurs at a depth of 68.33 mcd. These two zones, along with three other zones—top of *Thalassiosira torokina* (1.85 Ma; 57.705 mcd), top of *Thalassiosira insigna* (2.57 Ma; 56.495 mcd), and top of *Fragilariopsis interfrigidaria* (2.67 Ma; 76.53 mcd)—with similar ages and depth ranges are combined to give a mean age of 2.448 Ma for a mean depth of 64.308 mcd. Disagreement between magnetostratigraphic and biostratigraphic ages are generally no larger than the disagreement between ages estimated from the different biostratigraphic constraints. All predict similar ages near the top (e.g., note the similar depths for the Brunhes/Matuyama boundary in Fig. F7), the middle (e.g., note the similar depths for the onset of Subchron C3An.2n), and the base of the sedimentary section (e.g., all age constraints suggest that sediments below 450 mcd must be older than 9 Ma).

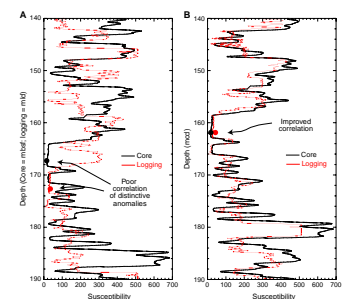
Our revised magnetostratigraphy for Site 1095 is also consistent with the downhole logging results presented by Williams et al. (Chap. 31, this volume) for the interval logged from 110 to 570 mbsf in Hole 1095B. The depths to reversals are available in graphical form in Figure F8, p. 19, of Williams et al. (Chap. 31, this volume). The logging depths are estimated from the wireline length during logging, whereas the mcd scale is built on between-hole correlation of recovered cores, whose depths were estimated from the length of the drill pipe. For a coeval feature, the logging depths average 4 to 6 m deeper than the mbsf depths for Hole 1095B or 5 to 11 m deeper than depths from the mcd scale. In Table T16, we give the offsets between the two depth scales. These were determined by correlating the susceptibility data from whole-core measurements to the susceptibility data from the second logging run of the Geologic High-Resolution Magnetic Tool (GHMT), which includes a susceptibility measurement sonde. The correlation was done using the program AnalySeries (Paillard et al., 1996), which outputs the user-selected tie points for the signals being correlated. Depths between tie-points are adjusted through linear interpolation between bounding tie-points. We use the susceptibility data because it was collected on the GHMT logging runs, from which the logging magnetostratigraphy is derived, and was collected along the core, from which the core magnetostratigraphy is derived. We focus on only the second run of the GHMT logging tool, although both runs gave comparable results (Williams et al., Chap. 31, this volume). Furthermore, both Barker (Chap. 6, this volume) and Acton et al. (Chap. 5, this volume) used the susceptibility data to construct mcd scales because it was the data type most easily correlated between holes at a site. We found that distinctive susceptibility anomalies could be easily correlated between the core and logging data sets (Fig. F14). Finally, use of susceptibility allows us to do core-logging correlation that is independent of the magnetostratigraphy, which thus allows us to compare the core and logging results and

F13. Split-core inclinations, Site 1095, p. 34.



T16. Correlation logging and mbsf and mcd depth scales, Hole 1095B, p. 61.

F14. Whole-core and GHMT susceptibilities, p. 35.



confirm that they give compatible magnetostratigraphies. When both the magnetic logging data and the paleomagnetic inclination data are plotted in the mcd scale, the excellent correlation between them is obvious (see Figure F9, p. 28, of Iwai et al., Chap. 36, this volume).

Below, we discuss our interpretation, working downhole. We focus the discussion on changes to the magnetostratigraphy presented in the Leg 178 *Initial Reports* volume (Shipboard Scientific Party, 1999a) and on complicated or interesting intervals. We note in Table T1 those intervals where the interpretation is similar or identical to that of the Shipboard Scientific Party (1999a).

1. None of the short polarity intervals occurring in the past 2.5 m.y., including the Jaramillo Subchron (Subchron C1r.1n), the Cobb Mountain Event (Cryptochron C1r.2r-1n), the Reunion Event (Subchron C2r.1n), or Cryptochron C2r.2r-1n can be confidently identified. The Jaramillo is the longest of these, spanning ~80 k.y., whereas the other three span <~20 k.y. We suspect that the low inclination interval between 18.05 and 20.00 mcd corresponds to the Jaramillo Subchron (Table T1). Similarly, a narrow normal polarity subzone spanning the top 52 cm of Core 178-1095D-6H could be Subchron C2r.1n, but a similar subzone is absent in Core 178-1095A-6H, which spans the same interval. Slow sedimentation rates, bioturbation, and complex magnetizations within the interval from 17 to 55 mcd (see discussion above and Fig. F8) probably contribute to the lack of resolution of these short polarity subchrons and cryptochrons.
2. Within the complexly magnetized interval, we interpret the normal polarity zone from 34.68 to 37.33 mcd as Chron C2n, which places the termination of Chron C2n about 20 m above the depth given by Shipboard Scientific Party (1999a). In the interpretation of Shipboard Scientific Party (1999a), all reversals from the termination of Chron C2n to the onset of Subchron C2An.1n were missing and assumed lost in a hiatus.
3. Within the interval that we interpret to be part of Chron C2An, the reversal boundaries for Subchron C2An.2n and the onset of Subchron C2An.1n cannot be accurately identified but are probably present within the interval from 77.64 to 80.20 mcd. A short reversed polarity subzone occurs from 77.66 to 77.95 mcd, but it is narrower than would be expected for Subchron C2An.1r unless an abrupt decrease in sedimentation rate had occurred at this time relative to the average rate during the Pliocene. Because there is also a large intensity spike in this narrow interval, we suspect that the subzone may be an artifact of the long-core magnetometer measurements rather than a true directional change.
4. The multiple holes cored in the upper part of the sedimentary section at Site 1095 resulted in recovery of a complete sedimentary section down to 91 mcd. Below this depth, coring was restricted to Hole 1095B, which extends to a total depth of 555.28 mcd. In this single-cored interval, gaps between cores and intervals of poor recovery, which range from several centimeters to several meters, add uncertainty to the precision at which some reversal boundaries can be determined.
5. Shallow positive inclinations between 104 and 109 mcd, within the reversed polarity zone interpreted to correspond to Chron C2Ar, are probably related to coring disturbance, which is visible

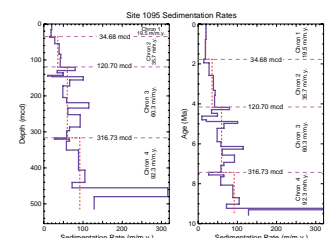
- within the upper and lower parts of Section 178-1095B-3H-6 and the upper part of Section 3H-7 (see core photos in “Site 1095 Visual Core Descriptions” in Barker, Camerlenghi, Acton, et al., 1999).
6. The normal polarity zone interpreted to correspond to Subchron C3n.1n is about two times thicker than would be expected if sedimentation rates were roughly constant in the upper middle part of the sedimentary section. This would indicate sedimentation rates during Subchron C3n.1n (4.18–4.29 Ma) were roughly twice as fast as they were a few hundred thousand years earlier or later (i.e., ~8 cm/k.y. relative to the average rate of ~4 cm/k.y. from 2 to 6 Ma).
  7. An excursion or short polarity subzone at 131.09–131.32 mcd is present within the polarity zone interpreted to correspond to Subchron C3n.1r. This feature has not been previously identified in Subchron C3n.1r as far as we know, though an anomalous spike is evident in intensity (a high) and in direction within Chronozone C3n.1r in Hole 845B cored during ODP Leg 138 (figure 2 of Schneider, 1995). It is unlikely that the inclination excursion in Hole 1095B is related to an intensity fluctuation, although an intensity low is present >20 cm uphole. This intensity low is unexceptional and fluctuations of similar size, which are present along the core, are not associated with directional changes.
  8. Shallow and intermediate inclinations at the top of Core 178-1095B-9H (153.5 mcd) down to the upper part of Core 10H (163.7 mcd) make determination of the termination of Subchron C3n.4n uncertain. Farther downhole in Core 178-1095B-10H, several other spurious intervals of shallow positive inclination occur in what is a dominantly negative inclination (normal polarity) interval interpreted to correspond to Subchron C3n.4n. We suspect that these and other unexpected shallow inclination spikes that occur farther downhole are noise related to core deformation rather than geomagnetic field behavior. Extended core barrel (XCB) cores nearly always contain core “biscuits” surrounded by core slurry. The biscuits are generally intact core pieces several centimeters long. These pieces usually retain their horizontal orientation and give accurate paleomagnetic inclinations, although ultimately some small pieces may get rotated or intervals of slurry may dominate, possibly causing spurious paleomagnetic results over short intervals.
  9. An excursion or anomalous interval occurs at 189.66–191.66 mcd in the reversed polarity zone that corresponds to Chron C3r. Further study of this interval is needed to evaluate the event. We are unaware of a geomagnetic event being previously identified in Chron C3r.
  10. The onset of Subchron C3An.1n occurs within a coring gap from 212.10 to 218.88 mcd (between Cores 178-1095B-15X and 16X). We place the reversal boundary near the base of the gap (at 218.8 mcd) because this location agrees well with the interpreted magnetic logging data (Williams et al., **Chap. 31**, this volume) and this placement gives a smoother variation in sedimentation rates over the interval from 150 to 250 mcd than if the midpoint of the gap is used.
  11. An excursion or anomalous interval with positive shallow inclinations is located between 244.76 and 247.74 mcd (interval 178-

- 1095B-18X-5, 76 cm, and 18X-6, 124 cm). This falls within the lower part of the polarity zone interpreted to be Subchron C3An.2n.
12. Within Chron C3Br, neither Subchron C3Br.1n nor Subchron C3Br.2n can be identified in the split-core measurements. Both subchrons have a short duration, spanning only ~35 k.y. Subchron C3Br.1n appeared to be present in the logging data as a discrete normal polarity interval that was ~2 m below Chron C3Bn (Shipboard Scientific Party, 1999a). The reprocessed logging data (Williams et al., [Chap. 31](#), this volume) no longer includes this feature.
  13. The inclination results are noisy within the polarity zone corresponding to Subchron C4n.2n. The noise is manifested as several intervals with shallow inclinations within the polarity zone, which is dominated by steep negative inclinations. The intensity of magnetization is low ( $\sim 10^{-3}$  A/m) relative to background values ( $\sim 10^{-2}$  A/m) where the shallow inclinations occur. Thus, these features could be caused by measurement artifacts or related to XCB core deformation.
  14. The long reversed polarity zone from 350.54 to 406.22 mcd corresponds to Chron C4r. Within Chron C4r, the GPTS includes two short normal polarity intervals, Subchron C4r.1n and Cryptochron C4r.2r-1, each of which span <40 k.y. (Cande and Kent, 1992a, 1992b, 1995). We cannot confidently identify the younger subchron, but it may correspond to an interval with intermediate positive inclinations at ~365 mcd. In contrast, a normal polarity zone from 394.6 to 399.5 mcd, which is interpreted to represent Cryptochron C4r.2r-1, is well defined and provides the best magnetostratigraphic record of this cryptochron to date (Acton et al., 1999).
  15. The reversal boundary between the polarity zones interpreted to represent Subchrons C4Ar.1r and C4An is poorly defined owing to the noisy results between 440 and 453 mcd.
  16. The normal polarity zone interpreted to represent Subchron C4Ar.1n is thicker than expected for a roughly constant rate of sedimentation. This implies a sedimentation rate for Subchron C4Ar.1n of 316 m/m.y., which is more than three times the overall Chron C4 average rate of 92 m/m.y.
  17. Below 480 mcd, the magnetostratigraphy becomes uncertain owing to poor core recovery. Both the core recovered and the magnetic logging data indicate that a reversed polarity zone is present from 480.3 to ~515 mcd, which we interpret to represent Subchron C4Ar.2r. A normal polarity zone appears to extend from ~515 mcd to the base of the hole, which could represent Subchron C4Ar.2n or some combination of Subchrons C4Ar.2n through C5n.2n.

### Site 1095 Sedimentation Rates

Using the revised magnetostratigraphy, we compute the sedimentation rates between the identified reversals. These are included in [Table T1](#) and are shown graphically in [Figure F15](#). As noted by Barker, Camerlenghi, Acton, et al. (1999), sedimentation rates increase downhole. Average rates were ~20 m/m.y. at the top of the hole and >100 m/m.y. near the bottom of the hole.

**F15.** Sedimentation rates, Site 1095, p. 36.



## SITE 1096

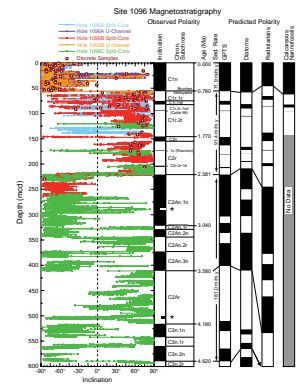
The paleomagnetic results from Site 1096 provide a magnetostratigraphy that correlates well with the GPTS starting from the onset of Subchron C3n.2n (4.620 Ma) at ~489.68 mcd upward through the Brunhes Chron (Fig. F16, F17). As at Site 1095, exceptions occur in a few intervals where core deformation, dropstones, overprints, or low recovery bias or obscure the paleomagnetic signal. Negligible coring gaps occur above ~140 mcd in the section that was double-APC cored in Holes 1096A and 1096B. Below this, gaps of several meters may occur between cores and with some shorter polarity zones may not have been recovered. Also, as at Site 1095, the interval from below Brunhes/Matuyama reversal to just above Subchron C2An.1n, spanning roughly 0.8 to 2.4 Ma, has the most complex magnetization and is the most difficult to interpret.

In Table T2, we list the depth range within which each reversal occurs along with the best estimate of the depth of the reversal boundary. Agreement between magnetostratigraphic ages and biostratigraphic ages, particularly those from diatom events, is excellent (Fig. F16). One exception is that the top of the *Lampromitra coronata* radiolarian zone indicates an age for the base of the sedimentary section that is ~0.5 m.y. younger than indicated by either the diatom events or the magnetostratigraphy.

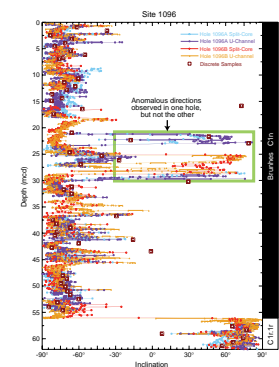
Revisions to the shipboard data are noted in Table T2 and are discussed further below. The most significant changes are the identification of Chron C2n, Subchron C2r.1n (the Reunion Subchron), the onset of Subchron C2An.1n, and Subchron C2An.2n. The relative stratigraphic locations of these newly identified polarity chrons and subchrons are compatible with the broader magnetostratigraphic framework constructed during Leg 178 (table T21 from Shipboard Scientific Party, 1999b). Details of the interpretation are given below.

1. The zones with positive inclinations (reversed polarity) between 20 and 30 mcd are probably related to coring deformation. None of the zones with positive inclinations are replicated where duplicate APC cores from Holes 1096A and 1096B exist (Fig. F17). The two positive inclination zones recorded in Hole 1096A are present in the upper 3.5 m of Cores 178-1096A-3H and 4H. Coring deformation is common in the upper meter of many APC cores but can extend downcore particularly when ship heave is large, which was common during Leg 178. The positive inclination zone in Hole 1096B extends from interval 178-1096B-4H-2, 56 cm, to 4H-5, 82 cm. Core photographs (Barker, Camerlenghi, Acton, et al., 1999) show drilling and or core-splitting disturbance, but the disturbance does not appear to extend over all of the interval and does not appear sufficient to remagnetize or reorient the core material so completely.
2. The Brunhes/Matuyama reversal boundary is a sharp contact between steep negative inclinations of the Brunhes Chron (C1n) and the steep positive inclinations of the upper Matuyama Chron (C1r.1r) (Fig. F17). The fluctuations in directions noted in the transition zone at Site 1095 are recorded neither here nor at Site 1101.
3. Neither the Jaramillo Subchron (Subchron C1r.1n) nor the Cobb Mountain Event (Cryptochron C1r.2r-1n) can be confidently

F16. Magnetostratigraphy, Site 1096, p. 37.



F17. U-channel, split-core, and discrete inclinations, Site 1096, p. 38.



identified within a noisy interval that extends from ~60 to 200 mcd. The Jaramillo Subchron could correspond to one of the short negative inclination zones between ~63 and 110 mcd, though these zones could merely represent noise. Although perhaps coincidental, it is interesting that the interval spanning Chrons C1r through C2r is the most complexly magnetized at both Site 1095 and Site 1096. The complexity is manifested in shallower than expected inclinations and in results that conflict in coeval zones from adjacent holes. Both sites are part of the same sediment drift and likely have similar magnetic mineralogy and depositional histories, even though the sedimentation rates are several times higher at Site 1096. As noted by the Shipboard Scientific Party (1999b; "Paleomagnetism" section), several, but not all, of the negative inclination zones from 60 to 200 mcd occur where the magnetization drops by more than an order of magnitude below the background level of ~0.04 A/m. Similarly, the susceptibility drops by about an order of magnitude where the lows in magnetization intensity occur. Instrument noise, lower concentrations of magnetic minerals, coarser magnetic mineral assemblages, abundant dropstones, and APC core deformation could all be factors. Whatever the cause, many of the narrow zones with negative inclinations from ~60 to 200 mcd, particularly those intervals with intermediate or shallow negative inclinations, do not appear to represent normal polarity zones or subzones.

4. The normal polarity zone located at ~146–147 mcd and sampled only in Hole 1096B is interpreted to represent the upper part of Chron C2n. On its own, this zone is narrower than would be expected for Chron C2n given the Pleistocene sedimentation rates at Site 1096. However, the base of Core 178-1096B-16H has sustained drilling disturbance, as is apparent for Section 16H-6 in the core photographs (Barker, Camerlenghi, Acton, et al., 1999). Thus, the reversal that appears to occur at the top of Section 178-1096B-16H-6 (~147 mcd) may be an artifact of the drilling disturbance. Below Core 178-1096B-16H there is an ~7-m coring gap. We suggest that the onset of Chron C2n occurs somewhere within the coring gap. Below the gap, the next reliable paleomagnetic inclinations come from the top of Core 178-1096B-19H, which clearly have reversed polarity and are interpreted to represent part of Chron C2r.
5. We speculate that the normal polarity subzone between ~173 and 174 mcd is Subchron C2r.1n (the Reunion Subchron). We base this speculation on the position of the normal polarity subzone relative to adjacent polarity zones and on the position of the subzone at the base of lithostratigraphic Unit II. As noted by Kyte (**Chap. 9**, this volume), the Reunion Subchron was identified at the base of lithostratigraphic Unit II at Site 1101 and Unit II is defined similarly at Sites 1096 and 1101, with its base occurring below the last of one or more foraminifer-bearing interglacial deposits. The inclination within the subzone is, however, shallower than other well-defined normal polarity zones, the magnetization and susceptibility are low within the subzone, and a discrete sample within the subzone indicated reversed rather than normal polarity. The subzone is located within the first two sections of Core 178-1096C-2H, of which the upper 105

cm of Section 2H-1 is affected by drilling disturbance, making the identification of the termination of the subzone uncertain.

6. A geomagnetic excursion or anomalous interval, located at 288.82–291.20 mcd (interval 178-1096C-10X-3, 28 cm, to 10X-4, 98 cm), is present in the normal polarity zone that corresponds to Subchron C2An.1n. Several other narrower anomalous intervals (<1 m thick) occur above and below this interval but are probably artifacts given the level of drilling disturbance common in XCB cores.
7. The reversed polarity zone at the top of Core 178-1096C-14X is interpreted to represent Subchron C2An.1r. The top of the zone is not observed because it occurs somewhere in the coring gap between Cores 178-1096C-13X and 14X. We prefer a location near the top of the coring gap because this minimizes sedimentation rate variations. This reversal boundary also defines the onset of Subchron C2An.1n. Given that the reversed polarity zone represents Subchron C2An.1r, it follows that the normal polarity zone below represents Subchron C2An.2n.
8. A normal polarity zone is present in Core 178-1096C-32X (501.47–506.75 mcd) that is also visible in the GHMT log (Williams et al., [Chap. 31](#), this volume). We interpret it as a geomagnetic excursion or as an anomalous zone. Alternatively, it could be interpreted as Subchron C3n.1n, but this results in more abrupt changes in sedimentation rates than our preferred interpretation. If it is Subchron C3n.1n, the lowest normal polarity zone in the hole would more likely be Subchron C3n.3n than our preferred interpretation of Subchron C3n.2n.
9. The locations of reversal boundaries for the termination of Subchron C2An.3n to the onset of Subchron C3n.2n agree with those of the Shipboard Scientific Party (1999b), although some minor modification has been made to the size of the transition zones (Table [T2](#)).

### Site 1096 Sedimentation Rates

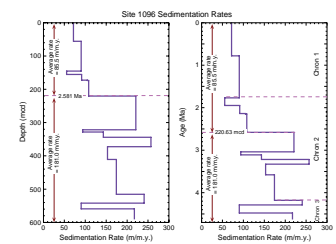
Using the revised magnetostratigraphy, we computed sedimentation rates between the identified reversals (Table [T2](#); Fig. [F18](#)). As noted by Barker, Camerlenghi, and Acton, et al. (1999), the sedimentation rates increase downhole with the largest increase at the termination of Subchron C2An.1n (2.581 Ma), which occurs at 220.63 mcd. The average sedimentation rate above this depth is 85.5 m/m.y. and below is 181.0 m/m.y.

### SITE 1101

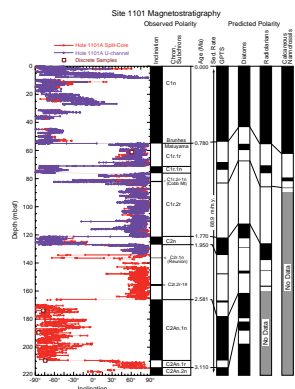
The paleomagnetic results from Site 1101 provide a magnetostratigraphy that correlates well with the GPTS from the onset of Subchron C2An.1n (3.040 Ma) at ~209.38 mcd upward through the Brunhes Chron (Table [T3](#); Fig. [F19](#)). As at the other sites, exceptions occur in a few intervals where core deformation, dropstones, overprints, or low core recovery bias or obscure the paleomagnetic signal. Unlike the other sites, Site 1101 was cored in a single hole (Hole 1101A). Thus, coring gaps are not filled by core recovered from other holes. Several large coring gaps occur in the upper 60 m. The lack of redundant coring also makes it difficult to evaluate the origin of anomalous paleomagnetic di-



**F18.** Sedimentation rates, Site 1096, p. 39.



**F19.** Magnetostratigraphy, Site 1101, p. 40



rections. Owing to the sea state, in which large swells were common, coring disturbance and associated anomalous directions were more common and more extreme than at the other sites. As was the case at the other sites, we do not consider data from intervals that are highly disturbed by drilling.

Because only one working half of the core was available for sampling, we decided to focus our efforts on U-channel sampling. We collected only four discrete samples from Hole 1101A and the results from these all agree well with coeval split-core and U-channel results. More than 47,200 vector measurements were made on over 5900 intervals from U-channel samples from the Cores 178-1101A-1H through 15H, which were progressively AF demagnetized up to 80 mT (Table T9). Directions estimated from PCA of the demagnetization results confirm the shipboard results and interpretations, which were based on AF demagnetization of the split-core sections at 30 mT (Fig. F5). Overall, deviations between U-channel, split-core, and discrete sample results are negligible. Hence, the revised magnetostratigraphy is virtually unchanged from that completed during Leg 178 (see table T21 and associated discussion by the Shipboard Scientific Party, 1999c). The slight adjustments that we make here are based mainly on the higher resolution of the U-channel measurements, as indicated in Table T3. We also defined the boundaries for Subchron C1r.2r-1n (the Cobb Mountain Subchron) and Subchron C2r.1n (the Reunion Event), which were discussed by the Shipboard Scientific Party (1999c) but which were not included in their table T21. The identification of both of these subchrons is speculative given the short intervals over which they occur and the level of drilling disturbance that affects some intervals cored in Hole 1101A.

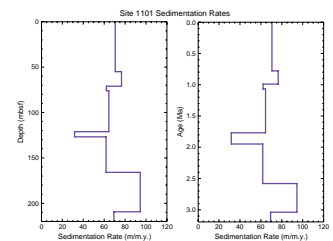
### Site 1101 Sedimentation Rates

Using the revised magnetostratigraphy, we computed sedimentation rates between the identified reversals (Table T3; Fig. F20). Because the magnetostratigraphy agrees well with that of the Shipboard Scientific Party (1999c), the sedimentation rates are also nearly equivalent. The average sedimentation rate is 68.9 m/m.y. over the 217.7-m section cored, with little overall variation. Sedimentation rates were also nearly constant over the past 3 m.y. at Sites 1095 and 1096. The most notable changes at Site 1101 are the slower sedimentation rates during Chron C2n and the faster rates during Subchron C2An.1n, a pattern similar to that observed at Site 1096.

## CONCLUSIONS

We provide revised magnetostratigraphic interpretations of paleomagnetic data from the three drift sites cored during Leg 178. We outline in detail the rationale for our interpretation, which is mainly based upon matching the pattern of the polarity zones recorded at the Leg 178 sites with the chrons of the geomagnetic polarity timescale. The revised interpretations are generally consistent with the biostratigraphic constraints, which on their own permit alternate magnetostratigraphic interpretations with the inclusion of one or two hiatuses at Site 1095 as discussed by Iwai et al. (Chap. 36, this volume). The magnetostratigraphic observations are, however, consistent with continuous sedimentation with decreasing sedimentation rates up section at Site 1095, a step decrease in sedimentation rates at Site 1096 from a mean of 181.0

F20. Sedimentation rates, Site 1101, p. 41.



m/m.y. before 2.581 Ma to 85.5 m/m.y. after, and a near-constant sedimentation rate of 68.9 m/m.y. over the interval cored at Site 1101. Our preferred interpretation includes no hiatuses at any of the sites.

We also provide a tabulated archive of more than 102,000 vector paleomagnetic measurements made at over 13,400 intervals along U-channel samples. Besides the raw data, we include the results from principal component analysis and stable end point determinations from these data. Similar data sets from shipboard measurements made on split-core sections and discrete samples are archived in Barker, Camerlenghi, Acton, et al. (1999). Together, these data provide the fundamental observations upon which our magnetostratigraphic interpretations have been based.

## **ACKNOWLEDGMENTS**

We thank Masao Iwai and Lisa Osterman for discussions concerning biostratigraphic events and Frank Kyte for his input on the location of the Reunion Subchron at Site 1096. We appreciate the thorough reviews by Andy Roberts and Suzanne Beske-Diehl and the comments of the editor, Peter Barker. We thank Jim Channell for allowing us access to the paleomagnetism laboratory at the University of Florida, Jean-Pierre Valet and Vincent Courtillot for allowing us access to the paleomagnetism laboratory at the Institut de Physique du Globe de Paris, and the staff at the Institute of Rock Magnetism at the University of Minnesota for assistance with rock magnetic measurements. This research used samples and data provided by the Ocean Drilling Program (ODP). The ODP is sponsored by the U.S. National Science Foundation (NSF) and participating countries under management of Joint Oceanographic Institutions (JOI), Inc. Funding for this research was provided by the United States Science Support Program (USSSP) (JOI/USSSP grant RF9801068RB1 at Texas A&M University).

## REFERENCES

- Acton, G.D., Brachfeld, S., and Guyodo, Y., 1999. The nature of a cryptochron: paleomagnetic results from ODP Site 1095, off the Pacific Coast of West Antarctica. *Eos*, 80 (Fall Meeting Supplement), F286.
- Acton, G.D., Okada, M., Clement, B.M., Lund, S.P., and Williams, T., 2002. Paleomagnetic overprints in ocean sediment cores and their relationship to shear deformation caused by piston coring. *J. Geophys. Res.*, 107:10.1029/2001JB000518.
- Barker, P.F., Camerlenghi, A., Acton, G.D., et al., 1999. *Proc. ODP, Init. Repts.*, 178 [CD-ROM]. Available from: Ocean Drilling Program, Texas A&M University, College Station, TX 77845-9547, U.S.A.
- Brachfeld, S., Acton, G.D., Guyodo, Y., and Banerjee, S.K., 2000. High-resolution paleomagnetic records from Holocene sediments from the Palmer Deep, western Antarctic Peninsula. *Earth Planet. Sci. Lett.*, 181:421–441.
- Cande, S.C., and Kent, D.V., 1992a. A new geomagnetic polarity time scale for the Late Cretaceous and Cenozoic. *J. Geophys. Res.*, 97:13917–13951.
- , 1992b. Ultrahigh resolution marine magnetic anomaly profiles: a record of continuous paleointensity variations? *J. Geophys. Res.*, 97:15075–15083.
- , 1995. Revised calibration of the geomagnetic polarity timescale for the Late Cretaceous and Cenozoic. *J. Geophys. Res.*, 100:6093–6095.
- Channell, J.E.T., 1999. Geomagnetic paleointensity and directional secular variation at Ocean Drilling Program (ODP) Site 984 (Bjorn Drift) since 500 ka: comparisons with ODP Site 983 (Gardar Drift). *J. Geophys. Res.*, 104:22937–22951.
- Channell, J.E.T., Hodell, D.A., and Lehman, B., 1997. Relative geomagnetic paleointensity and  $\delta^{18}\text{O}$  at ODP Site 983 (Gardar Drift, North Atlantic) since 350 ka. *Earth Planet. Sci. Lett.*, 153:103–118.
- Channell, J.E.T., and Kleiven, H.F., 2000. Geomagnetic palaeointensities and astrochronological ages for the Matuyama-Brunhes boundary and the boundaries of the Jaramillo Subchron: palaeomagnetic and oxygen isotope records from ODP Site 983. *Phil. Trans. R. Soc. Lond.*, 358:1027–1047.
- Day, R., Fuller, M., and Schmidt, V.A., 1977. Hysteresis properties of titanomagnetites: grain-size and compositional dependence. *Phys. Earth Planet. Inter.*, 13:260–267.
- Domack, E., Leventer, A., Dunbar, R., Taylor, F., Brachfeld, S., Sjunneskog, C., and ODP Leg 178 Science Party, 2001. Chronology of the Palmer Deep Site, Antarctic Peninsula: a Holocene paleoenvironmental reference for the circum-Antarctic. *The Holocene*, 11:1–9.
- Fisher, R.A., 1953. Dispersion on a sphere. *Proc. R. Soc. London A*, 217:295–305.
- Guyodo, Y., Acton, G.D., Brachfeld, S., and Channell, J.E.T., 2001. A sedimentary paleomagnetic record of the Matuyama Chron from the western Antarctic margin (ODP Site 1101). *Earth Planet. Sci. Lett.*, 191:61–74.
- Guyodo, Y., and Valet, J.P., 1999. Global changes in intensity of the Earth's magnetic field during the past 800 kyr. *Nature*, 399:249–252.
- Keigwin, L.D., Rio, D., Acton, G.D., et al., 1998. *Proc. ODP, Init. Repts.*, 172: College Station, TX (Ocean Drilling Program).
- Kirschvink, J.L., 1980. The least-squares line and plane and the analysis of palaeomagnetic data. *Geophys. J. R. Astron. Soc.*, 62:699–718.
- Nagy, E.A., and Valet, J.-P., 1993. New advances for paleomagnetic studies of sediment cores using U-channels. *Geophys. Res. Lett.*, 20:671–674.
- Paillard, D., Labeyrie, L., and Yiou, P., 1996. Macintosh program performs time-series analysis. *Eos*, 77:379.
- Roberts, A.P., Stoner, J.S., and Richter, C., 1996. Coring-induced magnetic overprints and limitations of the long-core paleomagnetic measurement technique: some observations from Leg 160, eastern Mediterranean Sea. In Emeis, K.-C., Robertson, A.H.F., Richter, C., et al., *Proc. ODP, Init. Repts.*, 160: College Station, TX (Ocean Drilling Program), 497–505.

- Schneider, D.A., 1995. Paleomagnetism of some Leg 138 sediments: detailing Miocene magnetostratigraphy. In Pias, N.G., Mayer, L.A., Janecek, T.R., Palmer-Julson, A., and van Andel, T.H. (Eds.), *Proc. ODP, Sci. Results*, 138: College Station, TX (Ocean Drilling Program), 59–72.
- Shipboard Scientific Party, 1999a. Site 1095. In Barker, P.F., Camerlenghi, A., Acton, G.D., et al., *Proc. ODP, Init. Repts.*, 178, 1–173 [CD-ROM]. Available from: Ocean Drilling Program, Texas A&M University, College Station, TX 77845-9547, U.S.A.
- , 1999b. Site 1096. In Barker, P.F., Camerlenghi, A., Acton, G.D., et al., *Proc. ODP, Init. Repts.*, 178, 1–144 [CD-ROM]. Available from: Ocean Drilling Program, Texas A&M University, College Station, TX 77845-9547, U.S.A.
- , 1999c. Site 1101. In Barker, P.F., Camerlenghi, A., Acton, G.D., et al., *Proc. ODP, Init. Repts.*, 178, 1–83 [CD-ROM]. Available from: Ocean Drilling Program, Texas A&M University, College Station, TX 77845-9547, U.S.A.
- Tauxe, L., LaBrecque, J.L., Dodson, R., and Fuller, M., 1983. “U” channels—a new technique for paleomagnetic analysis of hydraulic piston cores. *Eos*, 64:219.
- Weeks, R.J., Laj, C., Endignoux, L., Fuller, M.D., Roberts, A.P., Manganne, R., Blanchard, E., and Goree, W., 1993. Improvements in long-core measurement techniques: applications in palaeomagnetism and palaeoceanography. *Geophys. J. Int.*, 114:651–662.

Figure F1. Location map of Leg 178 drill sites on the western margin of the Antarctic Peninsula (modified from Barker, Camerlenghi, Acton, et al., 1999). DSDP = Deep Sea Drilling Project.

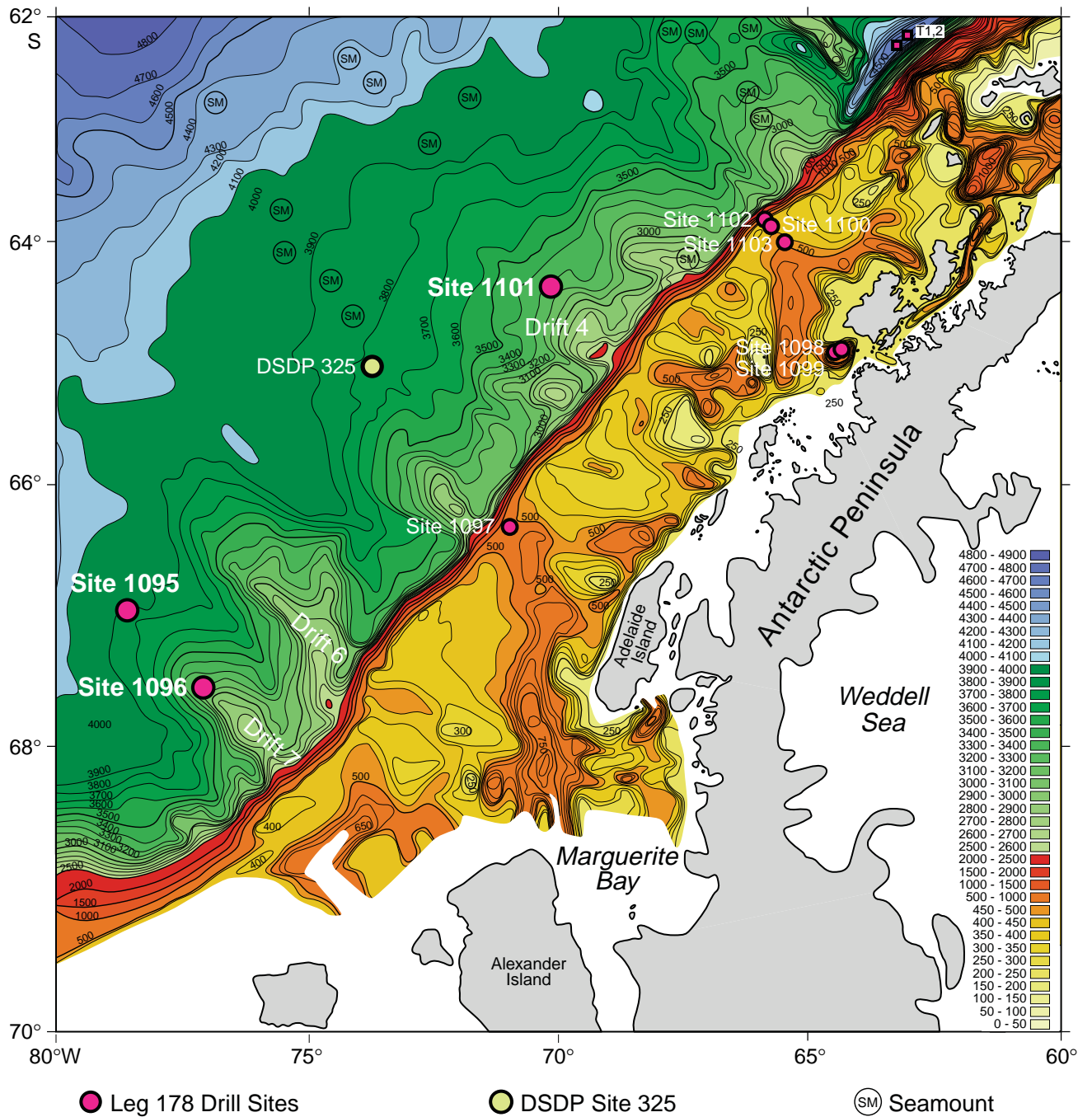


**Figure F2.** AF demagnetization results from U-channel samples from Site 1095. The top diagrams show the intensity variation with progressive demagnetization; the middle diagrams show vector end points on a vector demagnetization diagram (orthogonal projections: open squares = inclinations, solid squares = declinations); and the bottom diagrams show the magnetization directions on equal area projections (open squares = directions with negative inclinations). The first four intervals (A–D) are from U-channel samples taken from archive-half core sections, which had been subjected to peak AF demagnetizing fields of 20 mT during Leg 178. We remeasured the magnetization of each U-channel sample (0 mT step) prior to beginning progressive demagnetization at 20 mT; hence, the difference between the 0- and 20-mT steps is only indicative of the magnetization acquired since Leg 178 or of slight differences in the calibration of the demagnetization devices used on the ship and shore. Acquisition of small viscous components by the lowest-coercivity magnetic minerals is probably the cause of the difference because calibration differences appear to be negligible based on comparison of many demagnetization results. In contrast, the last two intervals (E and F) are from working-half core sections, which were not subject to any demagnetization prior to collection of the U-channel samples. Both intervals display a low-coercivity, steeply downward-directed component that is removed by demagnetization at 10–20 mT. This is a drilling overprint, which is evident to some degree in nearly every ODP core collected (e.g., Shipboard Scientific Party, 1999a). (A) Interval 178-1095A-1H-3, 114 cm (4.07 mbsf = 4.07 mcd), has a higher coercivity than deeper intervals. Similar behavior was also observed for the upper 18 m of Site 1096 (Brachfeld et al., [Chap. 14](#), this volume). A–C are all normal polarity intervals from the Brunhes Chron, D is a reversed polarity interval from the Matuyama Chron, E is a reversed polarity interval from Chron C2Ar, and F is a normal polarity interval from Subchron C3n.1n. NRM = natural remanent magnetization. ([Figure shown on next two pages.](#))

Figure F2 (continued). A. Sample 178-1095A-1H-3, 114 cm. B. Sample 178-1095A-2H-3, 46 cm. C. Sample 178-1095A-3H-4, 104 cm. (Continued on next page.)

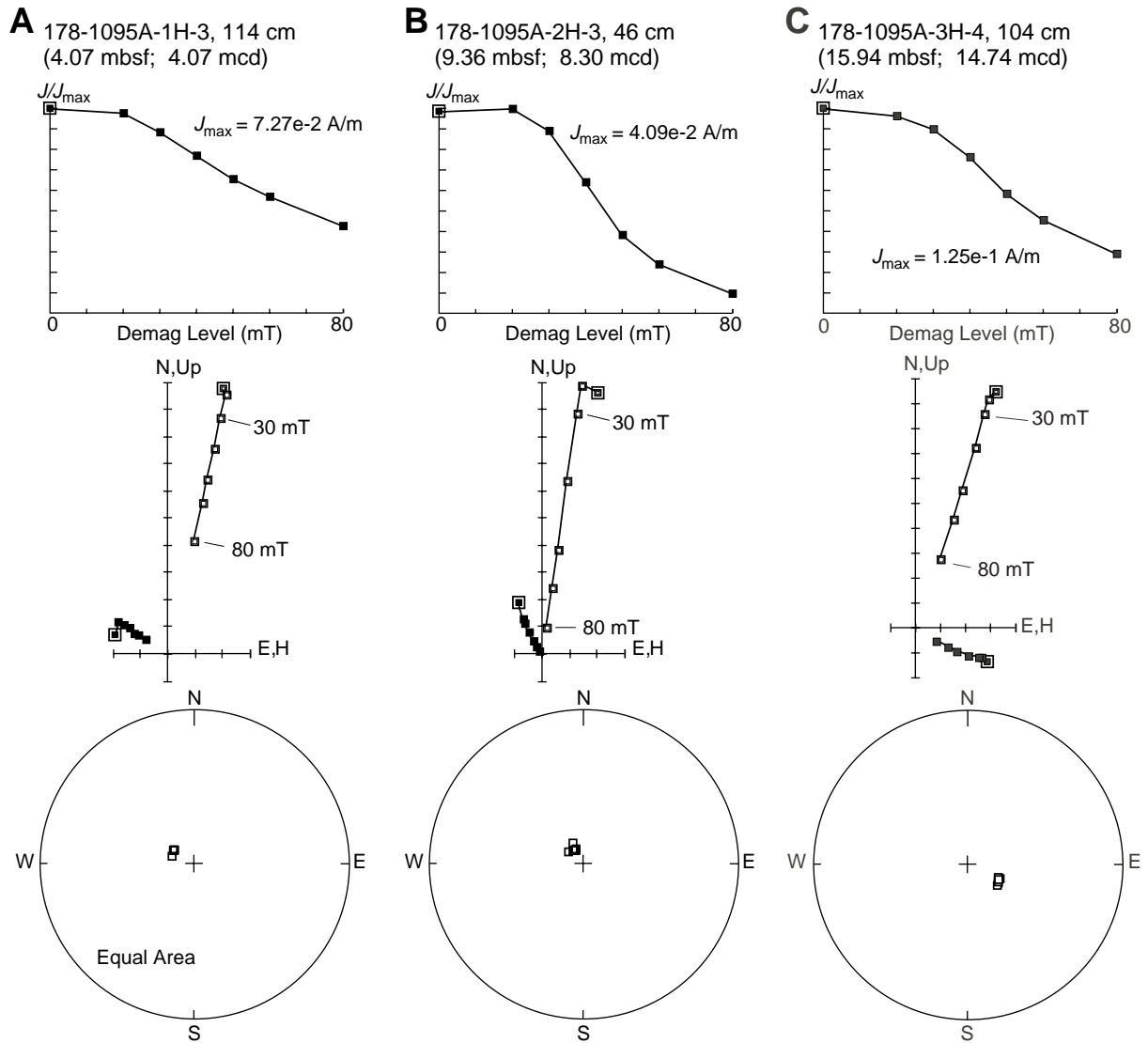
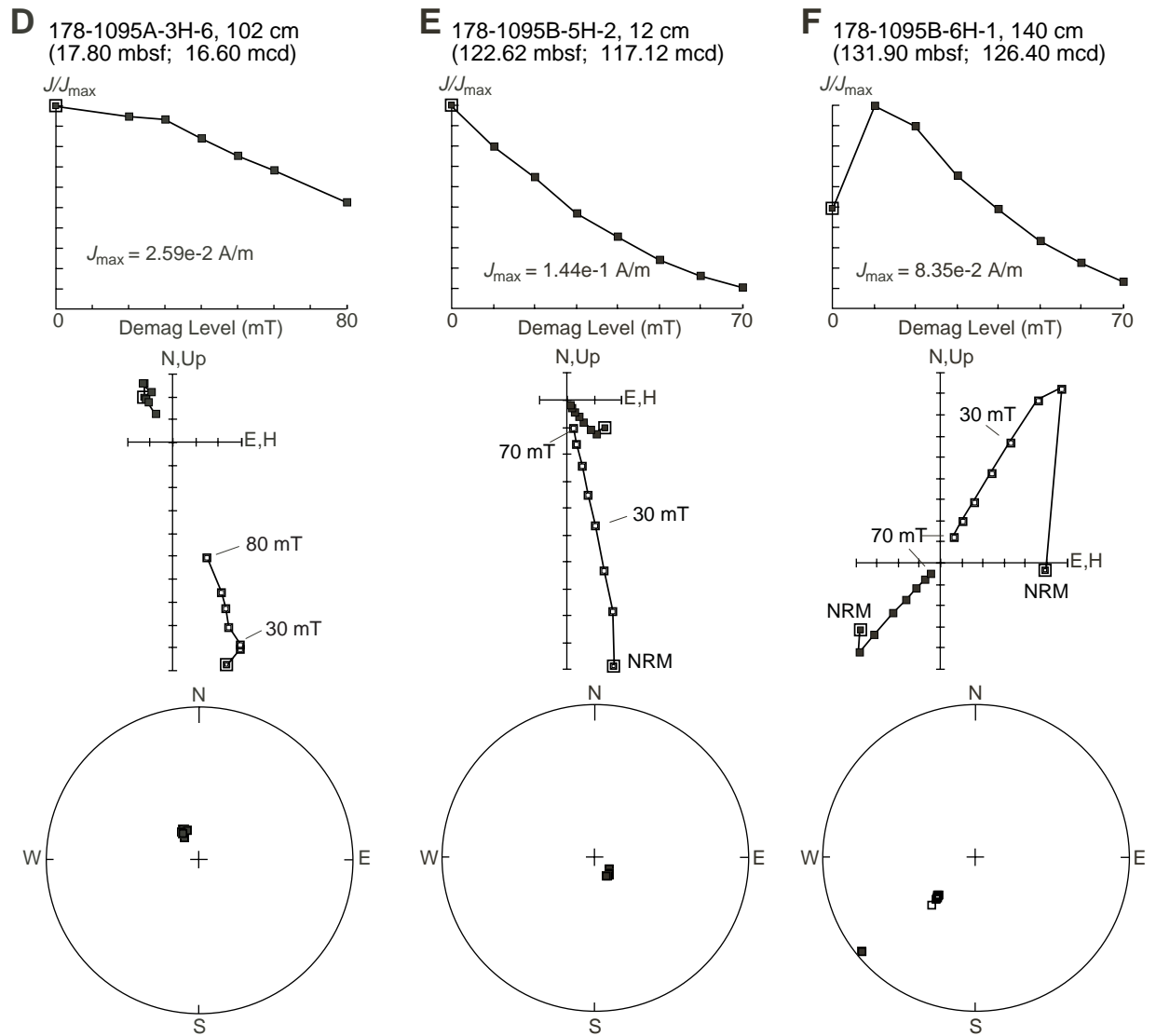


Figure F2 (continued). D. Sample 178-1095A-3H-6, 102 cm. E. Sample 178-1095B-5H-2, 12 cm. F. Sample 178-1095B-6H-1, 140 cm.



**Figure F3.** AF demagnetization results for two intervals from U-channel samples from Site 1096. See Figure F2, p. 21, for plot descriptions. Both intervals are from archive-half sections that had previously been subjected to demagnetization at 20 mT, and so the demagnetization of the U-channel samples was started at 20 mT. **A.** Sample 178-1096B-7H-3, 55 cm. **B.** Sample 178-1095B-7H-3, 95 cm.

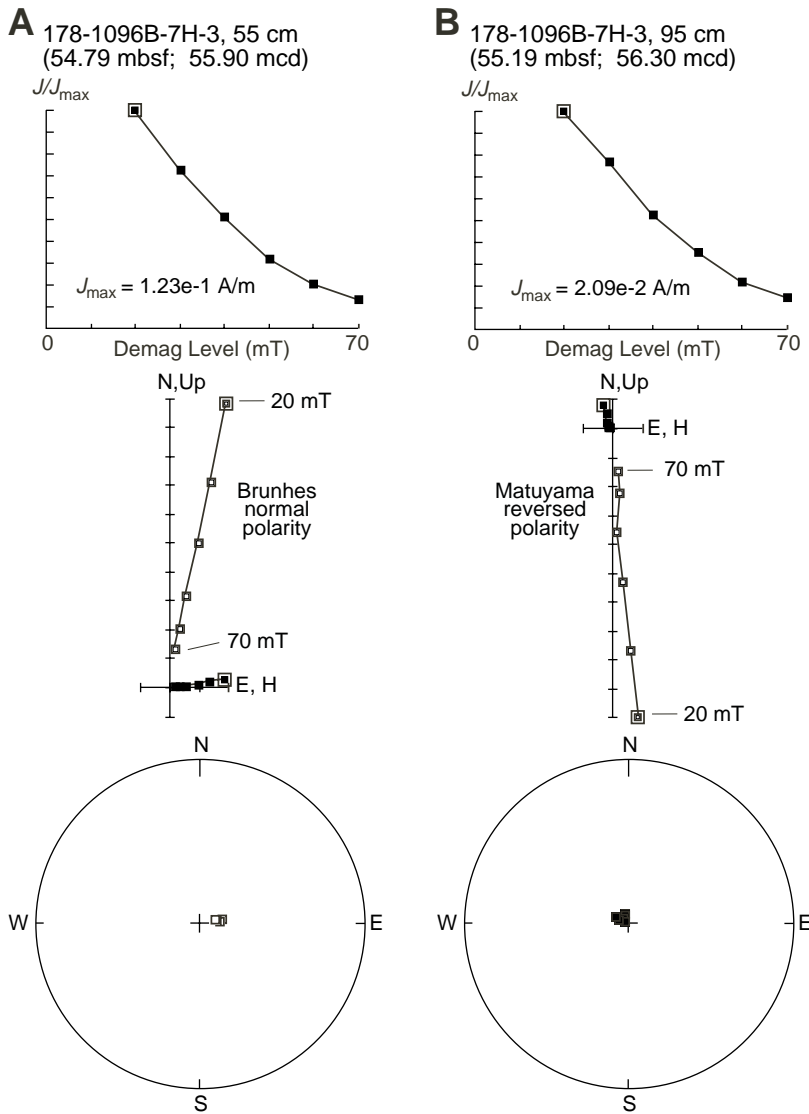


Figure F4. AF demagnetization results for two intervals from U-channel samples from Site 1101. See Figure F2, p. 21, for plot descriptions. A. Sample 178-1101A-7H-5, 35 cm. B. Sample 178-1101A-7H-6, 135 cm.

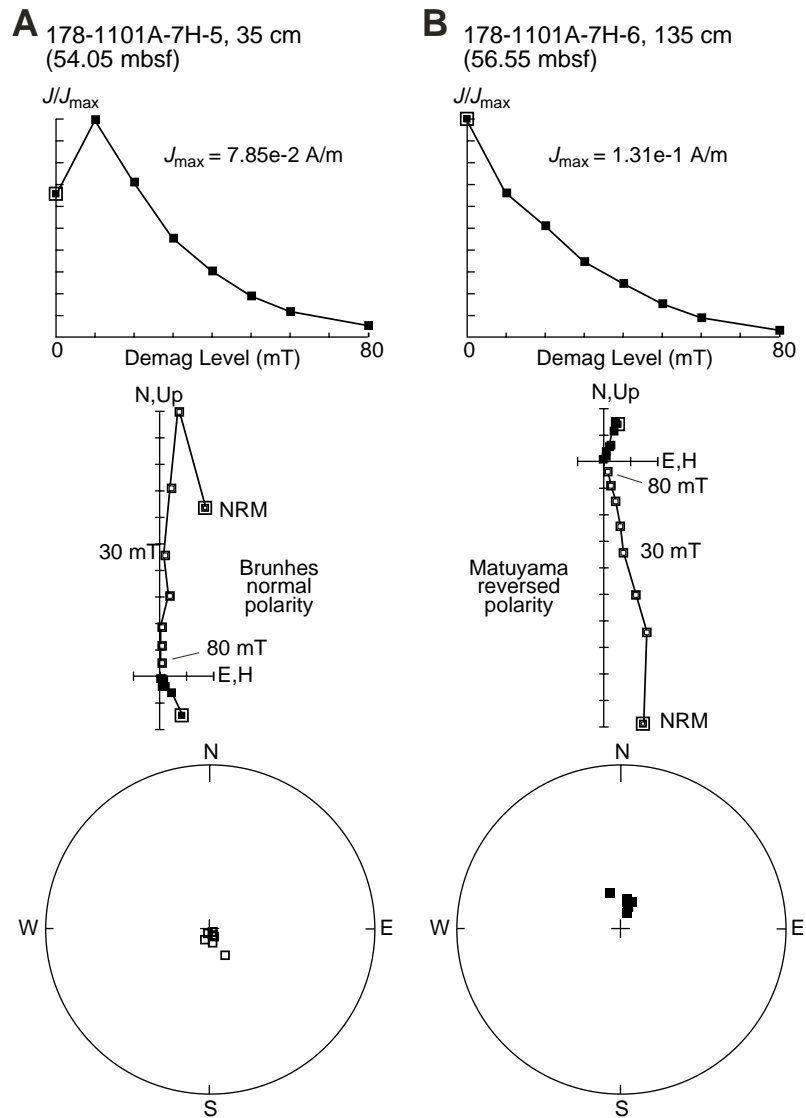
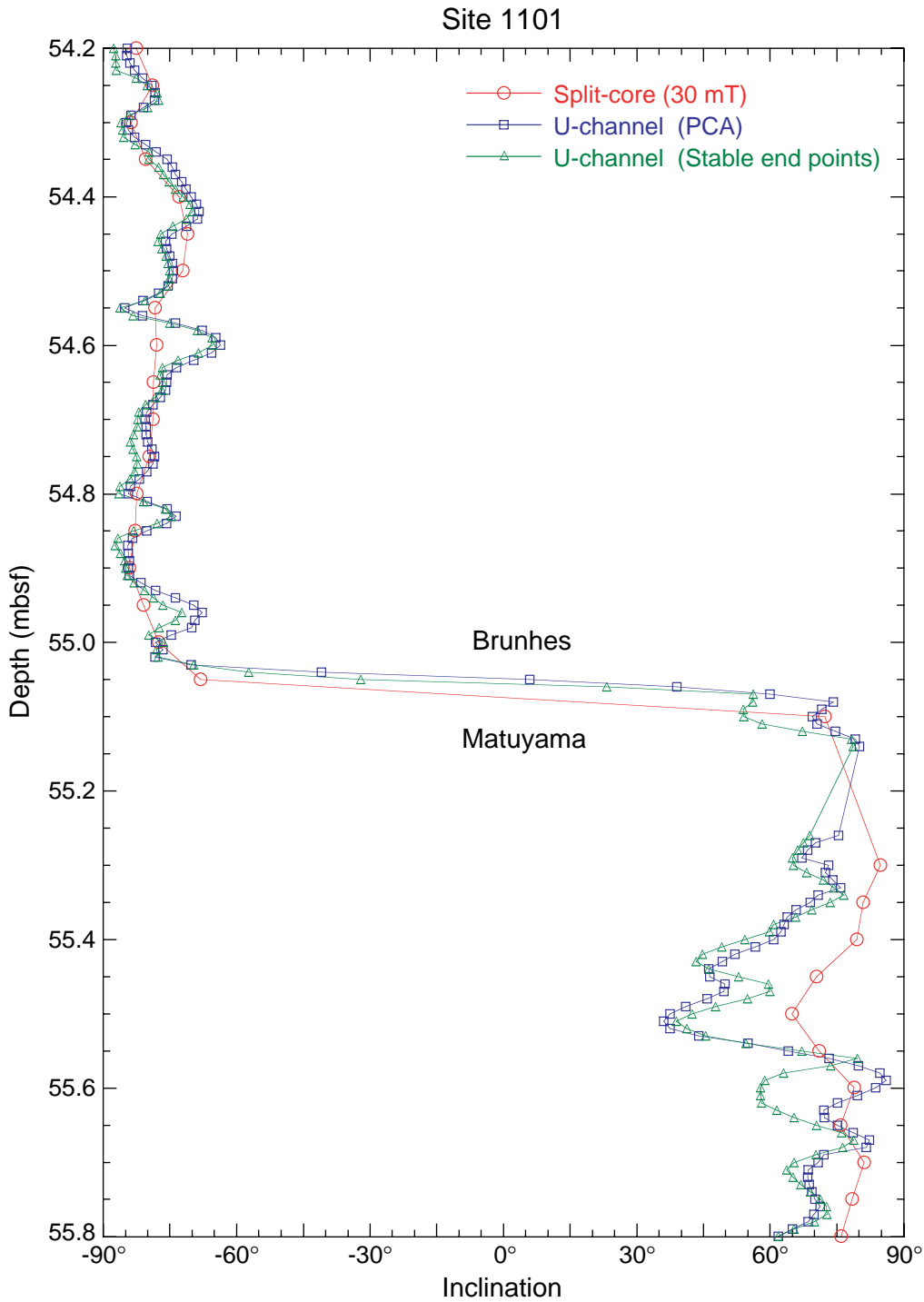
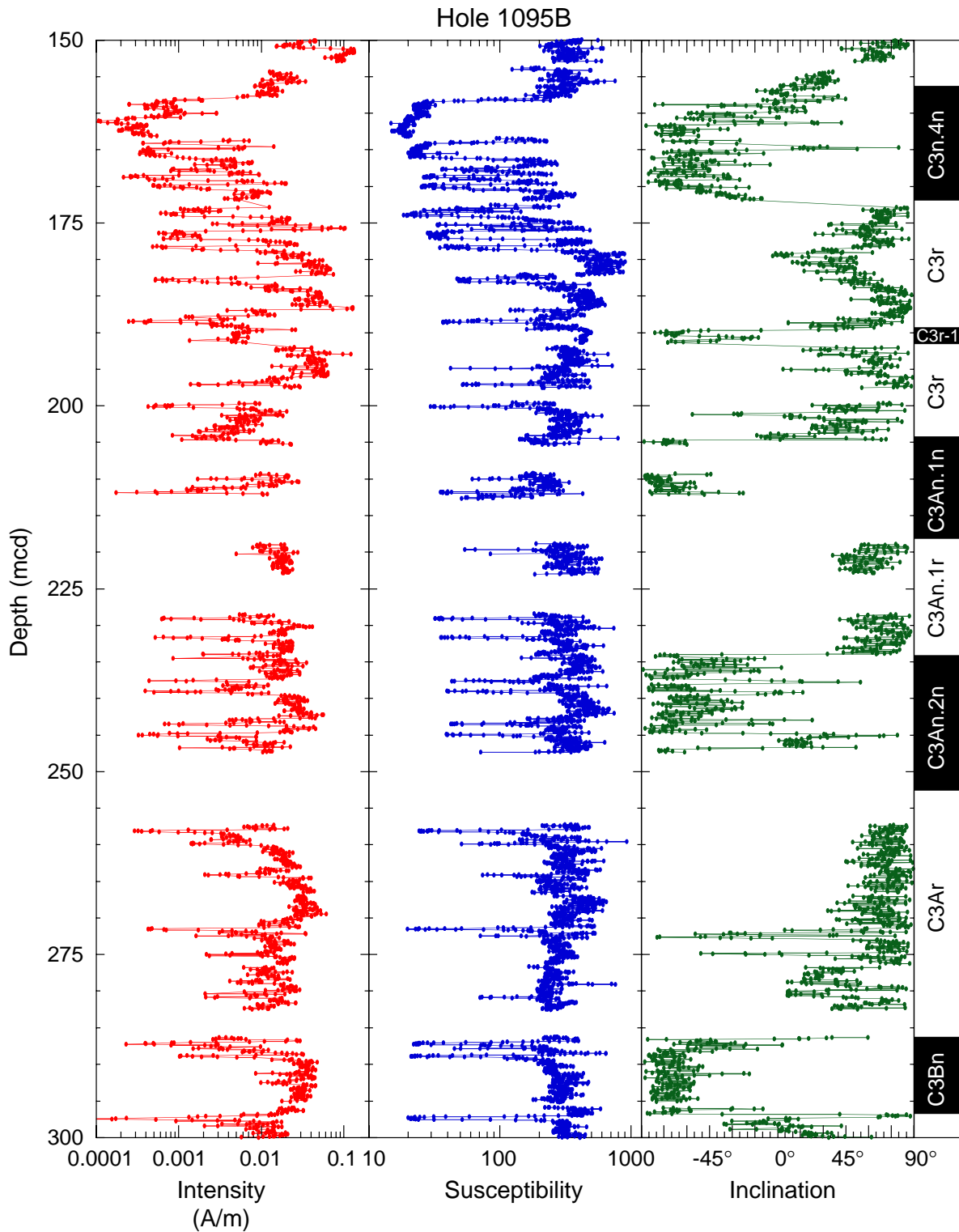


Figure F5. Example of the similar directions obtained from single-step demagnetization of split-core sections, PCA of progressive demagnetization data from U-channel samples, and stable end points obtained from the highest demagnetization steps from U-channel samples.



**Figure F6.** The notable susceptibility lows are shown for an interval from 150 to 300 mcd in Hole 1095B. Susceptibility is given in raw meter units, which can be converted to volume SI units by multiplying by  $\sim 0.7 \times 10^{-5}$ . The magnetic polarity (black = normal, white = reversed) and interpreted chrons are given to the far right.



**Figure F7.** The magnetostratigraphy for Site 1095 is shown with the paleomagnetic inclination data from split-core sections (after demagnetization of 20–30 mT), U-channel samples (PCA), and discrete samples (PCA). The interpreted magnetostratigraphy is also compared with the polarity zonation predicted from the geomagnetic polarity timescale (GPTS) for the case where the sedimentation rate was constant over long periods of time and for the case where the sediment ages are constrained by diatom, radiolarian, and calcareous nannofossil events of Iwai et al. (Chap. 36, this volume). Sed. Rate = sedimentation rate. \* = excursions, cryptochrons, or anomalous polarity zones observed in the inclination data; # = chrons and subchrons not identified in the sedimentary section.

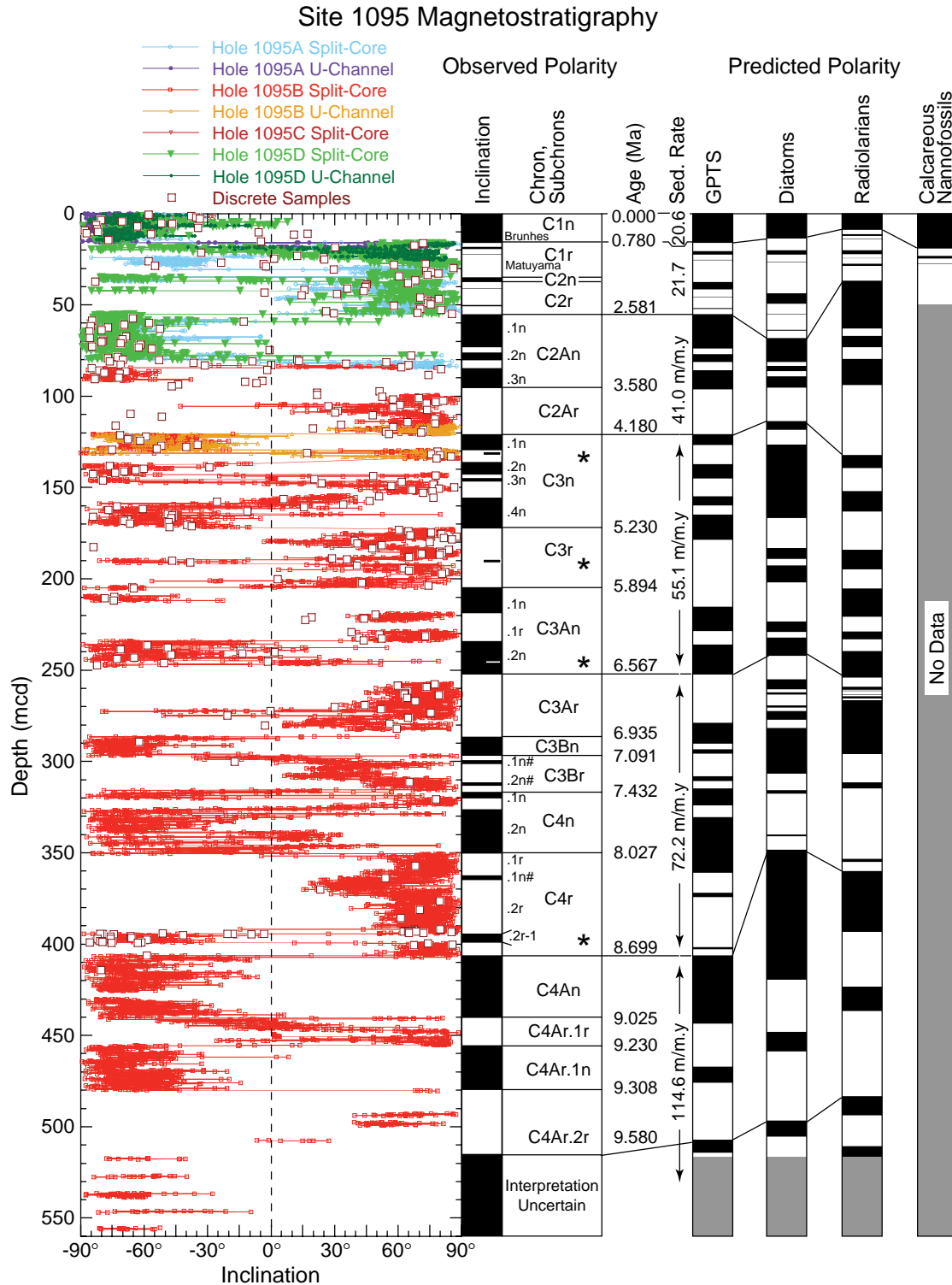


Figure F8. The magnetostratigraphy and paleomagnetic inclinations from the upper part of the sedimentary section at Site 1095. \* = excursions, cryptochrons, or anomalous polarity zones observed in the inclination data; # = chrons and subchrons not identified in the sedimentary section.

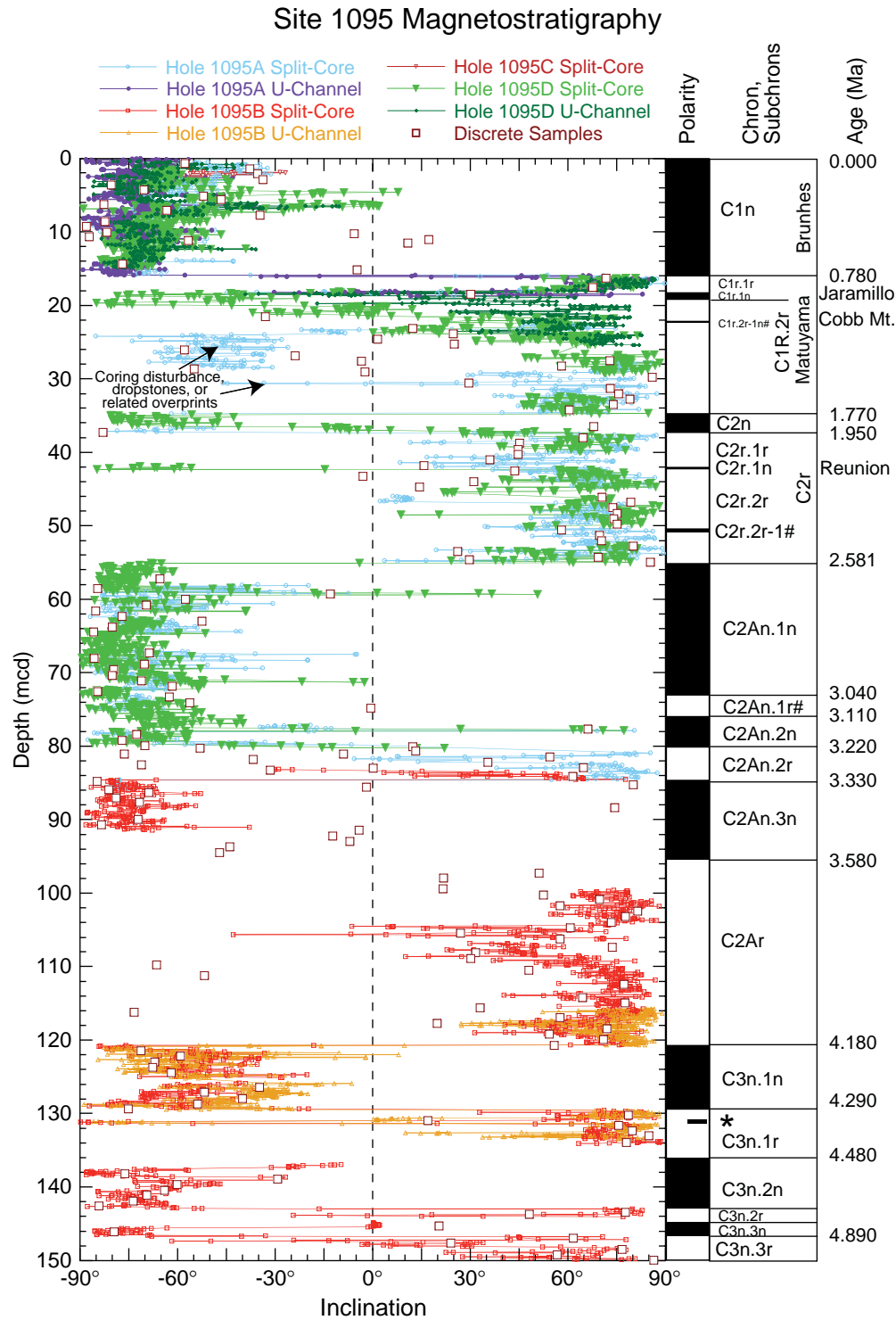


Figure F9. The magnetostratigraphy and paleomagnetic inclinations from the middle part of the sedimentary section at Site 1095. \* = excursions, cryptochrons, or anomalous polarity zones observed in the inclination data; # = chrons and subchrons not identified in the sedimentary section.

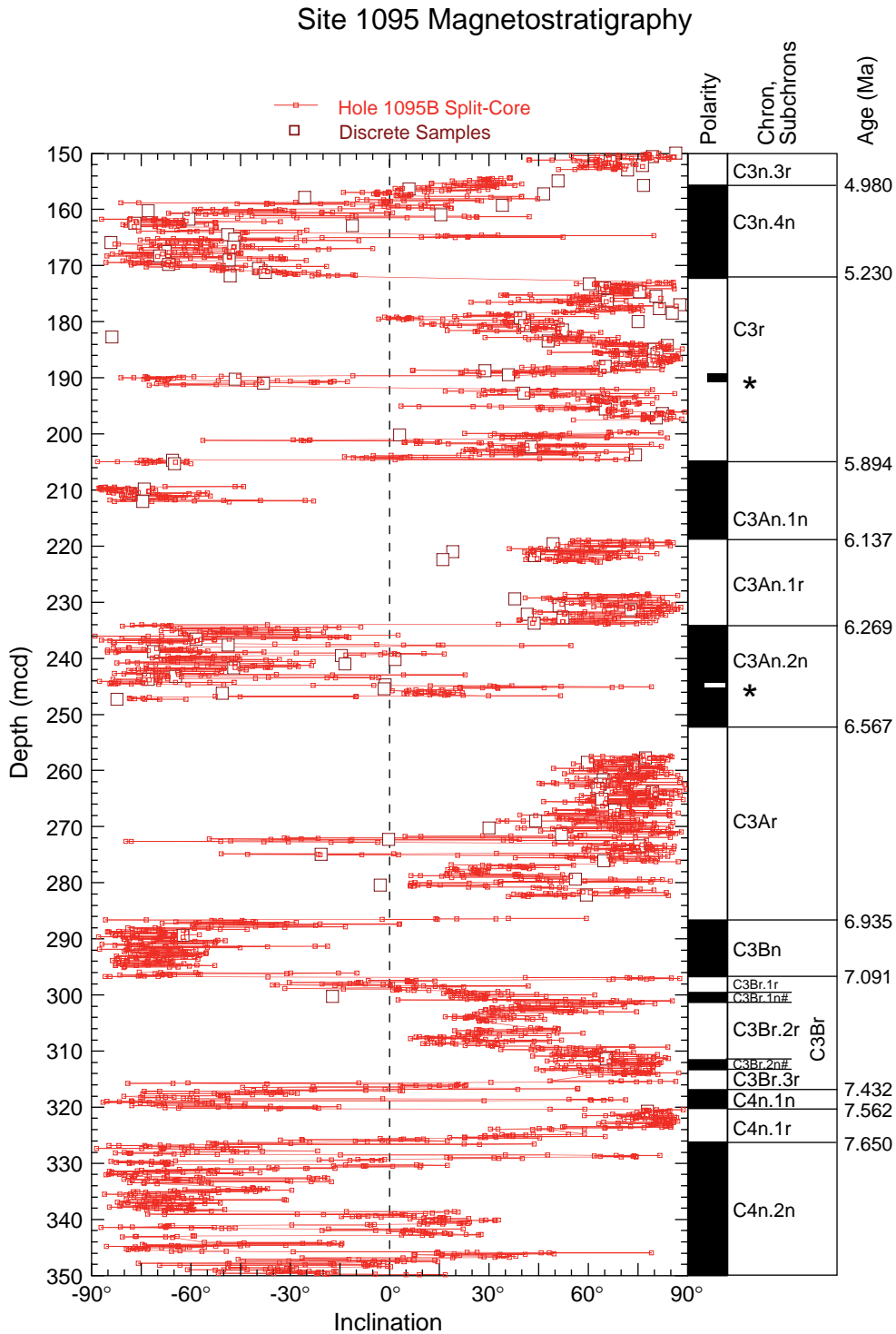
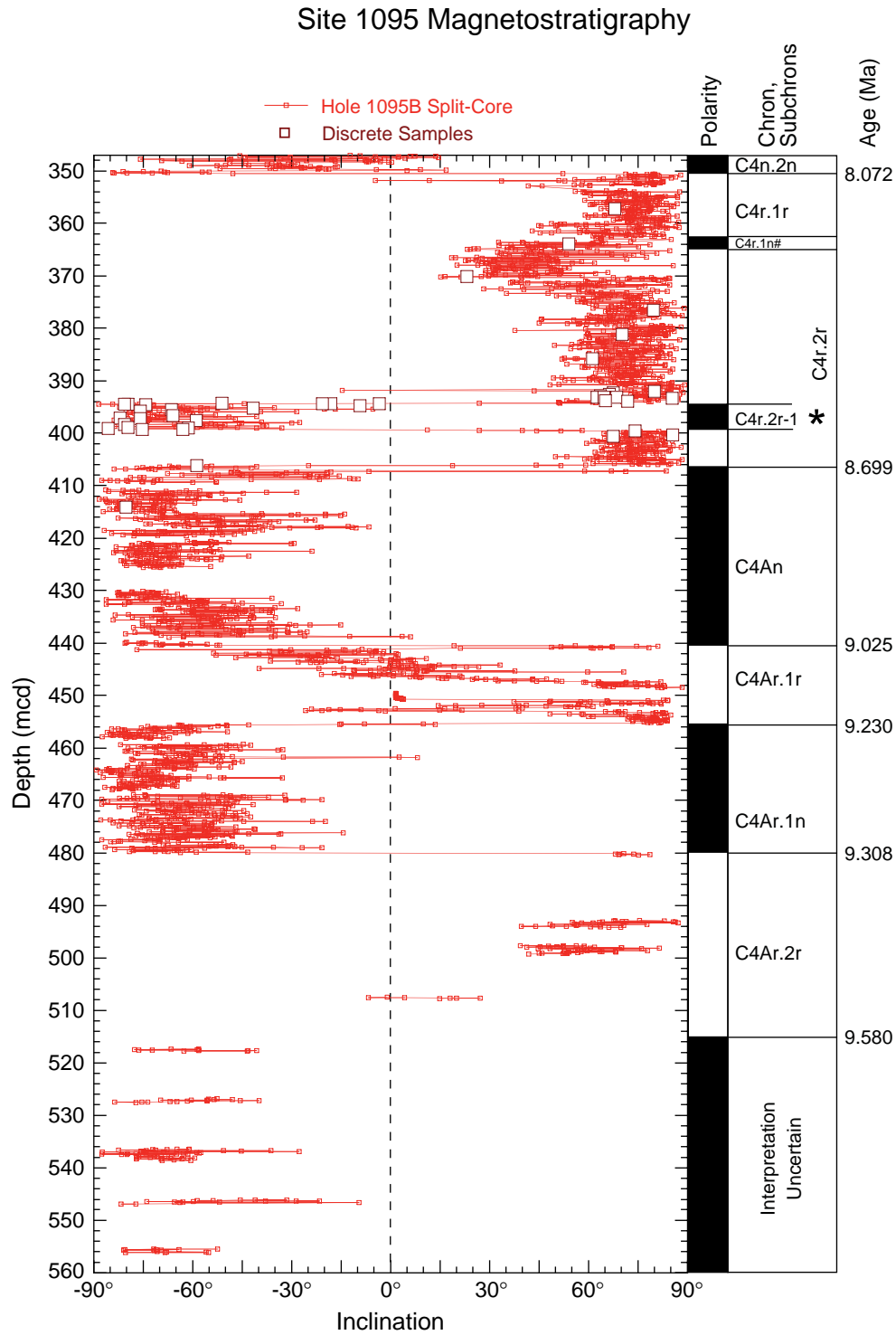


Figure F10. The magnetostratigraphy and paleomagnetic inclinations from the lower part of the sedimentary section at Site 1095. \* = excursions, cryptochrons, or anomalous polarity zones observed in the inclination data; # = chrons and subchrons not identified in the sedimentary section.



**Figure F11.** Comparison of U-channel (PCA) and split-core (20 mT) inclinations from the upper part of Hole 1095A illustrating the lack of agreement that occurs within some intervals of the core. The inset shows the details of the inclination variations in the transition zone of the Brunhes/Matuyama reversal. The reversal boundary (dashed line in the inset), as given in Table T1, p. 42, is placed in the middle of this zone.

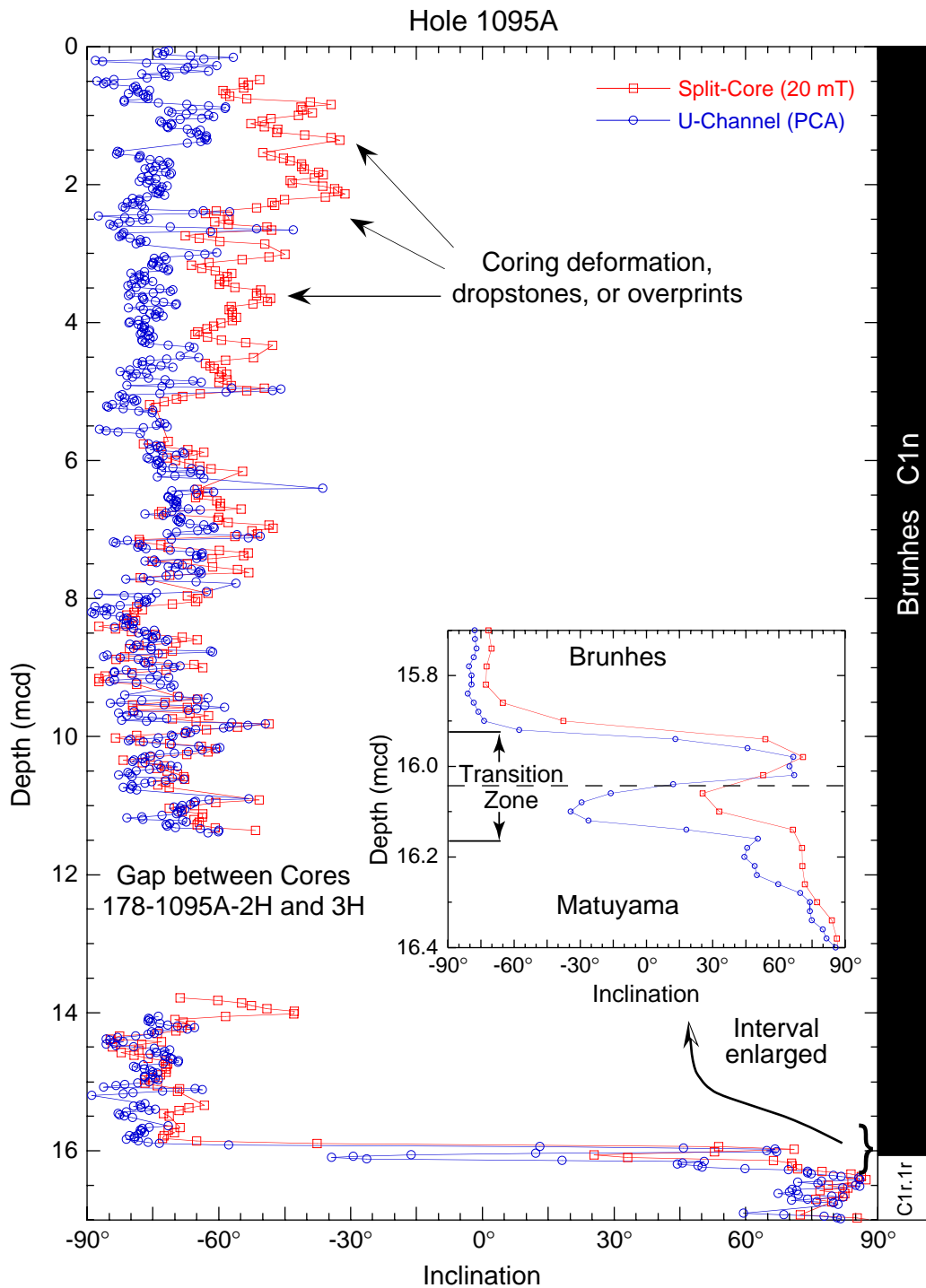


Figure F12. Comparison of U-channel (PCA) and split-core (20 mT) inclinations from the upper part of Hole 1095D illustrating the lack of agreement that occurs within some intervals of the core. Note that the Brunhes/Matuyama reversal occurs in a coring gap in Hole 1095D.

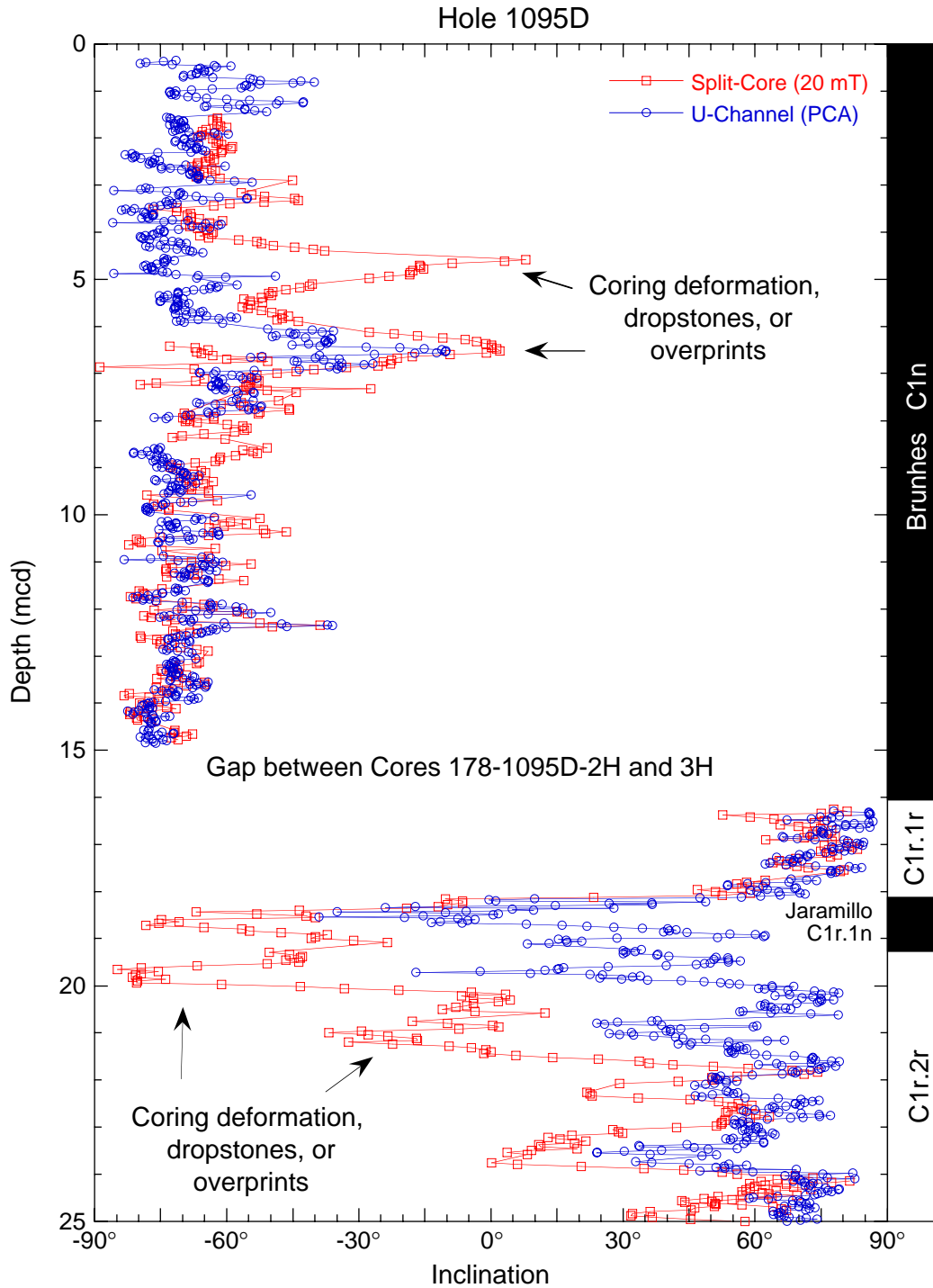
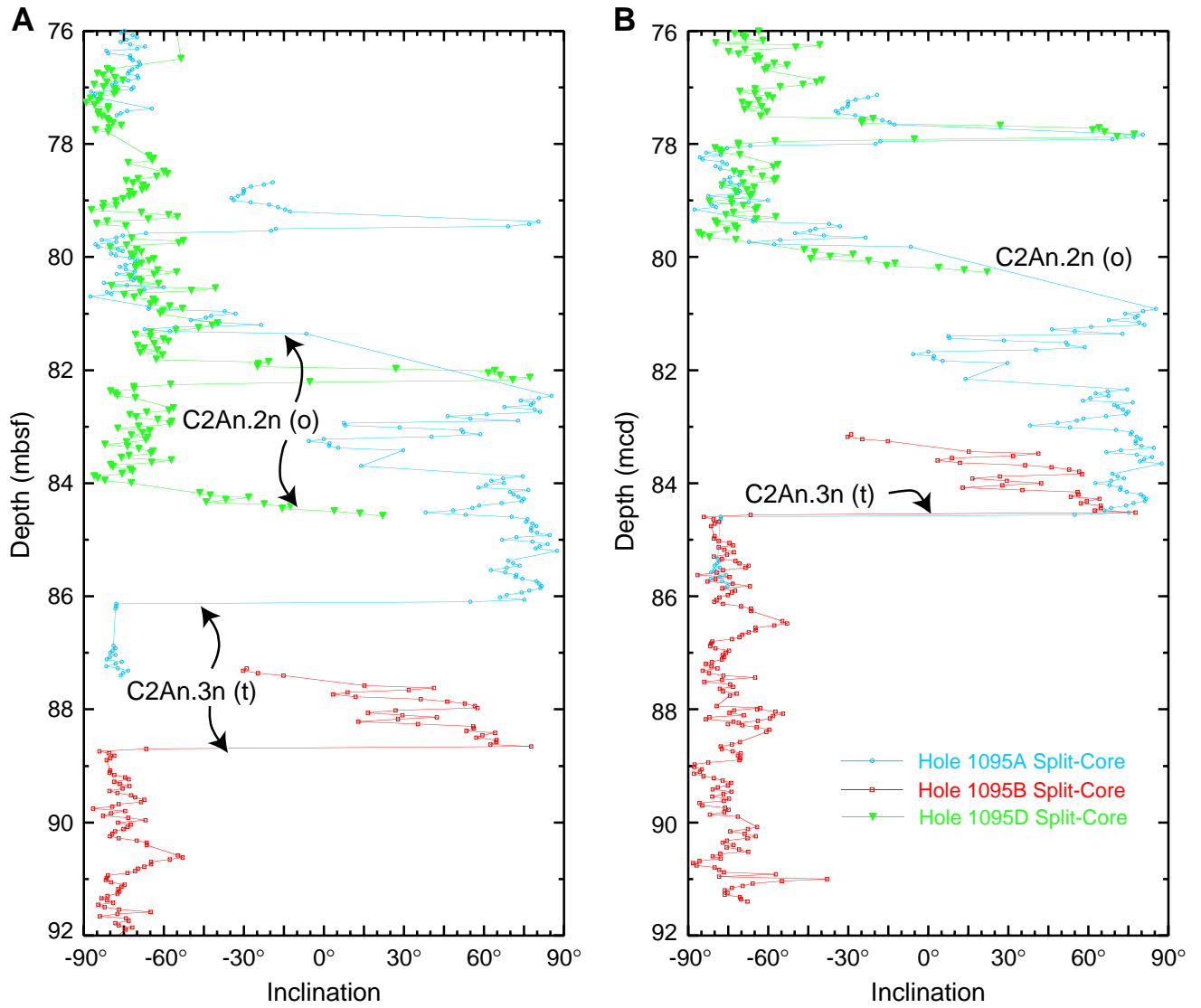


Figure F13. Split-core (20 mT) inclinations from Holes 1095A, 1095B, and 1095D plotted in the (A) mbsf and (B) mcd depth scales. Coeval reversal boundaries and other variations in the inclinations are artificially offset by inaccuracies in the mbsf depth scale, which are overcome by use of the mcd scale. For the reversal boundaries, o = onset and t = termination.



**Figure F14. A, B.** Susceptibility data from whole-core measurements (black) and from the second run of the GHMT logging tool (red). The core susceptibility data are plotted in the mbsf depth scale, which is estimated from the length of the drill pipe, and the logging susceptibility data are in the meters logging depth (mld), which is estimated from the length of the logging wireline. Both the core and logging data are plotted on the mcd depth scale using the offsets giving in Table T16, p. 61. This results in a notable improvement in the correlation of distinctive anomalies, such as those in the vicinity of the red and black dot. The logging susceptibility data have been divided by nine to scale them to the core susceptibility data. Core susceptibility is given in raw meter units, which can be converted to SI volume units when the raw values are multiplied by  $\sim 0.7 \times 10^{-5}$ . Both susceptibility data sets have been smoothed. The peak values for the logging data never exceed  $\sim 500$  in the plot, owing to the dynamic range of the logging tool.

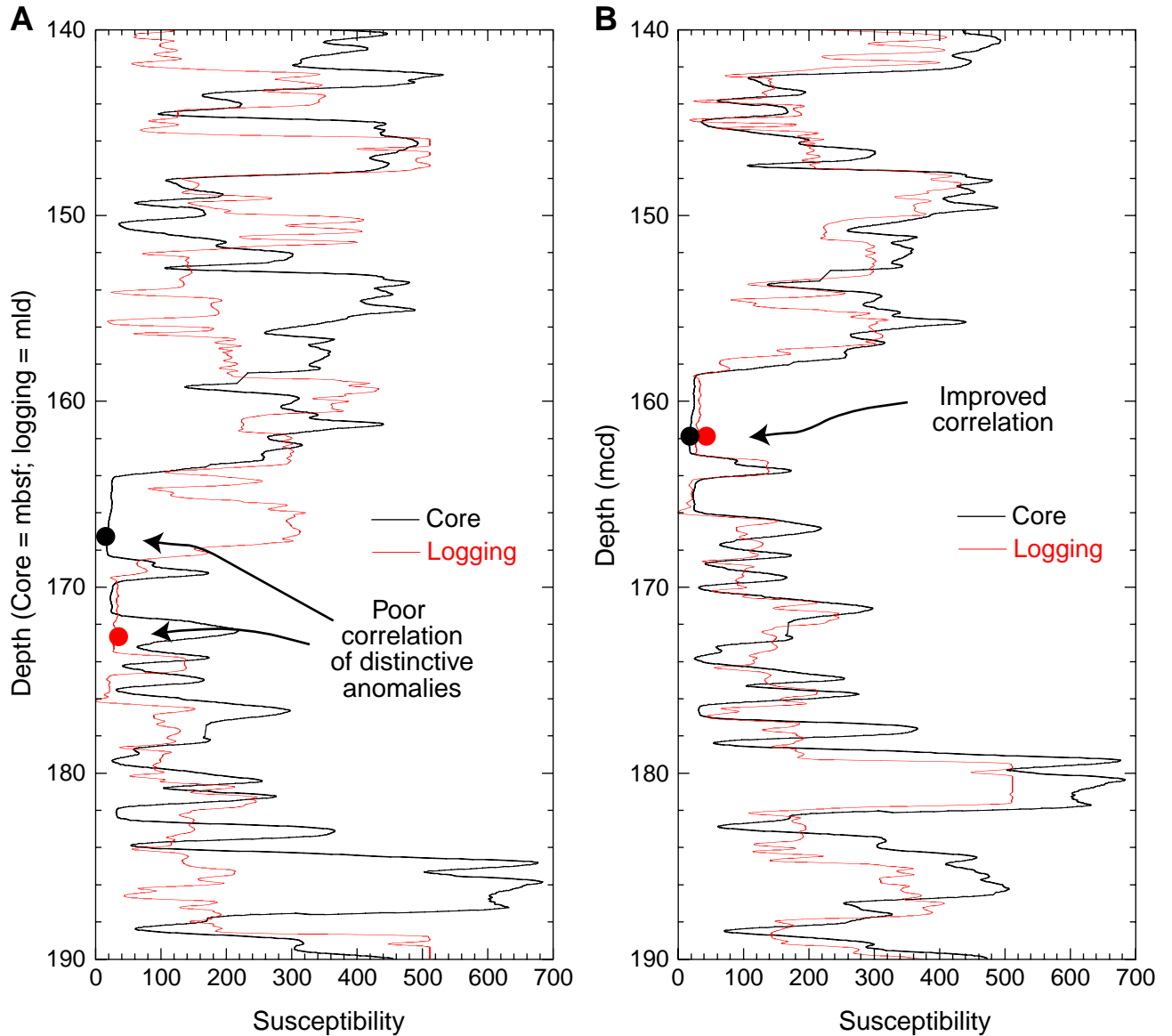
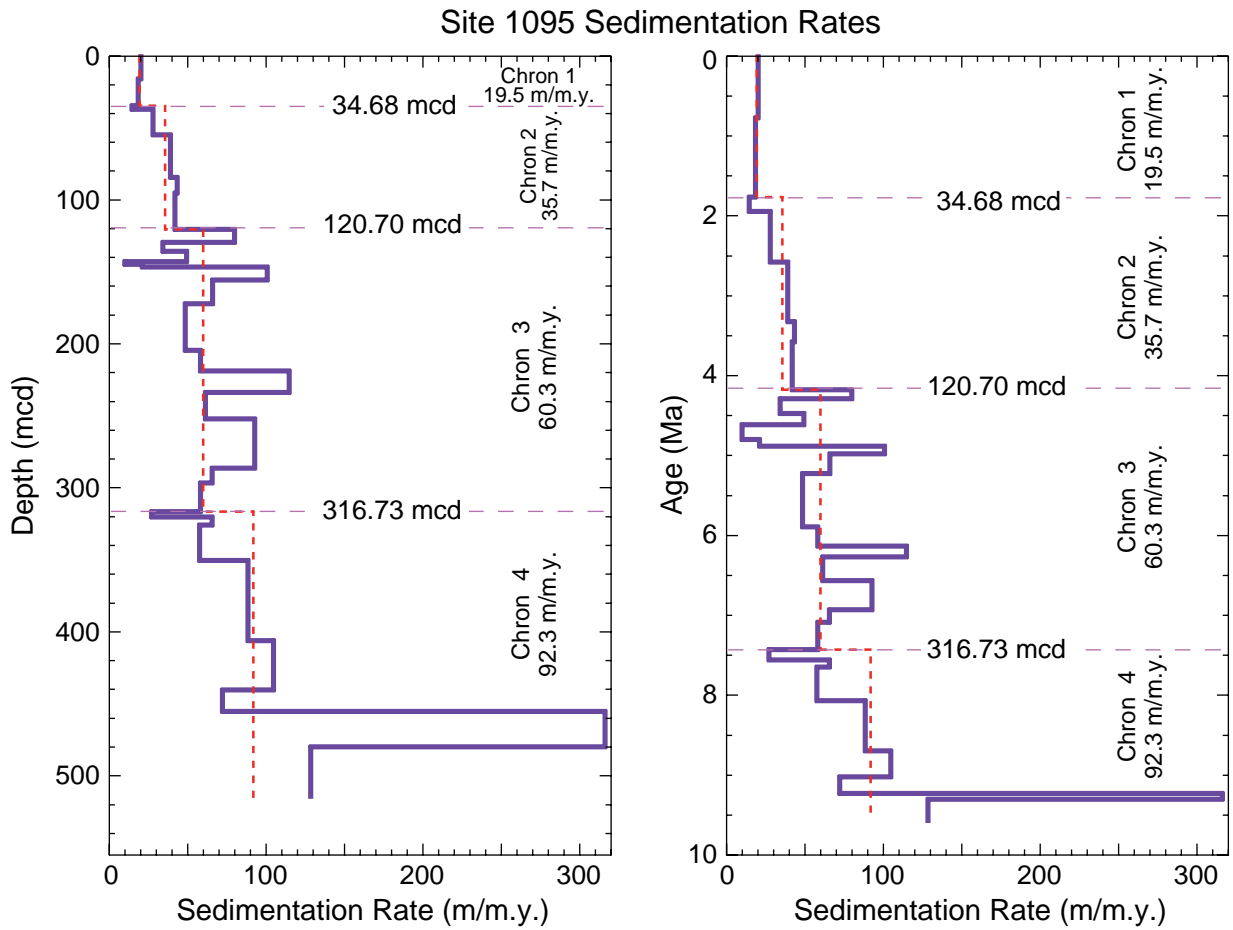


Figure F15. Sedimentation rates for Site 1095 plotted vs. depth and vs. the magnetostratigraphically-constrained age.



**Figure F16.** The magnetostratigraphy of Site 1096 is shown with the paleomagnetic inclination data from split-core sections (after demagnetization at 20 mT), U-channel samples (PCA), and discrete samples (PCA). The interpreted magnetostratigraphy is also compared with the polarity zonation predicted from the geomagnetic polarity timescale (GPTS) for the case where the sedimentation rate was constant over long periods of time and for the case where the sediment ages are constrained by diatom, radiolarian, and calcareous nannofossil events of Iwai et al. (**Chap. 36**, this volume). Sed. Rate = sedimentation rate. \* = excursions, cryptochrons, or anomalous polarity zones observed in the inclination data; # = chrons and subchrons not identified in the sedimentary section.

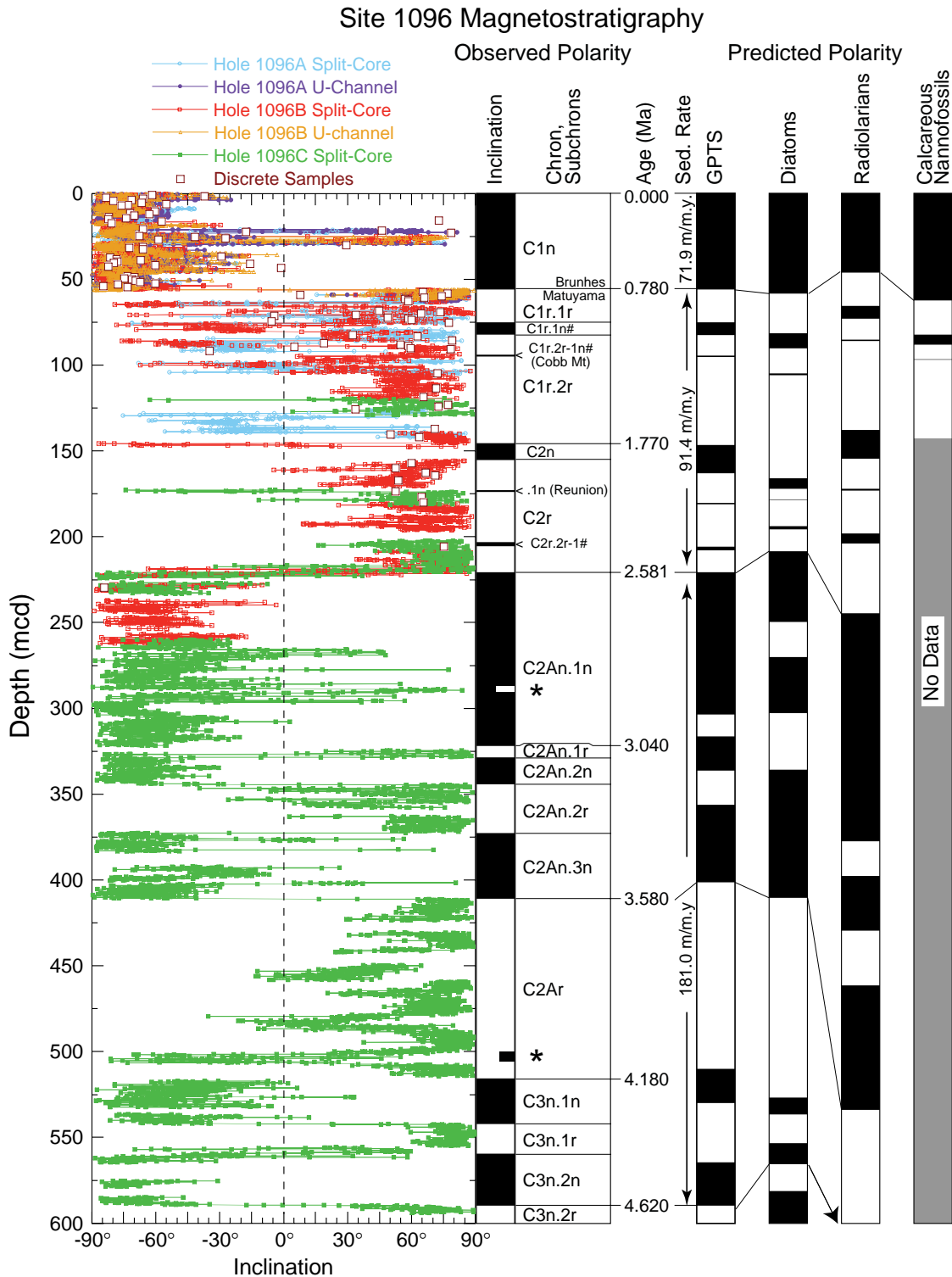


Figure F17. Comparison of U-channel (PCA), split-core (20 mT), and discrete (PCA) inclinations from the upper part of Site 1096.

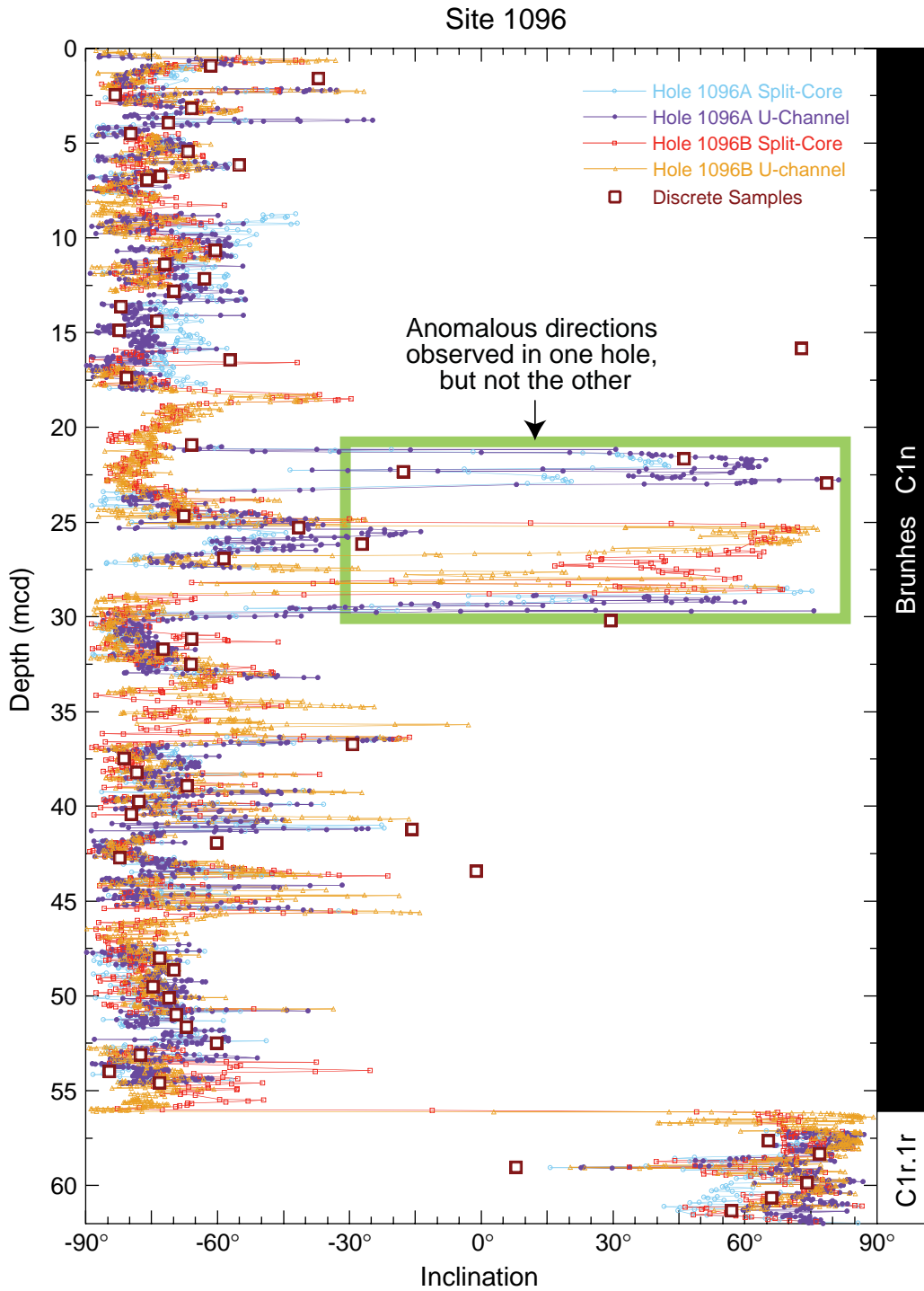


Figure F18. Sedimentation rates for Site 1096 plotted vs. depth and vs. the magnetostratigraphically constrained age.

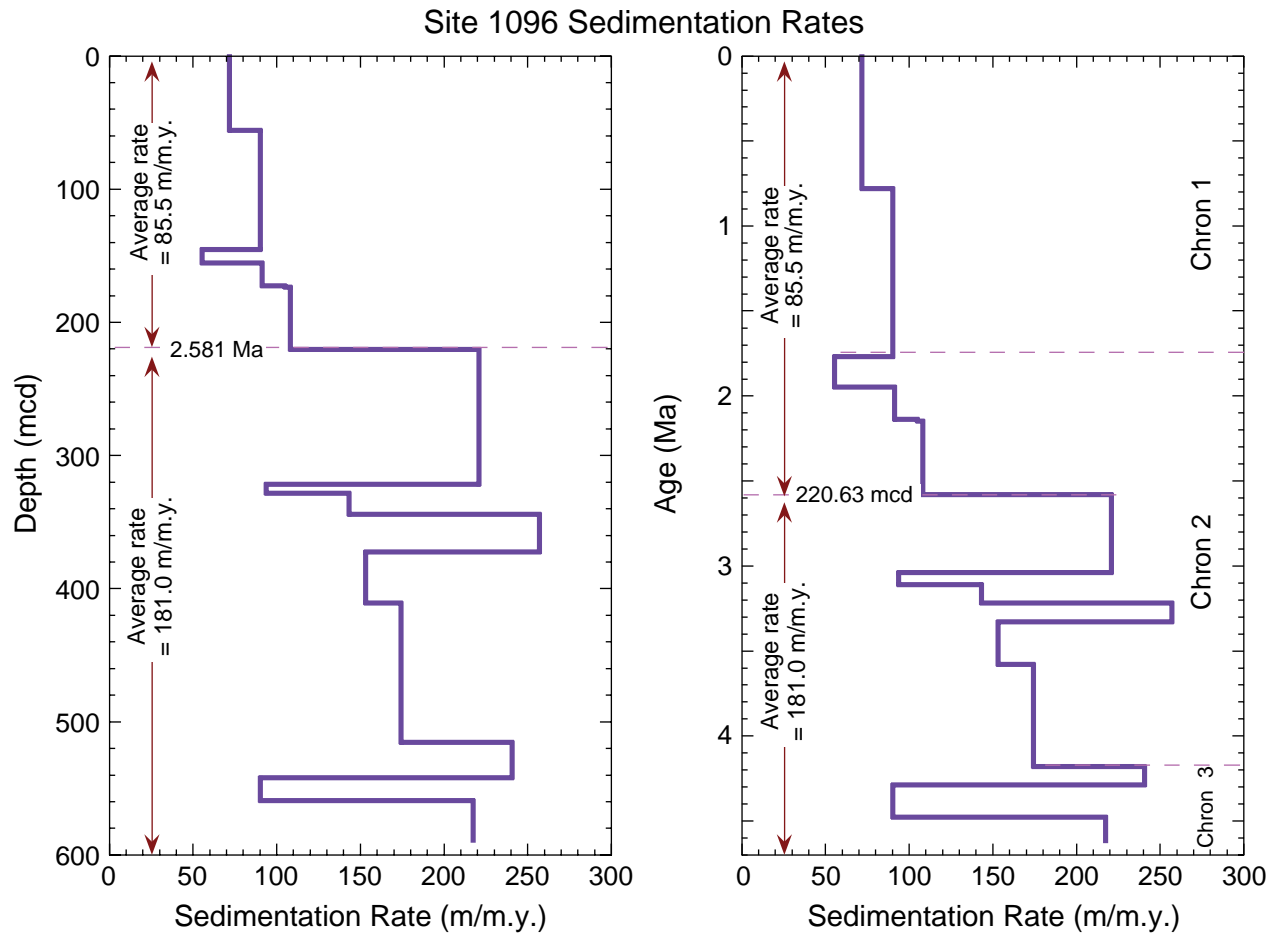


Figure F19. The magnetostratigraphy of Site 1101 is shown with the paleomagnetic inclination data from split-core sections (after demagnetization at 30 mT), U-channel samples (PCA), and discrete samples (PCA). Our interpreted magnetostratigraphy is compared with the polarity zonation predicted from the geomagnetic polarity timescale (GPTS) for the case where the sedimentation rate was constant and for the case where the sediment ages are constrained by diatom, radiolarian, and calcareous nannofossil events of Iwai et al. (Chap. 36, this volume). # = chrons and subchrons not identified in the sedimentary section.

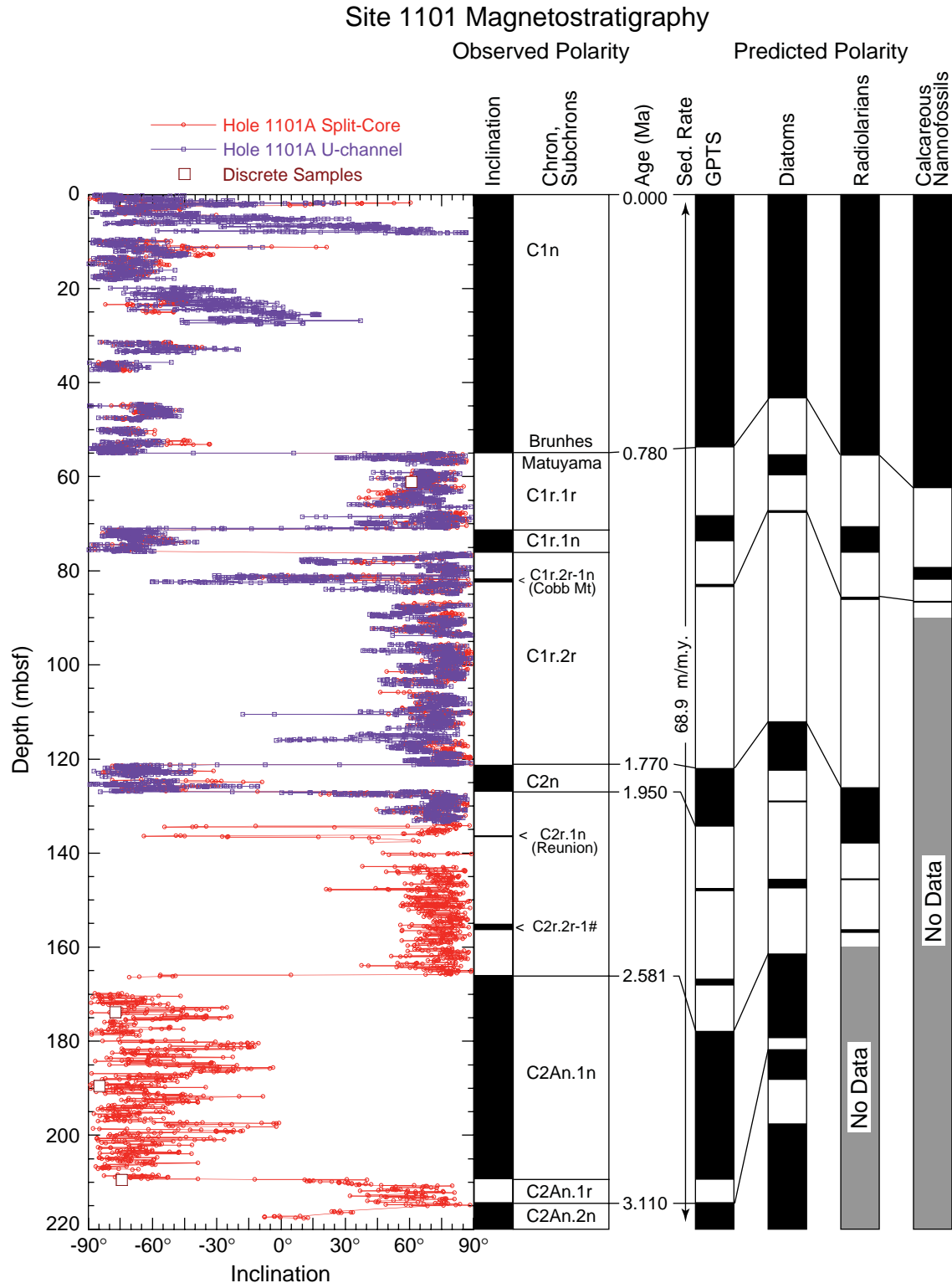
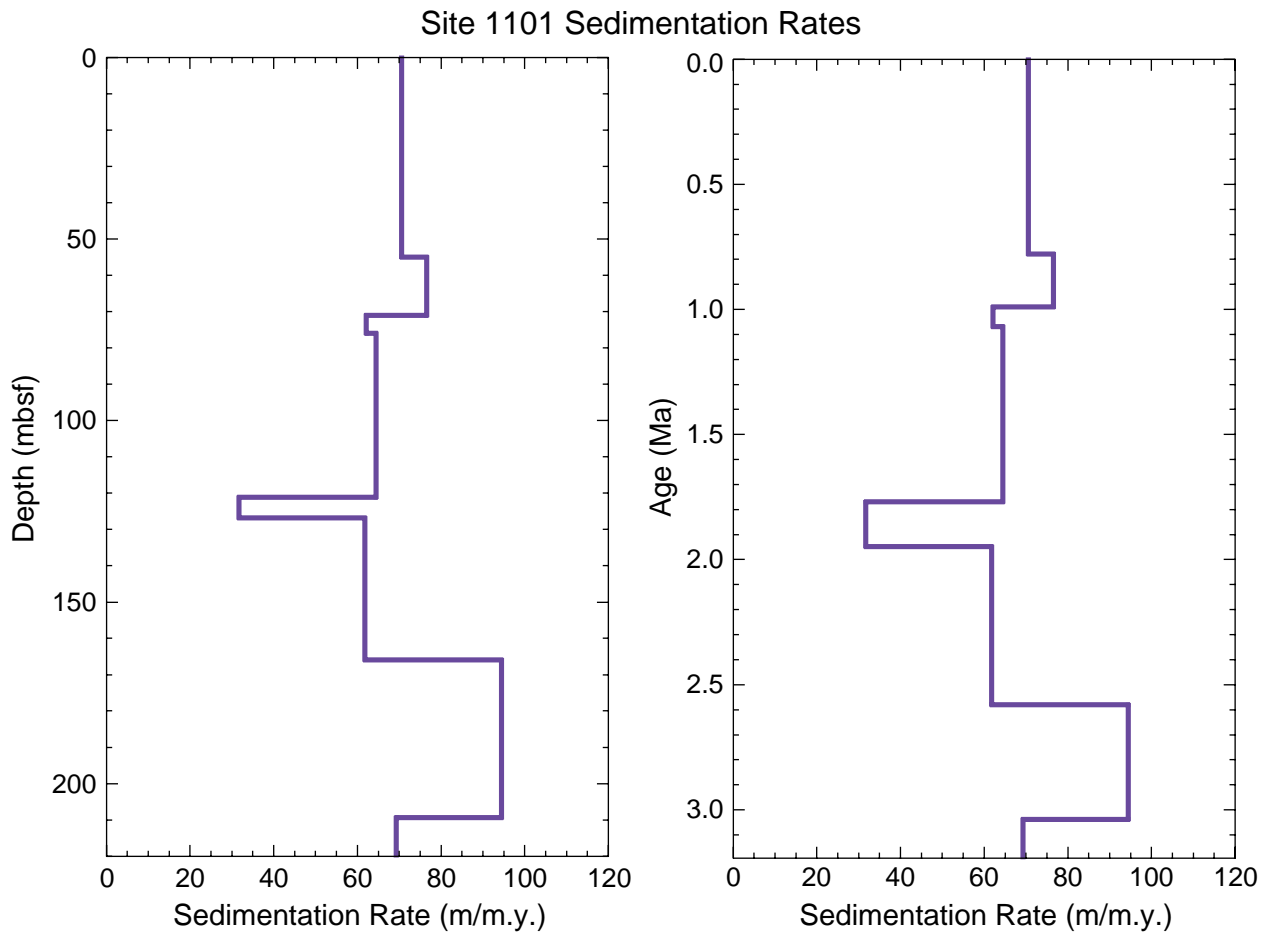


Figure F20. Sedimentation rates for Site 1101 plotted vs. depth and vs. the magnetostratigraphically constrained age.



**Table T1.** Magnetostratigraphy, Site 1095. (See table notes. Continued on next three pages.)

Polarity chron/ subchron	Reversal type	Age (Ma)	Range (mbsf)	Best estimate (mbsf)	Best estimate core, section, interval (cm)	Measurement type	Range (mbsf)	Best estimate (mbsf)	Best estimate core, section, interval (cm)	Measurement type
0	N	0.000	0.00-0.00		178- Mudline				178-	
C1n (o)	R→N	0.780	17.12-17.36	17.24	1095A-3H-6, 46	U-channel				
C1r.1n (t)	N→R	0.990	19.23-19.27	19.25	1095A-3H-8, 26	U-channel				
C1r.1n (o)	R→N	1.070	19.59-19.65	19.62	1095A-3H-8, 63	U-channel				
C1r.2r-1n (t)	N→R	1.201			Not identified					
C1r.2r-1n (t)	R→N	1.211			Not identified					
C2n (t)	N→R	1.770	38.12-38.16	38.14	1095A-5H-6, 34	Split-core				
C2n (o)	R→N	1.950	41.20-41.38	41.29	1095A-6H-1, 149	Split-core				
C2r.1n (t)	N→R	2.140			Not identified					
C2r.1n (o)	R→N	2.150			Not identified					
C2r.2r-1 (t)	Excursion	2.420			Not identified					
C2r.2r-1 (o)	Excursion	2.441			Not identified					
C2An.1n (t)	N→R	2.581	58.82-61.96		Between 1095A-7H and 8H	Split-core				
C2An.1n (o)	R→N	3.040	79.20-79.38	79.29	Between 1095A-10H-1 and 10H-2	Split-core				
C2An.2n (t)	N→R	3.110	79.46-79.58	79.52	1095A-10H-2, 22	Split-core				
C2An.2n (o)	R→N	3.220	81.36-82.46	81.91	Between 1095A-10H-3, 56, and 10H-4, 16	Split-core				
C2An.3n (t)	N→R	3.330	86.10-86.14	86.12	1095A-10H-6, 82	Split-core	88.66-88.70	88.68	1095B-1H-4, 118	Split-core
C2An.3n (o)	R→N	3.580					96.90-105.08	100.99	Between 1095B-2H-3, 140, and 3H-3, 8	Split-core
C3n.1 n (t)	N→R	4.180					126.18-126.22	126.20	1095B-5H-4, 70	U-channel
C3n.1n (o)	R→N	4.290					134.94-135.06	135.00	Between 1095B-6H-3, 144, and 6H-4, 6	U-channel
C3n.1n-1 (t)	N→R	?					136.08-136.56	136.32	1095B-6H-4, 132	U-channel
C3n.1n-1 (o)	R→N	?					136.80-136.84	136.82	1095B-6H-5, 32	U-channel
C3n.2n (t)	N→R	4.480					139.60-142.43	141.02	Between 1095B-6H and 7H	Split-core
C3n.2n (o)	R→N	4.620					148.43-148.51	148.47	1095B-7H-6, 100	Split-core
C3n.3n (t)	N→R	4.800					149.53-151.08	150.31	Between 1095B-7H and 8H	Split-core
C3n.3n (o)	R→N	4.890					152.20-152.24	152.22	1095B-8H-2, 122	Split-core
C3n.4n (t)	N→R	4.980					158.40-164.22	161.31	1095B-9H-2, 81	Split-core
C3n.4n (o)	R→N	5.230					177.32-178.40	177.86	Between 1095B-10H and 11H	Split-core
C3r-1 (t)	N→R	?					195.20-195.12	195.16	1095B-12H-6, 16	Split-core
C3r-1 (o)	R→N	?					196.82-197.50	197.16	Between 1095B-12H and 13H	Split-core
C3An.1n (t)	N→R	5.894					210.09-210.17	210.13	1095B-14X-4, 68	Split-core
C3An.1n (o)	R→N	6.137					217.60-224.38	224.30	Between 1095B-15X and 16X	Split-core
C3An.2n (t)	N→R	6.269					239.44-239.48	239.46	1095B-17X-4, 106	Split-core
C3An.2n (o)	R→N	6.567					252.82-262.78	257.80	Between 1095B-18X and 20X	Split-core
C3Bn (t)	N→R	6.935					292.02-292.06	292.04	1095B-23X-1, 34	Split-core
C3Bn (o)	R→N	7.091					302.30-302.34	302.32	1095B-24X-1, 102	Split-core
C3Br.1n (t)	N→R	7.135							Not identified	
C3Br.1n (o)	R→N	7.170							Not identified	
C3Br.2n (t)	N→R	7.341							Not identified	
C3Br.2n (o)	R→N	7.375							Not identified	
C4n.1n (t)	N→R	7.432					321.84-322.62	322.23	1095B-26X-2, 13	Split-core
C4n.1n (o)	R→N	7.562					325.78-325.82	325.80	1095B-26X-4, 70	Split-core
C4n.2n (t)	N→R	7.650					331.04-332.18	331.61	1095B-27X-1, 141	Split-core
C4n.2n (o)	R→N	8.072					356.02-356.06	356.04	1095B-29X-5, 54	Split-core
C4r.1n (t)	N→R	8.225								Split-core
C4r.1n (o)	R→N	8.257								Split-core
C4r.2r-1 (t)	N→R	8.635					399.84-399.88	399.86	1095B-34X-2, 106	Split-core

Table T1 (continued).

Polarity chron/ subchron	Reversal type	Age (Ma)	Range (mbsf)	Best estimate (mbsf)	Best estimate core, section, interval (cm)	Measurement type	Range (mcd)	Best estimate (mcd)	Sedimentation rate (m/m.y)	Comment
0	N	0.000	0.00-0.00	0	178- Mudline		0.00-0.00	0.00		(1)
C1n (o)	R→N	0.780	17.96-18.22	18.09	Between 1095D-2H and 3H	U-channel	15.92-16.16	16.04	20.56	Hole 1095A preferred*
C1r.1n (t)	N→R	0.990	20.08-20.10	20.09	1095D-3H-2, 49	U-channel	18.05-18.27	18.16	10.10	Hole 1095A preferred†
C1r.1n (o)	R→N	1.070	20.60-21.92	21.26	1095D-3H-3, 16	U-channel	18.42-20.00	19.21	13.13	Hole 1095D preferred†
C1r.2r-1n (t)	N→R	1.201			Not identified					Not identified
C1r.2r-1n (t)	R→N	1.211			Not identified					Not identified
C2n (t)	N→R	1.770	40.00-40.18	40.09	1095D-5H-2, 149	Split-core	34.66-34.70	34.68	18.83	(2) Hole 1095A preferred
C2n (o)	R→N	1.950	41.72-42.56	42.14	1095D-5H-4, 54	Split-core	37.24-37.42	37.33	14.72	(2) Hole 1095D preferred
C2r.1n (t)	N→R	2.140	45.12-46.68	46.60	Between 1095D-5H and 6H	Split-core	39.88-41.92	41.84	23.74	(3)†
C2r.1n (o)	R→N	2.150	47.08-47.16	47.12	1095D-6H-1, 52	Split-core	42.32-42.40	42.36	52.00	(3)†
C2r.2r-1 (t)	Excursion	2.420			Not identified					Not identified
C2r.2r-1 (o)	Excursion	2.441			Not identified					Not identified
C2An.1n (t)	N→R	2.581	58.84-58.92	58.88	1095D-7H-2, 128	Split-core	55.04-55.12	55.08	28.13	(4) Hole 1095D preferred*
C2An.1n (o)	R→N	3.040	81.94-81.98	81.96	1095D-9H-5, 86	Split-core	77.64-77.68	77.66	49.19	(5)†
C2An.2n (t)	N→R	3.110	82.18-82.26	82.22	1095D-9H-5, 112	Split-core	77.92-77.98	77.95	4.14	(5, 6)†
C2An.2n (o)	R→N	3.220	84.46-84.50	84.48	1095D-9H-7, 38	Split-core	80.16-80.20	80.18	20.27	(7) Hole 1095D preferred†
C2An.3n (t)	N→R	3.330					84.52-84.60	84.56	39.36	(8)
C2An.3n (o)	R→N	3.580					91.40-99.58	95.49	43.72	(9)‡
C3n.1 n (t)	N→R	4.180					120.68-120.72	120.70	42.02	‡
C3n.1n (o)	R→N	4.290					129.44-129.56	129.50	80.00	*
C3n.1n-1 (t)	N→R	?					130.58-131.60	131.09		(10)
C3n.1n-1 (o)	R→N	?					131.30-131.34	131.32		(10)
C3n.2n (t)	N→R	4.480					135.10-136.93	136.02	34.29	‡
C3n.2n (o)	R→N	4.620					142.93-143.01	142.97	49.68	*
C3n.3n (t)	N→R	4.800					144.03-145.58	144.81	10.19	(11)
C3n.3n (o)	R→N	4.890					146.70-146.74	146.72	21.28	(11)
C3n.4n (t)	N→R	4.980					152.90-158.72	155.81	101.00	(12)*
C3n.4n (o)	R→N	5.230					171.82-172.90	172.36	66.20	‡
C3r-1 (t)	N→R	?					189.62-189.70	189.66		(13)
C3r-1 (o)	R→N	?					191.32-192.00	191.66		(13)
C3An.1n (t)	N→R	5.894					204.59-204.67	204.63	48.60	*
C3An.1n (o)	R→N	6.137					212.10-218.88	218.80	58.31	(14)‡
C3An.2n (t)	N→R	6.269					233.94-233.98	233.96	114.85	‡
C3An.2n (o)	R→N	6.567					247.32-257.28	252.30	61.54	‡
C3Bn (t)	N→R	6.935					286.52-286.56	286.54	93.04	‡
C3Bn (o)	R→N	7.091					296.80-296.84	296.82	65.90	*
C3Br.1n (t)	N→R	7.135								Not identified
C3Br.1n (o)	R→N	7.170								Not identified
C3Br.2n (t)	N→R	7.341								Not identified
C3Br.2n (o)	R→N	7.375								Not identified
C4n.1n (t)	N→R	7.432					316.34-317.12	316.73	58.39	‡
C4n.1n (o)	R→N	7.562					320.28-320.32	320.30	27.46	‡
C4n.2n (t)	N→R	7.650					325.54-326.68	326.11	66.02	‡
C4n.2n (o)	R→N	8.072					350.52-350.56	350.54	57.89	‡
C4r.1n (t)	N→R	8.225								(15)
C4r.1n (o)	R→N	8.257								(15)
C4r.2r-1 (t)	N→R	8.635					394.34-394.38	394.36		(16)‡

**Table T1 (continued).**

Polarity chron/ subchron	Reversal type	Age (Ma)	Range (mbsf)	Best estimate (mbsf)	Best estimate core, section, interval (cm)	Measurement type	Range (mbsf)	Best estimate (mbsf)	Best estimate hole, core, section, interval (cm)	Measurement type
C4r.2r-1 (o)	R→N	8.651					404.81-404.88	404.85	1095B-34X-6, 5	Discrete/Split-core
C4An (t)	N→R	8.699					411.70-411.74	411.72	1095B-35X-4, 62	Split-core
C4An (o)	R→N	9.025					445.98-446.02	446.00	1095B-39X-1, 90	Split-core
C4Ar.1n (t)	N→R	9.230					460.70-461.04	460.87	1095B-40X-5, 7	Split-core
C4Ar.1n (o)	R→N	9.308					485.40-485.65	485.53	Between 1095B-43X-2 and 43X-CC	Split-core
C4Ar.2n (t)	N→R	9.580					504.74-522.88	520.50	Between 1095B-46X-2 and 48X-1	Split-core

Notes: Ages for chrons are from Cande and Kent (1995). (o) = onset, (t) = termination of a polarity chron. N→R = a reversal where the polarity of the field changed from normal to reversed, R→N = a reversal where the polarity of the field changed from reversed to normal. \* = the reversal boundary is the same as identified by Shipboard Scientific Party (1999a), but the location of the boundary has been adjusted slightly. † = identification of chron and reversal boundaries is speculative; therefore, these reversal boundaries are not used in the sedimentation rate plots. ‡ = the reversal boundary is identical to that given by Shipboard Scientific Party (1999a). Comments: (1) = depth to mudline in mbsf agrees to within 2 cm for the first core from Holes 1095A, 1095B, and 1095C. (2) = our interpretation places Chron C2n ~20 m higher in the section than that by Shipboard Scientific Party (1999a). (3) = the polarity subzone interpreted to represent Subchron C2r.1n is speculative. Rather than a geomagnetic origin, the subzone could be caused by coring disturbance at the top of Core 178-1095D-6H. We place the C2r.1n (t) reversal at the very top of Core 178-1095D-6H. This subchron was thought to be lost in a hiatus based on the interpretation of Shipboard Scientific Party (1999a). (4) = this reversal was interpreted to represent C2n (t) by Shipboard Scientific Party (1999a) and was thought to occur above a hiatus that removed reversals C2n (o) to C2An.1n (t). (5) = placing Subchron C2An.1n (o) at this locality produces a subchron (C2An.1r) that is short, with resulting sedimentation rates exceptionally slow relative to sedimentation rates above and below. (6) = average mcd depth taken from the best estimates from Holes 1095A and 1095D, which are 77.98 and 77.92 mcd. (7) = this reversal could be C2An.1n (o) instead of C2An.2n (o), in which case no Subchron C2An.2n appears to be recorded. (8) = average mcd depth taken from the best estimates for Holes 1095A and 1095B, which are 84.58 and 85.54 mcd. (9) = the reversal occurs within an interval that has some drilling disturbance. The best estimate for the location agrees with noisy discrete data. (10) = this is possibly a newly identified cryptochron, which we refer to as C3n.1r-1. (11) = Subchron C3n.3n was not previously identified by Shipboard Scientific Party (1999a). (12) = this poorly constrained reversal, C3n.4n (t), occurs somewhere within a broad zone of shallow inclinations. (13) = this is possibly a newly identified cryptochron, which we refer to as C3r-1. (14) = Subchron 3An.1n (o) is placed in the lower part of the coring gap (top of Core 178-1095B-16X) rather than the middle. (15) = reversals C4r.1n (t) and C4r.1n (o) possibly occur in a zone of shallow inclinations near 364 and 369 mcd, respectively. (16) = the transition zone for Subchron C4r.2r-1 (t) is from 393.94 to 394.48 mcd in discrete samples. This is a zone that is weakly magnetized. (17) = the transition zone for C4r.2r-1 (o) can only be limited to between Sections 178-1095B-34X-5 and 34X-6 in split-core data. (18) = the reversal C4Ar.2n (t) is arbitrarily placed near the top of Core 178-1095B-48X to better agree with logging estimate.

Table T1 (continued).

Polarity chron/ subchron	Reversal type	Age (Ma)	Range (mbsf)	Best estimate (mbsf)	Best estimate hole, core, section, interval (cm)	Measurement type	Range (mcd)	Best estimate (mcd)	Sedimentation rate (m/m.y)	Comment
C4r.2r-1 (o)	R→N	8.651					399.31-399.38	399.35		(17)*
C4An (t)	N→R	8.699					406.20-406.24	406.22	88.80	‡
C4An (o)	R→N	9.025					440.48-440.52	440.50	105.15	‡
C4Ar.1n (t)	N→R	9.230					455.20-455.54	455.37	72.54	‡
C4Ar.1n (o)	R→N	9.308					479.90-480.15	480.03	316.09	
C4Ar.2n (t)	N→R	9.580					499.24-517.38	515.00	128.58	(18)

**Table T2.** Magnetostratigraphy, Site 1096. (Continued on next page.)

Polarity chron/ subchron	Reversal type	Age (Ma)	Range (mbsf)	Best estimate (mbsf)	Best estimate (interval)	Measurement type	Range (mbsf)	Best Estimate (mbsf)	Best estimate core, section, interval (cm)	Measurement type
0	N	0.000			178-		0.00-0.00	0.00	178- Mudline	
C1n (o)	R→N	0.780	54.65-55.40	55.03	Between Cores 1096A-6H and 7H	U-channel	54.98-55.00	54.99	1096B-7H-3, 75	U-channel
C1r.1n (t)	N→R	0.990			Not identified				Not identified	
C1r.1n (o)	R→N	1.070			Not identified				Not identified	
C1r.2r-1n (t)	N→R	1.201			Not identified				Not identified	
C1r.2r-1n (t)	R→N	1.211			Not identified				Not identified	
C2n (t)	N→R	1.770					141.10-141.40	141.25	Between 1096B-16H-4, 140, and 16H-5, 20	Split-core
C2n (o)	R→N	1.950					142.60-151.50	151.24	Between 1096B-16H and 19H	Split-core
C2r.1n (t)	N→R	2.140							Not identified	
C2r.1n (o)	R→N	2.150							Not identified	
C2An.1n (t)	N→R	2.581					215.35-215.40	215.38	1096B-27X-3, 138	Split-core
C2An.1n (o)	R→N	3.040								
C2An.2n (t)	N→R	3.110								
C2An.2n (o)	R→N	3.220								
C2An.3n (t)	N→R	3.330								
C2An.3n (o)	R→N	3.580								
C2Ar-1 (t)	Excursion	?								
C2Ar-1 (o)	Excursion	?								
C3n.1n (t)	N→R	4.180								
C3n.1n (o)	R→N	4.290								
C3n.2n (t)	N→R	4.480								
C3n.2n (o)	R→N	4.620								

Notes: Ages for chrons are from Cande and Kent (1995). (o) = onset, (t) = termination of a polarity chron. N→R = a reversal where the polarity of the field changed from normal to reversed, R→N = a reversal where the polarity of the field changed from reversed to normal. \* = the reversal boundary is the same as identified by Shipboard Scientific Party (1999b), but the location of the boundary has been adjusted slightly. † = identification of chron and reversal boundaries is speculative; therefore, these reversal boundaries are not used in the sedimentation rate plots \*\* = reversal boundary is identical to that given by Shipboard Scientific Party (1999b). ‡ = reversal boundary not previously identified. Comments: (1) = the mudline was not recovered in Holes 1096A and 1096C. (2) = Chron 2An (o) is placed in the lower part of the coring gap (top of Core 178-1096B-19H). (3) = Hole 1096C split-core results give the best estimate and agree within 10 cm with those from Hole 1096B. (4) = Subchron C2An.1n (o) is placed in the upper part of the coring gap. (5) = excursion or possibly Subchron C3n.1n (see text). (6) = preferred location of the reversal boundary is near the base of the broad transition zone.

Table T2 (continued).

Polarity chron/ subchron	Reversal type	Age (Ma)	Range (mbsf)	Best estimate (mbsf)	Best estimate core, section, interval (cm)	Measurement type	Range (mcd)	Best estimate (mcd)	Sedimentation rate (mm/yr)	Comment
178-										
0	N	0.000					0.00-0.00	0.00		(1)
C1n (o)	R→N	0.780					56.09-56.11	56.10	71.92	Hole 1096B preferred*
C1r.1n (t)	N→R	0.990								Not identified
C1r.1n (o)	R→N	1.070								Not identified
C1r.2r-1n (t)	N→R	1.201								Not identified
C1r.2r-1n (t)	R→N	1.211								Not identified
C2n (t)	N→R	1.770					145.36-145.66	145.51	90.31	‡
C2n (o)	R→N	1.950					146.86-155.76	155.50	55.50	(2)‡
C2r.1n (t)	N→R	2.140	168.20-168.25	168.23	1096C-2H-1, 123	Split-core	172.84-172.89	172.87	91.39	† ‡
C2r.1n (o)	R→N	2.150	169.25-169.30	169.28	1096C-2H-2, 78	Split-core	173.89-173.94	173.92	105.00	† ‡
C2An.1n (t)	N→R	2.581	215.80-215.85	215.83	1096C-5X-3, 63	Split-core	220.60-20.65	220.63	108.38	(3)*‡
C2An.1n (o)	R→N	3.040	316.20-318.99	316.46	Between 1096C-13X and 14X	Split-core	321.74-324.53	322.00	220.86	(4)‡
C2An.2n (t)	N→R	3.110	322.99-323.04	323.02	1096C-14X-4, 113	Split-core	328.53-328.58	328.56	93.64	‡
C2An.2n (o)	R→N	3.220	338.75-338.80	338.78	1096C-16X-1, 78	Split-core	344.29-344.34	344.32	143.27	‡
C2An.3n (t)	N→R	3.330	367.05-367.10	367.08	1096C-19X-1, 18	Split-core	372.59-372.64	372.62	257.27	*
C2An.3n (o)	R→N	3.580	405.15-405.60	405.38	Between 1096C-22X and 23X	Split-core	410.69-411.14	410.92	153.20	*
C2Ar-1 (t)	Excursion	?	495.90-495.95	495.93	1096C-32X-3, 83	Split-core	501.44-501.49	501.47		(5)‡
C2Ar-1 (o)	Excursion	?	501.18-501.23	501.21	1096C-32X-7, 23	Split-core	506.72-506.77	506.75		(5)‡
C3n.1n (t)	N→R	4.180	508.54-511.55	510.05	Between 1096C-33X and 34X	Split-core	514.08-517.09	515.59	174.45	*
C3n.1n (o)	R→N	4.290	536.45-536.60	536.53	1096C-36X-4, 133	Split-core	541.99-542.14	542.07	240.73	**
C3n.2n (t)	N→R	4.480	550.60-553.70	553.70	1096C-38X-3, 60	Split-core	556.14-559.24	559.24	90.39	(6)*
C3n.2n (o)	R→N	4.620	583.85-584.05	583.95	1096C-41X-4, 35	Split-core	589.39-589.59	589.59	216.07	**

**Table T3.** Magnetostratigraphy, Site 1101.

Polarity Subchron	Reversal type	Age (Ma)	Range (mbsf)	Best estimate (mbsf)	Best estimate core, section, interval (cm)	Measurement type	Sedimentation rate (mm/yr)	Comment
0	N	0	0.00–0.00	0.00	178- Top of 1101A-1H			(1)
C1n (o)	R→N	0.78	55.04–55.06	55.05	1101A-7H-5, 135	U-channel	70.58	*
C1r.1n (t)	N→R	0.99	70.96–71.33	71.15	1101A-9H-3, 145	U-channel	76.64	*
C1r.1n (o)	R→N	1.07	75.95–76.29	76.12	Between 1101A-9H and 10H	U-channel	62.19	*
C1r.2r-1n (t)	N→R	1.201	80.96–82.26	81.61	1101A-10H-4, 46	U-channel	41.91	†*
C1r.2r-1n (t)	R→N	1.211	82.52–82.54	82.53	1101A-10H-5, 33	U-channel	92.00	†*
C2n (t)	N→R	1.77	121.24–121.26	121.25	1101A-14H-5, 105	U-channel	64.47	*
C2n (o)	R→N	1.95	126.95–126.97	126.96	1101A-15H-3, 26	U-channel	31.72	*
C2r.1n (t)	N→R	2.14	136.10–136.30	136.20	1101A-16H-2, 150	Split-core	48.63	†*
C2r.1n (o)	R→N	2.15	136.60–136.65	136.63	1101A-16H-3, 43	Split-core	42.50	†*
C2An.1n (t)	N→R	2.581	165.95–166.00	165.98	1101A-19X-3, 138	Split-core	61.83	**
C2An.1n (o)	R→N	3.04	209.35–209.40	209.38	1101A-24X-1, 128	Split-core	94.55	*

Notes: Ages for chrons are from Cande and Kent (1995). (o) = onset, (t) = termination of a polarity chron. N→R = a reversal where the polarity of the field changed from normal to reversed, R→N = a reversal where the polarity of the field changed from reversed to normal. \* = the reversal boundary is the same as identified by Shipboard Scientific Party (1999c), but the location of the boundary has been adjusted slightly. † = identification of chron and reversal boundaries is speculative; therefore, these reversal boundaries are not used in the sedimentation rate plots. \*\* = The reversal boundary location is identical to that given by Shipboard Scientific Party (1999c). Comments: (1) = the mudline is taken as 0-Ma sediment.

Table T4. Paleomagnetic data from U-channel samples, Hole 1095A.

Core, section	Interval (cm)	Depth		Inclination (°)	Declination (°)	Intensity (A/m)	Demagnetization step (mT)
		(mbsf)	(mcd)				
178-							
1095A-1H-1	6	0.06	0.06	-75.13	314.40	8.88E-02	0
1095A-1H-1	6	0.06	0.06	-73.02	318.49	8.42E-02	20
1095A-1H-1	6	0.06	0.06	-72.95	317.84	7.85E-02	30
1095A-1H-1	6	0.06	0.06	-73.02	318.61	7.09E-02	40
1095A-1H-1	6	0.06	0.06	-73.10	317.75	6.26E-02	50
1095A-1H-1	6	0.06	0.06	-73.79	321.19	5.54E-02	60
1095A-1H-1	6	0.06	0.06	-74.06	321.50	4.24E-02	80
1095A-1H-1	8	0.08	0.08	-75.27	310.33	9.77E-02	0
1095A-1H-1	8	0.08	0.08	-73.14	312.65	9.55E-02	20
1095A-1H-1	8	0.08	0.08	-73.03	312.16	8.97E-02	30
1095A-1H-1	8	0.08	0.08	-72.96	312.49	8.16E-02	40
1095A-1H-1	8	0.08	0.08	-73.01	312.02	7.25E-02	50
1095A-1H-1	8	0.08	0.08	-73.30	313.02	6.44E-02	60
1095A-1H-1	8	0.08	0.08	-73.49	312.99	4.98E-02	80
1095A-1H-1	10	0.10	0.10	-75.25	313.29	9.76E-02	0
1095A-1H-1	10	0.10	0.10	-73.40	314.14	9.71E-02	20
1095A-1H-1	10	0.10	0.10	-73.24	313.84	9.16E-02	30
1095A-1H-1	10	0.10	0.10	-73.08	313.60	8.37E-02	40
1095A-1H-1	10	0.10	0.10	-72.87	313.63	7.48E-02	50
1095A-1H-1	10	0.10	0.10	-72.87	313.22	6.66E-02	60
1095A-1H-1	10	0.10	0.10	-72.71	312.47	5.20E-02	80
1095A-1H-1	12	0.12	0.12	-72.87	310.10	9.32E-02	0
1095A-1H-1	12	0.12	0.12	-71.94	313.18	9.33E-02	20
1095A-1H-1	12	0.12	0.12	-71.64	312.84	8.81E-02	30
1095A-1H-1	12	0.12	0.12	-71.48	312.19	8.07E-02	40
1095A-1H-1	12	0.12	0.12	-71.13	312.37	7.24E-02	50
1095A-1H-1	12	0.12	0.12	-71.10	311.53	6.46E-02	60
1095A-1H-1	12	0.12	0.12	-70.78	310.24	5.07E-02	80
1095A-1H-1	14	0.14	0.14	-64.27	300.82	8.69E-02	0
1095A-1H-1	14	0.14	0.14	-65.21	304.08	8.76E-02	20
1095A-1H-1	14	0.14	0.14	-64.80	303.81	8.29E-02	30
1095A-1H-1	14	0.14	0.14	-64.64	303.38	7.62E-02	40
1095A-1H-1	14	0.14	0.14	-64.25	303.37	6.85E-02	50
1095A-1H-1	14	0.14	0.14	-63.90	302.59	6.13E-02	60
1095A-1H-1	14	0.14	0.14	-63.62	301.68	4.83E-02	80
1095A-1H-1	16	0.16	0.16	-55.23	296.20	7.26E-02	0
1095A-1H-1	16	0.16	0.16	-55.09	297.93	7.63E-02	20
1095A-1H-1	16	0.16	0.16	-54.81	297.82	7.26E-02	30
1095A-1H-1	16	0.16	0.16	-54.57	297.54	6.68E-02	40
1095A-1H-1	16	0.16	0.16	-54.40	297.60	6.04E-02	50
1095A-1H-1	16	0.16	0.16	-54.10	297.27	5.41E-02	60
1095A-1H-1	16	0.16	0.16	-53.42	296.62	4.29E-02	80
1095A-1H-1	18	0.18	0.18	-69.05	292.41	4.86E-02	0
1095A-1H-1	18	0.18	0.18	-62.10	294.75	5.17E-02	20
1095A-1H-1	18	0.18	0.18	-61.88	294.76	4.91E-02	30
1095A-1H-1	18	0.18	0.18	-61.58	294.60	4.55E-02	40
1095A-1H-1	18	0.18	0.18	-61.49	294.69	4.11E-02	50
1095A-1H-1	18	0.18	0.18	-61.54	294.52	3.67E-02	60
1095A-1H-1	18	0.18	0.18	-60.64	293.93	2.91E-02	80
1095A-1H-1	20	0.20	0.20	-87.74	181.47	5.53E-02	0
1095A-1H-1	20	0.20	0.20	-87.45	257.77	5.03E-02	20
1095A-1H-1	20	0.20	0.20	-87.24	263.13	4.78E-02	30
1095A-1H-1	20	0.20	0.20	-87.09	265.81	4.42E-02	40
1095A-1H-1	20	0.20	0.20	-86.92	269.27	3.99E-02	50
1095A-1H-1	20	0.20	0.20	-86.98	271.34	3.60E-02	60
1095A-1H-1	20	0.20	0.20	-86.27	274.36	2.82E-02	80
1095A-1H-1	22	0.22	0.22	-84.59	274.25	7.71E-02	0
1095A-1H-1	22	0.22	0.22	-85.16	279.56	7.11E-02	20
1095A-1H-1	22	0.22	0.22	-84.82	282.44	6.75E-02	30
1095A-1H-1	22	0.22	0.22	-84.54	284.47	6.24E-02	40
1095A-1H-1	22	0.22	0.22	-84.35	286.88	5.65E-02	50
1095A-1H-1	22	0.22	0.22	-83.95	288.91	5.09E-02	60
1095A-1H-1	22	0.22	0.22	-83.40	290.83	4.00E-02	80
1095A-1H-1	24	0.24	0.24	-74.42	294.96	9.67E-02	0

Note: Only a portion of this table appears here. The complete table is available in [ASCII format](#).

**Table T5.** Paleomagnetic data from U-channel samples, Hole 1095B.

Core, section	Interval (cm)	Depth		Inclination (°)	Declination (°)	Intensity (A/m)	Demagnetization step (mT)
		(mbsf)	(mcd)				
178-							
1095B-5H-1	22	121.22	115.72	85.45	214.71	1.64E-01	0
1095B-5H-1	22	121.22	115.72	84.32	217.11	1.30E-01	10
1095B-5H-1	22	121.22	115.72	84.24	220.20	1.02E-01	20
1095B-5H-1	22	121.22	115.72	84.29	219.83	7.46E-02	30
1095B-5H-1	22	121.22	115.72	83.82	218.16	5.60E-02	40
1095B-5H-1	22	121.22	115.72	85.01	222.96	3.91E-02	50
1095B-5H-1	22	121.22	115.72	84.96	225.67	2.67E-02	60
1095B-5H-1	22	121.22	115.72	85.18	214.36	1.67E-02	70
1095B-5H-1	24	121.24	115.74	86.77	155.43	1.58E-01	0
1095B-5H-1	24	121.24	115.74	86.49	168.61	1.27E-01	10
1095B-5H-1	24	121.24	115.74	86.77	175.10	9.99E-02	20
1095B-5H-1	24	121.24	115.74	86.95	178.38	7.36E-02	30
1095B-5H-1	24	121.24	115.74	86.14	178.56	5.56E-02	40
1095B-5H-1	24	121.24	115.74	87.07	166.84	3.90E-02	50
1095B-5H-1	24	121.24	115.74	87.27	174.69	2.68E-02	60
1095B-5H-1	24	121.24	115.74	86.54	159.31	1.69E-02	70
1095B-5H-1	26	121.26	115.76	86.48	293.53	1.46E-01	0
1095B-5H-1	26	121.26	115.76	86.15	279.11	1.18E-01	10
1095B-5H-1	26	121.26	115.76	85.88	278.46	9.32E-02	20
1095B-5H-1	26	121.26	115.76	85.84	278.41	6.91E-02	30
1095B-5H-1	26	121.26	115.76	86.12	265.20	5.24E-02	40
1095B-5H-1	26	121.26	115.76	86.60	282.32	3.69E-02	50
1095B-5H-1	26	121.26	115.76	86.56	284.33	2.54E-02	60
1095B-5H-1	26	121.26	115.76	86.91	268.41	1.62E-02	70
1095B-5H-1	28	121.28	115.78	73.96	306.18	1.46E-01	0
1095B-5H-1	28	121.28	115.78	72.77	302.39	1.18E-01	10
1095B-5H-1	28	121.28	115.78	72.76	301.75	9.24E-02	20
1095B-5H-1	28	121.28	115.78	73.08	302.09	6.84E-02	30
1095B-5H-1	28	121.28	115.78	73.75	300.46	5.19E-02	40
1095B-5H-1	28	121.28	115.78	73.87	304.48	3.67E-02	50
1095B-5H-1	28	121.28	115.78	74.80	306.23	2.53E-02	60
1095B-5H-1	28	121.28	115.78	75.52	301.27	1.62E-02	70
1095B-5H-1	30	121.30	115.80	74.44	309.40	1.48E-01	0
1095B-5H-1	30	121.30	115.80	72.13	305.45	1.19E-01	10
1095B-5H-1	30	121.30	115.80	71.89	304.97	9.29E-02	20
1095B-5H-1	30	121.30	115.80	72.05	305.79	6.87E-02	30
1095B-5H-1	30	121.30	115.80	72.88	304.71	5.22E-02	40
1095B-5H-1	30	121.30	115.80	73.05	308.25	3.69E-02	50
1095B-5H-1	30	121.30	115.80	74.58	310.24	2.54E-02	60
1095B-5H-1	30	121.30	115.80	75.77	306.63	1.62E-02	70
1095B-5H-1	32	121.32	115.82	86.99	300.01	1.39E-01	0
1095B-5H-1	32	121.32	115.82	85.46	288.04	1.10E-01	10
1095B-5H-1	32	121.32	115.82	84.83	288.62	8.63E-02	20
1095B-5H-1	32	121.32	115.82	84.65	292.54	6.39E-02	30
1095B-5H-1	32	121.32	115.82	85.19	286.72	4.86E-02	40
1095B-5H-1	32	121.32	115.82	85.44	299.02	3.42E-02	50
1095B-5H-1	32	121.32	115.82	86.50	301.13	2.36E-02	60
1095B-5H-1	32	121.32	115.82	86.99	285.56	1.52E-02	70
1095B-5H-1	34	121.34	115.84	87.33	155.39	1.51E-01	0
1095B-5H-1	34	121.34	115.84	85.80	162.26	1.19E-01	10
1095B-5H-1	34	121.34	115.84	85.79	164.97	9.40E-02	20
1095B-5H-1	34	121.34	115.84	85.92	163.15	6.95E-02	30
1095B-5H-1	34	121.34	115.84	85.39	162.01	5.26E-02	40
1095B-5H-1	34	121.34	115.84	86.21	157.18	3.68E-02	50
1095B-5H-1	34	121.34	115.84	85.81	150.18	2.54E-02	60
1095B-5H-1	34	121.34	115.84	85.61	159.82	1.62E-02	70
1095B-5H-1	36	121.36	115.86	87.02	127.33	1.74E-01	0
1095B-5H-1	36	121.36	115.86	84.82	143.90	1.33E-01	10
1095B-5H-1	36	121.36	115.86	84.27	145.14	1.05E-01	20
1095B-5H-1	36	121.36	115.86	84.07	143.00	7.78E-02	30
1095B-5H-1	36	121.36	115.86	83.47	143.38	5.85E-02	40
1095B-5H-1	36	121.36	115.86	84.07	140.57	4.09E-02	50
1095B-5H-1	36	121.36	115.86	83.51	137.01	2.81E-02	60

Note: Only a portion of this table appears here. The complete table is available in [ASCII format](#).

Table T6. Paleomagnetic data from U-channel samples, Hole 1095D.

Core, section	Interval (cm)	Depth		Inclination (°)	Declination (°)	Intensity (A/m)	Demagnetization step (mT)
		(mbsf)	(mcd)				
178-							
1095D-1H-1	36	0.36	0.36	-69.95	205.82	1.08E-04	0
1095D-1H-1	36	0.36	0.36	-73.98	200.68	1.09E-04	20
1095D-1H-1	36	0.36	0.36	-74.28	200.97	1.00E-04	30
1095D-1H-1	36	0.36	0.36	-74.75	201.08	9.31E-05	40
1095D-1H-1	36	0.36	0.36	-75.02	201.28	8.39E-05	50
1095D-1H-1	36	0.36	0.36	-75.46	201.66	7.52E-05	60
1095D-1H-1	36	0.36	0.36	-76.25	202.99	5.92E-05	80
1095D-1H-1	38	0.38	0.38	-73.25	220.93	1.24E-04	0
1095D-1H-1	38	0.38	0.38	-75.78	219.95	1.23E-04	20
1095D-1H-1	38	0.38	0.38	-76.01	220.05	1.13E-04	30
1095D-1H-1	38	0.38	0.38	-76.32	220.13	1.05E-04	40
1095D-1H-1	38	0.38	0.38	-76.51	220.29	9.52E-05	50
1095D-1H-1	38	0.38	0.38	-76.74	221.41	8.55E-05	60
1095D-1H-1	38	0.38	0.38	-77.13	222.65	6.76E-05	80
1095D-1H-1	40	0.40	0.40	-77.80	220.06	1.32E-04	0
1095D-1H-1	40	0.40	0.40	-79.41	223.52	1.31E-04	20
1095D-1H-1	40	0.40	0.40	-79.70	223.12	1.21E-04	30
1095D-1H-1	40	0.40	0.40	-79.95	222.77	1.12E-04	40
1095D-1H-1	40	0.40	0.40	-80.09	222.85	1.01E-04	50
1095D-1H-1	40	0.40	0.40	-80.23	223.93	9.10E-05	60
1095D-1H-1	40	0.40	0.40	-80.66	223.89	7.17E-05	80
1095D-1H-1	42	0.42	0.42	-77.44	198.08	1.27E-04	0
1095D-1H-1	42	0.42	0.42	-80.69	200.01	1.29E-04	20
1095D-1H-1	42	0.42	0.42	-80.88	198.95	1.18E-04	30
1095D-1H-1	42	0.42	0.42	-81.08	198.41	1.09E-04	40
1095D-1H-1	42	0.42	0.42	-81.27	197.95	9.82E-05	50
1095D-1H-1	42	0.42	0.42	-81.35	197.89	8.81E-05	60
1095D-1H-1	42	0.42	0.42	-81.78	196.73	6.92E-05	80
1095D-1H-1	44	0.44	0.44	-68.35	189.58	1.15E-04	0
1095D-1H-1	44	0.44	0.44	-73.89	186.38	1.17E-04	20
1095D-1H-1	44	0.44	0.44	-74.01	185.77	1.07E-04	30
1095D-1H-1	44	0.44	0.44	-74.29	185.45	9.90E-05	40
1095D-1H-1	44	0.44	0.44	-74.52	185.14	8.87E-05	50
1095D-1H-1	44	0.44	0.44	-74.73	184.93	7.94E-05	60
1095D-1H-1	44	0.44	0.44	-75.23	183.85	6.21E-05	80
1095D-1H-1	46	0.46	0.46	-58.09	191.94	1.07E-04	0
1095D-1H-1	46	0.46	0.46	-65.23	188.75	1.08E-04	20
1095D-1H-1	46	0.46	0.46	-65.67	188.42	9.86E-05	30
1095D-1H-1	46	0.46	0.46	-66.06	188.14	9.07E-05	40
1095D-1H-1	46	0.46	0.46	-66.53	188.06	8.10E-05	50
1095D-1H-1	46	0.46	0.46	-67.11	187.62	7.20E-05	60
1095D-1H-1	46	0.46	0.46	-67.72	187.08	5.60E-05	80
1095D-1H-1	48	0.48	0.48	-53.67	193.82	1.00E-04	0
1095D-1H-1	48	0.48	0.48	-61.54	191.87	1.01E-04	20
1095D-1H-1	48	0.48	0.48	-62.13	191.67	9.19E-05	30
1095D-1H-1	48	0.48	0.48	-62.68	191.30	8.42E-05	40
1095D-1H-1	48	0.48	0.48	-63.18	191.34	7.50E-05	50
1095D-1H-1	48	0.48	0.48	-63.93	191.17	6.65E-05	60
1095D-1H-1	48	0.48	0.48	-64.59	191.02	5.15E-05	80
1095D-1H-1	50	0.50	0.50	-52.77	187.75	9.31E-05	0
1095D-1H-1	50	0.50	0.50	-64.13	193.44	9.10E-05	20
1095D-1H-1	50	0.50	0.50	-64.57	192.92	8.28E-05	30
1095D-1H-1	50	0.50	0.50	-65.02	192.20	7.60E-05	40
1095D-1H-1	50	0.50	0.50	-65.16	191.67	6.77E-05	50
1095D-1H-1	50	0.50	0.50	-65.81	192.29	6.01E-05	60
1095D-1H-1	50	0.50	0.50	-66.27	192.08	4.65E-05	80
1095D-1H-1	52	0.52	0.52	-52.22	179.71	8.60E-05	0
1095D-1H-1	52	0.52	0.52	-66.87	190.25	8.06E-05	20
1095D-1H-1	52	0.52	0.52	-67.08	189.43	7.35E-05	30
1095D-1H-1	52	0.52	0.52	-67.23	188.75	6.77E-05	40
1095D-1H-1	52	0.52	0.52	-66.96	187.48	6.05E-05	50
1095D-1H-1	52	0.52	0.52	-67.53	188.57	5.38E-05	60
1095D-1H-1	52	0.52	0.52	-67.90	188.26	4.15E-05	80
1095D-1H-1	54	0.54	0.54	-57.21	188.38	7.55E-05	0

Note: Only a portion of this table appears here. The complete table is available in [ASCII format](#).

Table T7. Paleomagnetic data from U-channel samples, Hole 1096A.

Core, section	Interval (cm)	Depth		Inclination (°)	Declination (°)	Intensity (A/m)	Demagnetization step (mT)
		(mbsf)	(mcd)				
178-							
1096A-1H-1	12	0.12	0.36	-80.74	287.76	7.63E-02	0
1096A-1H-1	12	0.12	0.36	-80.00	287.09	7.04E-02	20
1096A-1H-1	12	0.12	0.36	-80.46	286.87	6.34E-02	30
1096A-1H-1	12	0.12	0.36	-80.69	283.43	5.75E-02	40
1096A-1H-1	12	0.12	0.36	-80.05	285.30	5.06E-02	50
1096A-1H-1	12	0.12	0.36	-80.71	285.86	4.49E-02	60
1096A-1H-1	12	0.12	0.36	-80.93	283.88	3.42E-02	80
1096A-1H-1	14	0.14	0.38	-85.82	300.19	8.65E-02	0
1096A-1H-1	14	0.14	0.38	-86.52	285.54	8.28E-02	20
1096A-1H-1	14	0.14	0.38	-86.75	286.79	7.47E-02	30
1096A-1H-1	14	0.14	0.38	-86.90	277.68	6.83E-02	40
1096A-1H-1	14	0.14	0.38	-86.54	283.48	6.06E-02	50
1096A-1H-1	14	0.14	0.38	-86.81	284.72	5.38E-02	60
1096A-1H-1	14	0.14	0.38	-86.83	284.49	4.14E-02	80
1096A-1H-1	16	0.16	0.40	-83.92	322.65	9.25E-02	0
1096A-1H-1	16	0.16	0.40	-85.91	316.17	8.91E-02	20
1096A-1H-1	16	0.16	0.40	-85.76	316.84	8.10E-02	30
1096A-1H-1	16	0.16	0.40	-86.03	311.64	7.44E-02	40
1096A-1H-1	16	0.16	0.40	-85.50	314.29	6.66E-02	50
1096A-1H-1	16	0.16	0.40	-85.43	315.05	5.95E-02	60
1096A-1H-1	16	0.16	0.40	-85.28	316.92	4.63E-02	80
1096A-1H-1	18	0.18	0.42	-83.20	328.00	9.38E-02	0
1096A-1H-1	18	0.18	0.42	-84.19	322.28	9.16E-02	20
1096A-1H-1	18	0.18	0.42	-84.19	322.48	8.39E-02	30
1096A-1H-1	18	0.18	0.42	-81.83	334.31	7.79E-02	40
1096A-1H-1	18	0.18	0.42	-83.95	322.30	6.98E-02	50
1096A-1H-1	18	0.18	0.42	-83.88	322.70	6.27E-02	60
1096A-1H-1	18	0.18	0.42	-83.79	324.40	4.92E-02	80
1096A-1H-1	20	0.20	0.44	-85.96	333.42	8.96E-02	0
1096A-1H-1	20	0.20	0.44	-86.16	324.13	8.82E-02	20
1096A-1H-1	20	0.20	0.44	-86.44	327.25	8.11E-02	30
1096A-1H-1	20	0.20	0.44	-83.91	341.75	7.56E-02	40
1096A-1H-1	20	0.20	0.44	-86.30	329.18	6.82E-02	50
1096A-1H-1	20	0.20	0.44	-86.32	330.92	6.13E-02	60
1096A-1H-1	20	0.20	0.44	-86.22	333.48	4.84E-02	80
1096A-1H-1	22	0.22	0.46	-85.15	302.29	8.48E-02	0
1096A-1H-1	22	0.22	0.46	-86.57	298.30	8.31E-02	20
1096A-1H-1	22	0.22	0.46	-86.89	299.28	7.67E-02	30
1096A-1H-1	22	0.22	0.46	-84.89	329.09	7.15E-02	40
1096A-1H-1	22	0.22	0.46	-87.01	301.10	6.46E-02	50
1096A-1H-1	22	0.22	0.46	-86.93	301.49	5.82E-02	60
1096A-1H-1	22	0.22	0.46	-86.85	304.02	4.61E-02	80
1096A-1H-1	24	0.24	0.48	-79.95	297.01	8.39E-02	0
1096A-1H-1	24	0.24	0.48	-81.56	290.68	8.12E-02	20
1096A-1H-1	24	0.24	0.48	-81.84	290.75	7.49E-02	30
1096A-1H-1	24	0.24	0.48	-80.53	307.32	6.99E-02	40
1096A-1H-1	24	0.24	0.48	-82.00	290.50	6.30E-02	50
1096A-1H-1	24	0.24	0.48	-81.88	290.23	5.69E-02	60
1096A-1H-1	24	0.24	0.48	-81.99	289.97	4.51E-02	80
1096A-1H-1	26	0.26	0.50	-79.41	302.80	8.24E-02	0
1096A-1H-1	26	0.26	0.50	-79.60	296.33	8.10E-02	20
1096A-1H-1	26	0.26	0.50	-79.90	296.92	7.45E-02	30
1096A-1H-1	26	0.26	0.50	-78.43	309.51	6.95E-02	40
1096A-1H-1	26	0.26	0.50	-79.98	297.04	6.24E-02	50
1096A-1H-1	26	0.26	0.50	-79.99	296.32	5.63E-02	60
1096A-1H-1	26	0.26	0.50	-80.24	295.31	4.44E-02	80
1096A-1H-1	28	0.28	0.52	-80.75	278.76	7.84E-02	0
1096A-1H-1	28	0.28	0.52	-81.24	284.41	7.81E-02	20
1096A-1H-1	28	0.28	0.52	-81.45	283.33	7.19E-02	30
1096A-1H-1	28	0.28	0.52	-80.29	299.38	6.69E-02	40
1096A-1H-1	28	0.28	0.52	-81.23	284.27	6.03E-02	50
1096A-1H-1	28	0.28	0.52	-81.28	283.29	5.44E-02	60
1096A-1H-1	28	0.28	0.52	-81.35	281.87	4.29E-02	80
1096A-1H-1	30	0.30	0.54	-71.63	253.38	7.91E-02	0

Note: Only a portion of this table appears here. The complete table is available in [ASCII format](#).

Table T8. Paleomagnetic data from U-channel samples, Hole 1096B.

Core, section	Interval (cm)	Depth		Inclination (°)	Declination (°)	Intensity (A/m)	Demagnetization step (mT)
		(mbsf)	(mcd)				
178-							
1096B-1H-1	12	0.12	0.12	-88.71	18.01	7.15E-02	0
1096B-1H-1	12	0.12	0.12	-88.61	23.77	6.90E-02	20
1096B-1H-1	12	0.12	0.12	-88.83	37.93	6.00E-02	30
1096B-1H-1	12	0.12	0.12	-88.82	34.97	5.38E-02	40
1096B-1H-1	12	0.12	0.12	-89.07	39.24	4.69E-02	50
1096B-1H-1	12	0.12	0.12	-89.16	11.34	4.08E-02	60
1096B-1H-1	12	0.12	0.12	-88.42	334.68	3.08E-02	80
1096B-1H-1	14	0.14	0.14	-84.54	296.03	8.55E-02	0
1096B-1H-1	14	0.14	0.14	-84.20	303.11	8.39E-02	20
1096B-1H-1	14	0.14	0.14	-84.38	302.07	7.40E-02	30
1096B-1H-1	14	0.14	0.14	-84.33	302.91	6.66E-02	40
1096B-1H-1	14	0.14	0.14	-84.72	298.43	5.80E-02	50
1096B-1H-1	14	0.14	0.14	-84.54	298.65	5.04E-02	60
1096B-1H-1	14	0.14	0.14	-83.31	296.45	3.79E-02	80
1096B-1H-1	16	0.16	0.16	-82.31	258.61	9.21E-02	0
1096B-1H-1	16	0.16	0.16	-82.48	268.38	9.10E-02	20
1096B-1H-1	16	0.16	0.16	-82.43	267.42	8.08E-02	30
1096B-1H-1	16	0.16	0.16	-82.43	266.25	7.29E-02	40
1096B-1H-1	16	0.16	0.16	-82.64	263.28	6.38E-02	50
1096B-1H-1	16	0.16	0.16	-82.57	263.42	5.57E-02	60
1096B-1H-1	16	0.16	0.16	-81.96	261.58	4.17E-02	80
1096B-1H-1	18	0.18	0.18	-80.53	244.72	9.41E-02	0
1096B-1H-1	18	0.18	0.18	-80.81	249.40	9.31E-02	20
1096B-1H-1	18	0.18	0.18	-80.86	248.82	8.31E-02	30
1096B-1H-1	18	0.18	0.18	-80.69	247.16	7.52E-02	40
1096B-1H-1	18	0.18	0.18	-80.95	246.27	6.62E-02	50
1096B-1H-1	18	0.18	0.18	-80.72	246.34	5.79E-02	60
1096B-1H-1	18	0.18	0.18	-80.56	244.51	4.36E-02	80
1096B-1H-1	20	0.20	0.20	-80.50	255.74	9.35E-02	0
1096B-1H-1	20	0.20	0.20	-80.72	256.67	9.28E-02	20
1096B-1H-1	20	0.20	0.20	-81.00	255.43	8.33E-02	30
1096B-1H-1	20	0.20	0.20	-80.84	254.15	7.56E-02	40
1096B-1H-1	20	0.20	0.20	-81.09	254.15	6.68E-02	50
1096B-1H-1	20	0.20	0.20	-80.85	253.39	5.87E-02	60
1096B-1H-1	20	0.20	0.20	-81.05	253.53	4.45E-02	80
1096B-1H-1	22	0.22	0.22	-82.48	268.78	9.25E-02	0
1096B-1H-1	22	0.22	0.22	-82.27	272.67	9.18E-02	20
1096B-1H-1	22	0.22	0.22	-82.56	271.81	8.30E-02	30
1096B-1H-1	22	0.22	0.22	-82.54	270.40	7.55E-02	40
1096B-1H-1	22	0.22	0.22	-82.69	270.33	6.71E-02	50
1096B-1H-1	22	0.22	0.22	-82.69	269.17	5.92E-02	60
1096B-1H-1	22	0.22	0.22	-83.08	268.73	4.54E-02	80
1096B-1H-1	24	0.24	0.24	-86.32	250.47	9.65E-02	0
1096B-1H-1	24	0.24	0.24	-86.35	267.42	9.50E-02	20
1096B-1H-1	24	0.24	0.24	-86.40	266.44	8.65E-02	30
1096B-1H-1	24	0.24	0.24	-86.52	263.78	7.90E-02	40
1096B-1H-1	24	0.24	0.24	-86.57	262.12	7.05E-02	50
1096B-1H-1	24	0.24	0.24	-86.77	257.72	6.28E-02	60
1096B-1H-1	24	0.24	0.24	-86.75	251.46	4.89E-02	80
1096B-1H-1	26	0.26	0.26	-84.68	234.67	1.07E-01	0
1096B-1H-1	26	0.26	0.26	-85.77	240.96	1.05E-01	20
1096B-1H-1	26	0.26	0.26	-85.72	241.09	9.58E-02	30
1096B-1H-1	26	0.26	0.26	-85.86	237.08	8.78E-02	40
1096B-1H-1	26	0.26	0.26	-85.76	235.27	7.91E-02	50
1096B-1H-1	26	0.26	0.26	-85.74	234.28	7.10E-02	60
1096B-1H-1	26	0.26	0.26	-85.35	232.62	5.57E-02	80
1096B-1H-1	28	0.28	0.28	-79.71	262.06	1.13E-01	0
1096B-1H-1	28	0.28	0.28	-80.82	265.27	1.12E-01	20
1096B-1H-1	28	0.28	0.28	-80.98	264.42	1.03E-01	30
1096B-1H-1	28	0.28	0.28	-81.07	263.15	9.53E-02	40
1096B-1H-1	28	0.28	0.28	-80.88	263.35	8.64E-02	50
1096B-1H-1	28	0.28	0.28	-80.80	263.87	7.77E-02	60
1096B-1H-1	28	0.28	0.28	-80.54	263.40	6.12E-02	80
1096B-1H-1	30	0.30	0.30	-74.73	278.25	1.11E-01	0

Note: Only a portion of this table appears here. The complete table is available in [ASCII format](#).

Table T9. Paleomagnetic data from U-channel samples, Hole 1101A.

Core, section	Interval (cm)	Depth (mbsf)	Inclination (°)	Declination (°)	Intensity (A/m)	Demagnetization step (mT)
178-						
1101A-1H-1	8	0.08	-74.80	91.30	4.91E-02	0
1101A-1H-1	8	0.08	-77.90	76.40	5.90E-02	10
1101A-1H-1	8	0.08	-78.10	75.80	4.92E-02	20
1101A-1H-1	8	0.08	-78.00	73.30	4.02E-02	30
1101A-1H-1	8	0.08	-77.70	71.40	3.39E-02	40
1101A-1H-1	8	0.08	-77.50	69.20	2.79E-02	50
1101A-1H-1	8	0.08	-77.20	63.00	2.30E-02	60
1101A-1H-1	8	0.08	-76.90	62.30	1.65E-02	80
1101A-1H-1	9	0.09	-74.60	86.80	4.84E-02	0
1101A-1H-1	9	0.09	-78.90	80.20	5.77E-02	10
1101A-1H-1	9	0.09	-79.10	79.00	4.82E-02	20
1101A-1H-1	9	0.09	-79.10	76.80	3.92E-02	30
1101A-1H-1	9	0.09	-78.80	74.70	3.31E-02	40
1101A-1H-1	9	0.09	-78.60	72.20	2.72E-02	50
1101A-1H-1	9	0.09	-78.00	64.50	2.25E-02	60
1101A-1H-1	9	0.09	-77.40	62.80	1.61E-02	80
1101A-1H-1	10	0.10	-75.10	89.50	4.70E-02	0
1101A-1H-1	10	0.10	-80.00	94.10	5.66E-02	10
1101A-1H-1	10	0.10	-80.30	93.20	4.72E-02	20
1101A-1H-1	10	0.10	-80.40	91.70	3.83E-02	30
1101A-1H-1	10	0.10	-80.00	88.20	3.23E-02	40
1101A-1H-1	10	0.10	-80.10	85.00	2.66E-02	50
1101A-1H-1	10	0.10	-79.70	74.60	2.19E-02	60
1101A-1H-1	10	0.10	-78.90	70.90	1.57E-02	80
1101A-1H-1	11	0.11	-75.70	101.30	4.59E-02	0
1101A-1H-1	11	0.11	-79.80	111.50	5.63E-02	10
1101A-1H-1	11	0.11	-80.10	112.60	4.69E-02	20
1101A-1H-1	11	0.11	-80.20	113.00	3.81E-02	30
1101A-1H-1	11	0.11	-80.10	108.50	3.21E-02	40
1101A-1H-1	11	0.11	-80.40	106.30	2.64E-02	50
1101A-1H-1	11	0.11	-80.60	95.20	2.17E-02	60
1101A-1H-1	11	0.11	-79.90	87.80	1.55E-02	80
1101A-1H-1	12	0.12	-75.00	116.10	4.55E-02	0
1101A-1H-1	12	0.12	-78.70	122.10	5.69E-02	10
1101A-1H-1	12	0.12	-78.90	124.20	4.75E-02	20
1101A-1H-1	12	0.12	-78.90	124.90	3.87E-02	30
1101A-1H-1	12	0.12	-79.00	121.70	3.26E-02	40
1101A-1H-1	12	0.12	-79.20	120.30	2.68E-02	50
1101A-1H-1	12	0.12	-79.80	112.70	2.20E-02	60
1101A-1H-1	12	0.12	-79.20	104.20	1.56E-02	80
1101A-1H-1	13	0.13	-73.50	124.60	4.60E-02	0
1101A-1H-1	13	0.13	-78.00	125.00	5.81E-02	10
1101A-1H-1	13	0.13	-78.10	127.10	4.87E-02	20
1101A-1H-1	13	0.13	-78.10	128.10	3.98E-02	30
1101A-1H-1	13	0.13	-78.30	124.60	3.35E-02	40
1101A-1H-1	13	0.13	-78.30	124.20	2.76E-02	50
1101A-1H-1	13	0.13	-78.90	118.90	2.26E-02	60
1101A-1H-1	13	0.13	-78.30	111.30	1.61E-02	80
1101A-1H-1	14	0.14	-72.50	126.70	4.72E-02	0
1101A-1H-1	14	0.14	-78.10	125.00	5.94E-02	10
1101A-1H-1	14	0.14	-78.20	126.60	4.99E-02	20
1101A-1H-1	14	0.14	-78.30	128.40	4.08E-02	30
1101A-1H-1	14	0.14	-78.50	125.00	3.45E-02	40
1101A-1H-1	14	0.14	-78.20	124.80	2.84E-02	50
1101A-1H-1	14	0.14	-78.90	120.20	2.34E-02	60
1101A-1H-1	14	0.14	-78.10	113.80	1.67E-02	80
1101A-1H-1	15	0.15	-72.60	126.20	4.84E-02	0
1101A-1H-1	15	0.15	-79.60	126.20	6.02E-02	10
1101A-1H-1	15	0.15	-79.70	127.70	5.07E-02	20
1101A-1H-1	15	0.15	-79.80	131.80	4.16E-02	30
1101A-1H-1	15	0.15	-80.10	128.90	3.51E-02	40
1101A-1H-1	15	0.15	-79.60	129.40	2.90E-02	50
1101A-1H-1	15	0.15	-80.50	124.40	2.39E-02	60

Note: Only a portion of this table appears here. The complete table is available in [ASCII format](#).

**Table T10.** Principal component analysis results from U-channel paleomagnetic data, Hole 1095A.

Core, section	Interval (cm)	Depth		Principal component analysis								Stable end point				
		(mbsf)	(mcd)	Inclination (°)	Declination (°)	MAD (°)	Length (A/m)	Deviation angle (°)	Number of steps	Lowest step (mT)	Highest step (mT)	Inclination (°)	Declination (°)	k	N	Angular distance (°)
178-																
1095A-1H-1	6	0.06	0.06	-71.4	313.7	1.36	3.62E-01	2.53	5	30	80	-73.7	320.1	11,052.2	3	3.0
1095A-1H-1	8	0.08	0.08	-72.3	311.1	0.57	3.99E-01	0.90	5	30	80	-73.3	312.7	76,959.7	3	1.1
1095A-1H-1	10	0.10	0.10	-73.9	315.7	0.46	3.96E-01	1.10	5	30	80	-72.8	313.1	167,772.2	3	1.3
1095A-1H-1	12	0.12	0.12	-72.7	316.5	0.65	3.75E-01	2.01	5	30	80	-71.0	311.4	41,120.6	3	2.3
1095A-1H-1	14	0.14	0.14	-66.5	307.1	0.76	3.46E-01	2.76	5	30	80	-63.9	302.5	27,594.1	3	3.2
1095A-1H-1	16	0.16	0.16	-56.7	299.6	0.34	2.97E-01	2.69	5	30	80	-54.0	297.2	19,373.2	3	3.1
1095A-1H-1	18	0.18	0.18	-63.4	295.9	0.77	2.00E-01	1.99	5	30	80	-61.2	294.4	22,369.6	3	2.3
1095A-1H-1	20	0.20	0.20	-88.1	230.5	0.54	1.96E-01	1.93	5	30	80	-86.7	271.8	36,954.2	3	2.2
1095A-1H-1	22	0.22	0.22	-86.5	258.9	0.64	2.75E-01	3.04	5	30	80	-83.9	289.0	24,174.7	3	3.5
1095A-1H-1	24	0.24	0.24	-76.5	292.2	0.79	3.56E-01	3.14	5	30	80	-73.6	300.8	25,970.9	3	3.6
1095A-1H-1	26	0.26	0.26	-65.7	298.4	1.14	4.00E-01	3.97	5	30	80	-61.8	304.1	19,553.9	3	4.6
1095A-1H-1	28	0.28	0.28	-60.4	302.0	1.12	3.84E-01	4.49	5	30	80	-55.9	306.9	15,947.9	3	5.2
1095A-1H-1	30	0.30	0.30	-67.1	305.9	1.14	3.65E-01	5.93	5	30	80	-60.5	309.5	7,194.3	3	6.8
1095A-1H-1	32	0.32	0.32	-73.1	305.2	1.35	4.11E-01	5.33	5	30	80	-67.0	305.6	10,578.3	3	6.1
1095A-1H-1	34	0.34	0.34	-67.7	302.7	0.96	4.90E-01	2.17	5	30	80	-65.7	299.0	79,891.5	3	2.5
1095A-1H-1	36	0.36	0.36	-62.4	302.2	0.66	4.91E-01	1.44	5	30	80	-62.5	298.5	89,240.5	3	1.7
1095A-1H-1	38	0.38	0.38	-72.3	310.4	1.15	4.11E-01	0.75	5	30	80	-71.5	311.2	38,304.1	3	0.8
1095A-1H-1	40	0.40	0.40	-77.6	338.2	0.84	4.15E-01	3.36	5	30	80	-73.8	335.2	24,456.6	3	3.9
1095A-1H-1	42	0.42	0.42	-72.1	331.3	0.92	4.36E-01	3.96	5	30	80	-67.6	328.7	19,645.5	3	4.5
1095A-1H-1	44	0.44	0.44	-71.3	324.9	0.61	4.15E-01	3.15	5	30	80	-67.7	324.6	25,970.9	3	3.6
1095A-1H-1	46	0.46	0.46	-76.3	321.7	0.63	3.73E-01	2.28	5	30	80	-73.7	323.3	50,840.0	3	2.6
1095A-1H-1	48	0.48	0.48	-83.9	319.7	0.42	3.47E-01	0.76	5	30	80	-83.1	318.7	195,083.9	3	0.9
1095A-1H-1	50	0.50	0.50	-87.8	304.5	0.32	3.45E-01	1.18	5	30	80	-86.5	296.4	114,912.4	3	1.4
1095A-1H-1	52	0.52	0.52	-85.7	312.8	0.46	3.50E-01	1.54	5	30	80	-84.0	308.7	69,327.3	3	1.8
1095A-1H-1	54	0.54	0.54	-86.2	321.5	0.38	3.49E-01	1.22	5	30	80	-84.8	318.4	174,762.7	3	1.4
1095A-1H-1	56	0.56	0.56	-83.9	299.9	0.31	3.49E-01	0.55	5	30	80	-83.3	302.9	699,050.7	3	0.7
1095A-1H-1	58	0.58	0.58	-79.0	305.5	0.21	3.29E-01	0.44	5	30	80	-78.7	307.4	1,398,101.4	3	0.5
1095A-1H-1	60	0.60	0.60	-79.4	323.0	0.29	2.58E-01	0.78	4	40	80	-78.6	324.2	335,544.3	3	0.9
1095A-1H-1	62	0.62	0.62	-78.6	312.8	0.63	3.24E-01	1.26	5	30	80	-77.2	315.7	289,262.3	3	1.5
1095A-1H-1	64	0.64	0.64	-75.8	296.9	0.42	3.34E-01	0.93	5	30	80	-75.1	300.3	493,447.5	3	1.1
1095A-1H-1	66	0.66	0.66	-78.4	289.2	0.39	3.43E-01	0.57	5	30	80	-78.1	292.0	559,240.6	3	0.7

Notes: The mean paleomagnetic direction is estimated from the demagnetization data using the principal component analysis (PCA) method of Kirschvink (1980). The best-fit line that passes through the vector demagnetization data is not forced to be anchored to the origin of vector demagnetization space, but is allowed to freely fit the data. To avoid data possibly contaminated by the drilling overprint, we do not use demagnetization steps <20 mT. We use an iterative search program to find and delete demagnetization steps in any interval that give directions that are outliers relative to directions from other demagnetization steps from that interval. PCA parameters, in addition to the direction (inclination and declination), are MAD = maximum angular deviation, length = distance from origin of the vector demagnetization space to the centroid of the data used to find the best-fit line, deviation angle = the angle between the best-fit line and a line that passes through the origin and centroid, number of steps = number of demagnetization steps used in finding the best-fit line, lowest step = the lowest demagnetization step used in finding the best-fit line, highest step = the highest demagnetization step used in finding the best-fit line. For comparison, we also compute a Fisherian mean of the highest three or four demagnetization steps for each interval from a U-channel sample. This is referred to as the stable end point direction. Typically only the highest three demagnetization steps are used in the average, unless the mean of these three directions has a dispersion parameter <200, in which case the fourth highest demagnetization step is included. When the dispersion parameter is <200, we also use an iterative search to find and remove the direction that is the largest outlier. Stable end point parameters, in addition to the mean direction (inclination and declination), are k = the Fisherian dispersion parameter and N = the number of directions from the three highest demagnetization steps that were averaged. Angular distance = the angular distance between the PCA direction and the stable end point direction. Only a portion of this table appears here. The complete table is available in [ASCII format](#).

**Table T11.** Principal component analysis results from U-channel paleomagnetic data, Hole 1095B.

Core, section	Interval (cm)	Depth		Principal component analysis								Stable end point				Angular distance (°)
		(mbsf)	(mcd)	Inclination (°)	Declination (°)	MAD (°)	Length (A/m)	Deviation angle (°)	Number of steps	Lowest step (mT)	Highest step (mT)	Inclination (°)	Declination (°)	k	N	
178-																
1095B-5H-1	22	121.22	115.72	83.9	219.7	0.59	8.51E-01	0.45	6	20	70	85.1	221.1	24,385.5	3	1.1
1095B-5H-1	24	121.24	115.74	86.7	179.1	0.69	8.30E-01	0.26	6	20	70	87.0	166.3	21,290.9	3	0.8
1095B-5H-1	26	121.26	115.76	85.6	277.9	0.76	7.70E-01	0.58	6	20	70	86.7	278.7	23,629.9	3	1.1
1095B-5H-1	28	121.28	115.78	72.1	301.0	0.71	7.63E-01	1.40	6	20	70	74.7	304.0	5,920.0	3	2.7
1095B-5H-1	30	121.30	115.80	71.0	304.1	0.64	7.67E-01	1.84	6	20	70	74.5	308.4	3,151.2	3	3.7
1095B-5H-1	32	121.32	115.82	84.2	288.0	0.67	7.12E-01	1.07	6	20	70	86.3	296.0	7,417.0	3	2.2
1095B-5H-1	34	121.34	115.84	85.8	167.7	0.51	7.78E-01	0.45	6	20	70	85.9	155.7	29,228.6	3	0.9
1095B-5H-1	36	121.36	115.86	84.3	146.3	0.56	8.74E-01	0.52	6	20	70	83.8	140.3	32,388.4	3	0.8
1095B-5H-1	38	121.38	115.88	84.8	138.4	0.93	6.23E-01	0.58	5	30	70	84.1	135.0	45,100.0	3	0.8
1095B-5H-1	40	121.40	115.90	86.3	252.8	1.11	6.51E-01	1.39	5	30	70	88.1	225.5	48,489.1	3	2.2
1095B-5H-1	42	121.42	115.92	74.7	282.4	0.92	7.46E-01	3.34	5	30	70	80.2	286.0	3,102.3	3	5.6
1095B-5H-1	44	121.44	115.94	71.2	283.9	0.71	1.15E+00	4.36	6	20	70	80.1	283.4	1,076.6	3	8.9
1095B-5H-1	46	121.46	115.96	77.6	282.2	0.58	8.95E-01	3.89	6	20	70	85.2	263.5	1,009.6	3	8.0
1095B-5H-1	48	121.48	115.98	74.0	308.4	0.70	6.64E-01	2.55	6	20	70	79.2	306.3	2,188.0	3	5.2
1095B-5H-1	50	121.50	116.00	63.2	312.9	0.61	6.27E-01	2.03	6	20	70	67.3	311.6	3,440.8	3	4.2
1095B-5H-1	52	121.52	116.02	69.9	311.2	0.82	5.88E-01	2.55	6	20	70	75.0	308.7	3,363.5	3	5.2
1095B-5H-1	54	121.54	116.04	83.9	301.4	1.13	3.63E-01	3.41	4	30	70	87.6	241.2	2,922.9	3	5.4
1095B-5H-1	56	121.56	116.06	84.4	276.2	1.39	5.43E-01	2.15	6	20	70	85.9	232.7	3,512.8	3	3.9
1095B-5H-1	58	121.58	116.08	69.6	305.2	0.96	5.83E-01	1.26	6	20	70	71.9	304.5	6,074.3	3	2.3
1095B-5H-1	60	121.60	116.10	52.3	312.7	0.87	6.99E-01	1.32	6	20	70	55.1	313.0	3,385.2	3	2.8
1095B-5H-1	62	121.62	116.12	57.2	314.1	1.09	6.32E-01	1.74	6	20	70	60.9	314.7	2,542.8	3	3.7
1095B-5H-1	64	121.64	116.14	83.9	305.0	1.13	4.67E-01	1.94	6	20	70	87.7	313.8	4,092.0	3	3.8
1095B-5H-1	66	121.66	116.16	78.3	147.9	1.04	4.67E-01	1.38	6	20	70	76.2	141.6	5,924.2	3	2.5
1095B-5H-1	68	121.68	116.18	75.0	147.4	1.06	4.94E-01	0.80	6	20	70	73.8	147.9	25,890.8	3	1.2
1095B-5H-1	70	121.70	116.20	78.3	148.8	0.65	3.54E-01	1.00	4	30	70	77.3	153.8	32,388.4	3	1.5
1095B-5H-1	72	121.72	116.22	86.4	134.3	0.86	3.73E-01	1.99	4	30	70	83.6	149.0	15,335.7	3	3.0
1095B-5H-1	74	121.74	116.24	84.8	18.1	1.22	5.55E-01	2.27	5	20	70	86.5	74.3	24,244.5	3	4.4
1095B-5H-1	76	121.76	116.26	83.5	30.8	1.08	5.24E-01	1.21	6	20	70	84.7	48.5	8,481.9	3	2.2
1095B-5H-1	78	121.78	116.28	86.2	23.2	1.24	4.96E-01	1.35	6	20	70	88.0	53.7	5,071.7	3	2.4
1095B-5H-1	80	121.80	116.30	85.0	329.7	1.21	5.12E-01	1.86	5	20	70	88.5	281.4	9,597.9	3	4.2
1095B-5H-1	82	121.82	116.32	84.1	323.7	1.29	5.34E-01	2.44	5	20	70	88.5	254.8	11,715.9	3	5.5

Notes: The mean paleomagnetic direction is estimated from the demagnetization data using the principal component analysis (PCA) method of Kirschvink (1980). The best-fit line that passes through the vector demagnetization data is not forced to be anchored to the origin of vector demagnetization space, but is allowed to freely fit the data. To avoid data possibly contaminated by the drilling overprint, we do not use demagnetization steps <20 mT. We use an iterative search program to find and delete demagnetization steps in any interval that give directions that are outliers relative to directions from other demagnetization steps from that interval. PCA parameters, in addition to the direction (inclination and declination), are MAD = maximum angular deviation, length = distance from origin of the vector demagnetization space to the centroid of the data used to find the best-fit line, deviation angle = the angle between the best-fit line and a line that passes through the origin and centroid, number of steps = number of demagnetization steps used in finding the best-fit line, lowest step = the lowest demagnetization step used in finding the best-fit line, highest step = the highest demagnetization step used in finding the best-fit line. For comparison, we also compute a Fisherian mean of the highest three or four demagnetization steps for each interval from a U-channel sample. This is referred to as the stable end point direction. Typically only the highest three demagnetization steps are used in the average, unless the mean of these three directions has a dispersion parameter <200, in which case the fourth highest demagnetization step is included. When the dispersion parameter is <200, we also use an iterative search to find and remove the direction that is the largest outlier. Stable end point parameters, in addition to the mean direction (inclination and declination), are k = the Fisherian dispersion parameter and N = the number of directions from the three highest demagnetization steps that were averaged. Angular distance = the angular distance between the PCA direction and the stable end point direction. Only a portion of this table appears here. The complete table is available in [ASCII format](#).

**Table T12.** Principal component analysis results from U-channel paleomagnetic data, Hole 1095D.

Core, section	Interval (cm)	Depth		Principal component analysis								Stable end point				Angular distance (°)	
		(mbsf)	(mcd)	Inclination (°)	Declination (°)	MAD (°)	Length (A/m)	Deviation angle (°)	Number of steps	Lowest step (mT)	Highest step (mT)	Inclination (°)	Declination (°)	k	N		
178-																	
1095D-1H-1	36	0.36	0.36	-71.6	198.8	0.66	4.11E-04	3.55	5	30	80	-75.6	202.0	15,006.5	3	4.1	
1095D-1H-1	38	0.38	0.38	-74.4	216.6	0.61	4.55E-04	2.32	5	30	80	-76.8	221.4	38,304.1	3	2.7	
1095D-1H-1	40	0.40	0.40	-78.4	221.6	0.48	4.90E-04	1.69	5	30	80	-80.3	223.5	66,052.0	3	2.0	
1095D-1H-1	42	0.42	0.42	-79.7	201.2	0.35	4.86E-04	1.63	5	30	80	-81.5	197.5	76,959.7	3	1.9	
1095D-1H-1	44	0.44	0.44	-72.4	187.9	0.41	4.50E-04	2.23	5	30	80	-74.8	184.7	39,756.4	3	2.6	
1095D-1H-1	46	0.46	0.46	-62.9	189.8	0.86	4.27E-04	3.66	5	30	80	-67.1	187.6	16,810.8	3	4.3	
1095D-1H-1	48	0.48	0.48	-59.0	192.2	1.14	4.05E-04	4.18	5	30	80	-63.9	191.2	13,046.0	3	5.0	
1095D-1H-1	50	0.50	0.50	-62.4	193.4	1.21	3.64E-04	2.87	5	30	80	-65.7	192.0	20,020.5	3	3.4	
1095D-1H-1	52	0.52	0.52	-66.0	190.5	0.48	3.21E-04	1.48	4	30	80	-67.5	188.1	24,174.7	3	1.7	
1095D-1H-1	54	0.54	0.54	-66.4	194.9	1.02	2.85E-04	0.78	5	30	80	-67.1	193.3	79,137.8	3	0.9	
1095D-1H-1	56	0.56	0.56	-65.1	207.2	0.40	2.89E-04	0.77	5	30	80	-65.9	206.4	838,860.8	3	0.9	
1095D-1H-1	58	0.58	0.58	-64.0	210.9	0.50	3.19E-04	1.18	5	30	80	-65.3	212.0	335,544.3	3	1.4	
1095D-1H-1	60	0.60	0.60	-65.1	211.6	0.48	3.41E-04	1.85	5	30	80	-66.9	214.5	63,072.2	3	2.2	
1095D-1H-1	62	0.62	0.62	-66.8	211.5	0.37	3.62E-04	1.66	5	30	80	-68.4	214.1	66,576.3	3	1.9	
1095D-1H-1	64	0.64	0.64	-67.0	212.3	0.37	3.80E-04	1.02	5	30	80	-68.1	213.3	279,620.3	3	1.2	
1095D-1H-1	66	0.66	0.66	-68.0	216.9	0.60	3.92E-04	1.24	5	30	80	-69.3	218.2	270,600.2	3	1.4	
1095D-1H-1	68	0.68	0.68	-69.8	220.0	0.48	3.99E-04	1.37	5	30	80	-71.3	221.5	164,482.5	3	1.6	
1095D-1H-1	70	0.70	0.70	-69.9	212.5	0.47	3.90E-04	1.37	5	30	80	-71.5	212.2	94,254.0	3	1.6	
1095D-1H-1	72	0.72	0.72	-63.2	207.7	0.60	4.43E-04	1.77	6	20	80	-65.4	207.0	46,863.7	3	2.2	
1095D-1H-1	74	0.74	0.74	-54.7	212.6	0.84	3.73E-04	1.88	5	30	80	-56.8	213.8	78,398.2	3	2.2	
1095D-1H-1	76	0.76	0.76	-54.0	217.7	0.66	4.10E-04	2.09	5	30	80	-55.4	221.2	66,576.3	3	2.5	
1095D-1H-1	78	0.78	0.78	-52.4	218.2	1.11	4.55E-04	4.32	5	30	80	-56.0	224.4	12,139.8	3	5.1	
1095D-1H-1	80	0.80	0.80	-43.2	211.3	1.06	3.21E-04	10.34	4	30	60	-53.9	220.9	3,548.5	3	12.5	
1095D-1H-1	82	0.82	0.82	-40.1	206.5	1.47	3.17E-04	11.23	4	30	60	-52.7	214.3	2,789.7	3	13.7	
1095D-1H-1	84	0.84	0.84	-44.9	203.8	1.23	2.51E-04	8.16	4	30	60	-53.8	210.2	5,533.4	3	9.9	
1095D-1H-1	86	0.86	0.86	-52.6	212.1	1.16	3.30E-04	4.68	5	30	80	-56.4	219.0	9,576.0	3	5.6	
1095D-1H-1	88	0.88	0.88	-55.6	228.0	0.59	3.31E-04	3.99	5	30	80	-57.5	235.7	9,521.7	3	4.7	
1095D-1H-1	90	0.90	0.90	-55.9	240.6	0.57	3.60E-04	3.67	5	30	80	-58.0	247.5	12,925.4	3	4.3	
1095D-1H-1	92	0.92	0.92	-54.6	238.8	0.97	2.52E-04	6.98	4	30	60	-61.3	248.0	8,313.8	3	8.3	
1095D-1H-1	94	0.94	0.94	-56.7	224.3	1.02	2.61E-04	8.80	4	30	60	-66.4	232.9	4,969.6	3	10.5	
1095D-1H-1	96	0.96	0.96	-63.3	206.9	1.38	3.85E-04	6.07	5	30	80	-70.0	212.9	5,940.9	3	7.1	
1095D-1H-1	98	0.98	0.98	-68.0	202.1	0.82	3.57E-04	4.94	5	30	80	-73.2	209.3	8,281.0	3	5.7	

Notes: The mean paleomagnetic direction is estimated from the demagnetization data using the principal component analysis (PCA) method of Kirschvink (1980). The best-fit line that passes through the vector demagnetization data is not forced to be anchored to the origin of vector demagnetization space, but is allowed to freely fit the data. To avoid data possibly contaminated by the drilling overprint, we do not use demagnetization steps <20 mT. We use an iterative search program to find and delete demagnetization steps in any interval that give directions that are outliers relative to directions from other demagnetization steps from that interval. PCA parameters, in addition to the direction (inclination and declination), are MAD = maximum angular deviation, length = distance from origin of the vector demagnetization space to the centroid of the data used to find the best-fit line, deviation angle = the angle between the best-fit line and a line that passes through the origin and centroid, number of steps = number of demagnetization steps used in finding the best-fit line, lowest step = the lowest demagnetization step used in finding the best-fit line, highest step = the highest demagnetization step used in finding the best-fit line. For comparison, we also compute a Fisherian mean of the highest three or four demagnetization steps for each interval from a U-channel sample. This is referred to as the stable end point direction. Typically only the highest three demagnetization steps are used in the average, unless the mean of these three directions has a dispersion parameter <200, in which case the fourth highest demagnetization step is included. When the dispersion parameter is <200, we also use an iterative search to find and remove the direction that is the largest outlier. Stable end point parameters, in addition to the mean direction (inclination and declination), are k = the Fisherian dispersion parameter and N = the number of directions from the three highest demagnetization steps that were averaged. Angular distance = the angular distance between the PCA direction and the stable end point direction. Only a portion of this table appears here. The complete table is available in [ASCII format](#).

**Table T13.** Principal component analysis results from U-channel paleomagnetic data, Hole 1096A.

Core, section	Interval (cm)	Depth		Principal component analysis								Stable end point				Angular distance (°)
		(mbsf)	(mcd)	Inclination (°)	Declination (°)	MAD (°)	Length (A/m)	Deviation angle (°)	Number of steps	Lowest step (mT)	Highest step (mT)	Inclination (°)	Declination (°)	k	N	
178-																
1096A-1H-1	12	0.12	0.36	-80.0	287.5	1.12	2.91E-01	0.73	4	30	80	-80.6	285.0	27,685.2	3	0.7
1096A-1H-1	14	0.14	0.38	-86.8	282.5	1.21	3.33E-01	0.05	5	30	80	-86.7	284.2	239,674.5	3	0.1
1096A-1H-1	16	0.16	0.40	-86.7	315.4	0.98	4.28E-01	1.01	6	20	80	-85.4	315.4	270,600.2	3	1.3
1096A-1H-1	18	0.18	0.42	-84.7	319.2	0.39	3.47E-01	0.84	4	30	80	-83.9	323.1	310,689.2	3	0.9
1096A-1H-1	20	0.20	0.44	-86.6	316.6	0.21	3.27E-01	0.86	4	30	80	-86.3	331.2	289,262.3	3	1.0
1096A-1H-1	22	0.22	0.46	-86.9	292.1	0.31	3.06E-01	0.48	4	30	80	-86.9	302.2	466,033.8	3	0.5
1096A-1H-1	24	0.24	0.48	-81.7	291.9	0.33	2.99E-01	0.33	4	30	80	-82.0	290.2	1,048,576.0	3	0.4
1096A-1H-1	26	0.26	0.50	-79.4	299.3	0.28	3.01E-01	0.78	4	30	80	-80.1	296.2	152,520.1	3	0.9
1096A-1H-1	28	0.28	0.52	-81.6	285.9	0.67	2.90E-01	0.44	4	30	80	-81.3	283.1	178,481.0	3	0.5
1096A-1H-1	30	0.30	0.54	-75.8	252.8	0.70	2.80E-01	0.82	4	30	80	-75.0	253.7	81,442.8	3	0.9
1096A-1H-1	32	0.32	0.56	-64.8	255.1	0.66	2.96E-01	0.81	4	30	80	-64.0	255.8	80,659.7	3	0.9
1096A-1H-1	34	0.34	0.58	-58.0	260.8	0.37	3.26E-01	0.97	4	30	80	-57.0	261.2	149,796.6	3	1.1
1096A-1H-1	36	0.36	0.60	-56.5	260.4	0.45	3.38E-01	0.91	4	30	80	-55.5	260.2	116,508.4	3	1.0
1096A-1H-1	38	0.38	0.62	-59.0	255.3	0.20	3.21E-01	1.54	4	30	80	-57.5	254.0	70,492.5	3	1.7
1096A-1H-1	40	0.40	0.64	-63.9	245.6	0.35	2.82E-01	2.36	4	30	80	-61.4	243.7	42,153.8	3	2.6
1096A-1H-1	42	0.42	0.66	-66.5	239.9	0.76	2.47E-01	3.78	4	30	80	-62.3	238.2	20,311.4	3	4.2
1096A-1H-1	44	0.44	0.68	-58.3	244.4	1.49	2.56E-01	5.00	4	30	80	-52.8	243.0	15,224.3	3	5.6
1096A-1H-1	46	0.46	0.70	-50.0	246.3	0.86	2.98E-01	4.80	4	30	80	-44.8	244.7	14,098.5	3	5.3
1096A-1H-1	48	0.48	0.72	-49.7	248.9	1.03	3.07E-01	4.48	4	30	80	-45.1	246.3	18,766.5	3	5.0
1096A-1H-1	50	0.50	0.74	-53.9	251.4	1.42	2.72E-01	4.09	4	30	80	-49.9	247.9	30,393.5	3	4.6
1096A-1H-1	40	0.40	0.64	-63.9	245.6	0.35	2.82E-01	2.36	4	30	80	-61.4	243.7	42,153.8	3	2.6
1096A-1H-1	42	0.42	0.66	-66.5	239.9	0.76	2.47E-01	3.78	4	30	80	-62.3	238.2	20,311.4	3	4.2
1096A-1H-1	44	0.44	0.68	-58.3	244.4	1.49	2.56E-01	5.00	4	30	80	-52.8	243.0	15,224.3	3	5.6
1096A-1H-1	46	0.46	0.70	-50.0	246.3	0.86	2.98E-01	4.80	4	30	80	-44.8	244.7	14,098.5	3	5.3
1096A-1H-1	48	0.48	0.72	-49.7	248.9	1.03	3.07E-01	4.48	4	30	80	-45.1	246.3	18,766.5	3	5.0
1096A-1H-1	50	0.50	0.74	-53.9	251.4	1.42	2.72E-01	4.09	4	30	80	-49.9	247.9	30,393.5	3	4.6
1096A-1H-1	52	0.52	0.76	-58.9	251.9	1.39	2.18E-01	3.17	4	30	80	-55.8	248.6	65,028.0	3	3.6
1096A-1H-1	54	0.54	0.78	-60.8	270.7	0.84	1.82E-01	1.44	4	30	80	-59.4	269.3	335,544.3	3	1.6
1096A-1H-1	56	0.56	0.80	-59.1	303.0	1.27	1.93E-01	0.91	4	30	80	-58.1	302.6	63,072.2	3	1.0
1096A-1H-1	58	0.58	0.82	-61.2	313.0	0.89	2.24E-01	0.40	4	30	80	-61.2	312.1	209,715.2	3	0.5
1096A-1H-1	60	0.60	0.84	-62.8	299.5	1.18	2.64E-01	0.75	4	30	80	-63.2	297.9	158,275.6	3	0.9
1096A-1H-1	62	0.62	0.86	-58.5	286.5	1.50	3.27E-01	1.10	4	30	80	-59.6	287.8	171,196.1	3	1.3

Notes: The mean paleomagnetic direction is estimated from the demagnetization data using the principal component analysis (PCA) method of Kirschvink (1980). The best-fit line that passes through the vector demagnetization data is not forced to be anchored to the origin of vector demagnetization space, but is allowed to freely fit the data. To avoid data possibly contaminated by the drilling overprint, we do not use demagnetization steps <20 mT. We use an iterative search program to find and delete demagnetization steps in any interval that give directions that are outliers relative to directions from other demagnetization steps from that interval. PCA parameters, in addition to the direction (inclination and declination), are MAD = maximum angular deviation, length = distance from origin of the vector demagnetization space to the centroid of the data used to find the best-fit line, deviation angle = the angle between the best-fit line and a line that passes through the origin and centroid, number of steps = number of demagnetization steps used in finding the best-fit line, lowest step = the lowest demagnetization step used in finding the best-fit line, highest step = the highest demagnetization step used in finding the best-fit line. For comparison, we also compute a Fisherian mean of the highest three or four demagnetization steps for each interval from a U-channel sample. This is referred to as the stable end point direction. Typically only the highest three demagnetization steps are used in the average, unless the mean of these three directions has a dispersion parameter <200, in which case the fourth highest demagnetization step is included. When the dispersion parameter is <200, we also use an iterative search to find and remove the direction that is the largest outlier. Stable end point parameters, in addition to the mean direction (inclination and declination), are k = the Fisherian dispersion parameter and N = the number of directions from the three highest demagnetization steps that were averaged. Angular distance = the angular distance between the PCA direction and the stable end point direction. Only a portion of this table appears here. The complete table is available in [ASCII format](#).

**Table T14.** Principal component analysis results from U-channel paleomagnetic data, Hole 1096B.

Core, section	Interval (cm)	Depth		Principal component analysis								Stable end point				Angular distance (°)
		(mbsf)	(mcd)	Inclination (°)	Declination (°)	MAD (°)	Length (A/m)	Deviation angle (°)	Number of steps	Lowest step (mT)	Highest step (mT)	Inclination (°)	Declination (°)	k	N	
178-																
1096B-1H-1	12	0.12	0.12	-87.7	76.9	0.86	2.93E-01	1.88	5	30	80	-89.0	1.5	11,715.9	3	2.3
1096B-1H-1	14	0.14	0.14	-85.2	311.7	1.42	3.60E-01	1.36	5	30	80	-84.2	297.7	10,852.0	3	1.6
1096B-1H-1	16	0.16	0.16	-82.6	275.2	0.71	4.93E-01	1.25	6	20	80	-82.4	262.7	41,323.2	3	1.6
1096B-1H-1	18	0.18	0.18	-81.0	253.0	0.66	3.96E-01	0.99	5	30	80	-80.7	245.7	97,542.0	3	1.2
1096B-1H-1	20	0.20	0.20	-80.9	257.2	0.63	3.89E-01	0.47	5	30	80	-81.0	253.7	322,638.8	3	0.6
1096B-1H-1	22	0.22	0.22	-81.9	274.6	0.41	3.76E-01	0.97	5	30	80	-82.8	269.4	107,546.3	3	1.2
1096B-1H-1	24	0.24	0.24	-85.6	280.4	0.29	4.61E-01	1.52	6	20	80	-86.7	257.2	61,230.7	3	1.9
1096B-1H-1	26	0.26	0.26	-86.0	253.8	0.63	4.90E-01	1.21	6	20	80	-85.6	234.0	103,563.1	3	1.5
1096B-1H-1	28	0.28	0.28	-81.7	264.9	0.55	4.21E-01	0.88	5	30	80	-80.7	263.5	195,083.9	3	1.0
1096B-1H-1	30	0.30	0.30	-76.3	280.7	0.35	4.14E-01	0.92	5	30	80	-75.3	281.3	381,300.4	3	1.1
1096B-1H-1	32	0.32	0.32	-74.2	287.3	0.22	3.73E-01	0.51	5	30	80	-73.6	286.7	559,240.6	3	0.6
1096B-1H-1	34	0.34	0.34	-76.8	285.2	0.21	3.15E-01	0.45	5	30	80	-76.7	283.0	493,447.5	3	0.5
1096B-1H-1	36	0.36	0.36	-78.8	273.6	0.34	3.38E-01	0.48	6	20	80	-78.2	272.9	335,544.3	3	0.6
1096B-1H-1	38	0.38	0.38	-75.7	266.3	0.60	2.82E-01	0.76	5	30	80	-75.0	268.6	254,200.2	3	0.9
1096B-1H-1	40	0.40	0.40	-73.7	268.9	0.57	2.82E-01	0.77	5	30	80	-73.2	271.6	4,194,304.0	3	0.9
1096B-1H-1	42	0.42	0.42	-75.8	266.1	0.95	2.72E-01	0.15	5	30	80	-75.6	266.3	171,196.1	3	0.2
1096B-1H-1	44	0.44	0.44	-73.3	231.2	0.96	2.77E-01	0.53	5	30	80	-72.7	230.9	172,944.4	3	0.6
1096B-1H-1	46	0.46	0.46	-64.5	220.2	1.03	3.10E-01	1.11	5	30	80	-64.1	223.0	144,631.2	3	1.3
1096B-1H-1	48	0.48	0.48	-59.0	222.3	1.23	3.25E-01	0.92	5	30	80	-58.7	224.3	133,152.5	3	1.1
1096B-1H-1	50	0.50	0.50	-54.7	218.4	1.18	3.14E-01	0.40	5	30	80	-54.6	219.2	103,563.1	3	0.5
1096B-1H-1	52	0.52	0.52	-52.3	213.7	0.98	2.87E-01	1.03	5	30	80	-52.6	215.6	215,092.5	3	1.2
1096B-1H-1	54	0.54	0.54	-53.0	218.3	0.95	2.54E-01	2.27	5	30	80	-53.0	222.6	50,533.8	3	2.6
1096B-1H-1	56	0.56	0.56	-50.2	229.6	1.19	2.26E-01	2.36	5	30	80	-49.6	233.7	45,590.3	3	2.7
1096B-1H-1	58	0.58	0.58	-40.9	222.4	0.86	1.30E-01	3.88	4	30	60	-42.2	227.8	45,343.8	3	4.2
1096B-1H-1	60	0.60	0.60	-36.9	222.1	1.42	2.20E-01	1.23	5	30	80	-37.1	223.9	111,848.1	3	1.5
1096B-1H-1	62	0.62	0.62	-35.1	238.4	1.30	2.05E-01	0.84	5	30	80	-35.0	239.6	98,689.5	3	1.0
1096B-1H-1	64	0.64	0.64	-33.2	260.1	1.00	1.39E-01	1.85	5	30	80	-33.6	262.7	92,182.5	3	2.2
1096B-1H-1	66	0.66	0.66	-37.5	292.3	1.45	3.75E-02	12.91	4	30	60	-43.6	311.1	2,589.9	3	15.5
1096B-1H-1	68	0.68	0.68	-48.1	42.8	1.64	3.30E-02	11.29	4	30	80	-52.0	62.1	2,462.9	3	13.0
1096B-1H-1	70	0.70	0.70	-42.2	147.0	1.43	8.01E-02	6.63	4	30	80	-42.8	157.2	8,490.5	3	7.5
1096B-1H-1	72	0.72	0.72	-39.4	182.0	1.25	2.11E-01	3.79	4	30	80	-40.0	187.6	24,036.1	3	4.3
1096B-1H-1	74	0.74	0.74	-43.8	203.0	0.67	3.64E-01	2.00	5	30	80	-43.3	206.0	75,573.0	3	2.3
1096B-1H-1	76	0.76	0.76	-51.9	212.7	0.69	4.56E-01	1.74	5	30	80	-50.9	215.4	215,092.5	3	2.0

Notes: The mean paleomagnetic direction is estimated from the demagnetization data using the principal component analysis (PCA) method of Kirschvink (1980). The best-fit line that passes through the vector demagnetization data is not forced to be anchored to the origin of vector demagnetization space, but is allowed to freely fit the data. To avoid data possibly contaminated by the drilling overprint, we do not use demagnetization steps <20 mT. We use an iterative search program to find and delete demagnetization steps in any interval that give directions that are outliers relative to directions from other demagnetization steps from that interval. PCA parameters, in addition to the direction (inclination and declination), are MAD = maximum angular deviation, length = distance from origin of the vector demagnetization space to the centroid of the data used to find the best-fit line, deviation angle = the angle between the best-fit line and a line that passes through the origin and centroid, number of steps = number of demagnetization steps used in finding the best-fit line, lowest step = the lowest demagnetization step used in finding the best-fit line, highest step = the highest demagnetization step used in finding the best-fit line. For comparison, we also compute a Fisherian mean of the highest three or four demagnetization steps for each interval from a U-channel sample. This is referred to as the stable end point direction. Typically only the highest three demagnetization steps are used in the average, unless the mean of these three directions has a dispersion parameter <200, in which case the fourth highest demagnetization step is included. When the dispersion parameter is <200, we also use an iterative search to find and remove the direction that is the largest outlier. Stable end point parameters, in addition to the mean direction (inclination and declination), are k = the Fisherian dispersion parameter and N = the number of directions from the three highest demagnetization steps that were averaged. Angular distance = the angular distance between the PCA direction and the stable end point direction. Only a portion of this table appears here. The complete table is available in [ASCII format](#).

**Table T15.** Principal component analysis results from U-channel paleomagnetic data, Hole 1101A.

Core, section	Interval (cm)	Depth (mbsf)	Principal component analysis								Stable end point				Angular distance (°)
			Inclination (°)	Declination (°)	MAD (°)	Length (A/m)	Deviation angle (°)	Number of steps	Lowest step (mT)	Highest step (mT)	Inclination (°)	Declination (°)	k	N	
178-															
1101A-1H-1	8	0.08	-78.4	84.6	0.75	3.27E-01	2.95	6	20	80	-77.2	64.8	8,313.8	3	4.3
1101A-1H-1	9	0.09	-79.6	90.2	0.74	3.22E-01	3.26	6	20	80	-78.0	66.3	4,621.8	3	4.8
1101A-1H-1	10	0.10	-80.3	107.6	0.86	3.16E-01	3.60	6	20	80	-79.6	76.6	3,132.4	3	5.4
1101A-1H-1	11	0.11	-79.1	129.2	1.03	2.27E-01	4.49	5	30	80	-80.4	96.3	2,523.6	3	5.9
1101A-1H-1	12	0.12	-77.8	137.0	0.83	2.32E-01	3.86	5	30	80	-79.5	112.4	2,799.9	3	5.1
1101A-1H-1	13	0.13	-77.3	137.8	0.83	2.37E-01	3.26	5	30	80	-78.5	118.1	3,618.9	3	4.3
1101A-1H-1	14	0.14	-77.9	137.5	0.95	2.41E-01	2.84	5	30	80	-78.4	119.6	4,536.8	3	3.7
1101A-1H-1	15	0.15	-79.5	140.4	1.12	2.45E-01	2.29	5	30	80	-80.0	124.0	5,265.9	3	3.0
1101A-1H-1	16	0.16	-82.0	149.0	1.21	2.44E-01	1.24	5	30	80	-83.0	139.8	7,767.2	3	1.6
1101A-1H-1	17	0.17	-84.6	162.2	1.11	2.43E-01	1.24	4	30	80	-85.7	174.9	11,382.1	3	1.6
1101A-1H-1	18	0.18	-86.3	188.7	1.21	2.38E-01	2.01	4	30	80	-86.6	230.7	8,924.1	3	2.6
1101A-1H-1	19	0.19	-86.5	216.5	1.45	2.32E-01	2.61	5	30	80	-85.9	266.9	6,388.9	3	3.3
1101A-1H-1	20	0.20	-86.1	218.0	1.27	2.25E-01	3.41	5	30	80	-86.3	286.3	4,514.9	3	4.3
1101A-1H-1	21	0.21	-86.1	206.7	1.24	2.18E-01	3.76	5	30	80	-87.9	308.3	4,373.6	3	4.8
1101A-1H-1	22	0.22	-87.2	178.6	1.09	2.09E-01	3.21	5	30	80	-88.5	40.0	6,759.6	3	4.1
1101A-1H-1	23	0.23	-86.7	129.6	1.08	1.97E-01	2.77	5	30	80	-86.1	72.2	9,049.2	3	3.5
1101A-1H-1	24	0.24	-84.5	125.1	1.18	1.81E-01	3.22	5	30	80	-83.9	84.0	6,283.6	3	4.1
1101A-1H-1	25	0.25	-81.8	140.6	1.75	1.24E-01	4.85	4	40	80	-82.7	99.0	3,432.3	3	5.6
1101A-1H-1	26	0.26	-75.4	155.2	1.18	1.51E-01	7.43	5	30	80	-81.3	117.8	1,373.6	3	9.3
1101A-1H-1	27	0.27	-64.8	163.7	1.07	1.15E-01	12.93	4	40	80	-77.3	137.1	504.2	3	14.9
1101A-1H-1	28	0.28	-48.5	169.2	1.34	1.82E-01	15.97	5	20	60	-70.5	147.1	230.1	3	24.4
1101A-1H-1	29	0.29	-45.3	168.9	0.92	1.55E-01	18.91	4	40	80	-64.1	154.4	135.8	4	20.4
1101A-1H-1	30	0.30	-45.9	172.8	1.26	2.38E-01	17.43	4	30	80	-61.3	160.6	822.0	3	17.0
1101A-1H-1	31	0.31	-51.8	173.9	1.16	3.28E-01	12.86	4	20	80	-68.3	159.7	164.6	4	17.8
1101A-1H-1	32	0.32	-67.3	175.7	1.24	1.65E-01	5.72	4	30	60	-75.3	157.7	214.8	3	9.8
1101A-1H-1	33	0.33	-74.8	172.2	1.25	2.42E-01	3.94	5	20	60	-80.4	151.0	425.2	3	7.1
1101A-1H-1	34	0.34	-79.7	161.3	1.34	1.70E-01	3.18	4	30	60	-83.0	132.8	826.1	3	5.3
1101A-1H-1	35	0.35	-80.7	162.3	1.16	2.56E-01	5.65	5	30	80	-84.0	112.8	1,542.9	3	7.1
1101A-1H-1	36	0.36	-81.2	166.1	1.09	2.57E-01	5.79	4	30	80	-84.8	105.9	1,784.1	3	7.7
1101A-1H-1	37	0.37	-79.7	173.6	1.09	2.56E-01	6.08	4	30	80	-85.1	122.8	1,852.2	3	8.1

Notes: The mean paleomagnetic direction is estimated from the demagnetization data using the principal component analysis (PCA) method of Kirschvink (1980). The best-fit line that passes through the vector demagnetization data is not forced to be anchored to the origin of vector demagnetization space, but is allowed to freely fit the data. To avoid data possibly contaminated by the drilling overprint, we do not use demagnetization steps <20 mT. We use an iterative search program to find and delete demagnetization steps in any interval that give directions that are outliers relative to directions from other demagnetization steps from that interval. PCA parameters, in addition to the direction (inclination and declination), are MAD = maximum angular deviation, length = distance from origin of the vector demagnetization space to the centroid of the data used to find the best-fit line, deviation angle = the angle between the best-fit line and a line that passes through the origin and centroid, number of steps = number of demagnetization steps used in finding the best-fit line, lowest step = the lowest demagnetization step used in finding the best-fit line, highest step = the highest demagnetization step used in finding the best-fit line. For comparison, we also compute a Fisherian mean of the highest three or four demagnetization steps for each interval from a U-channel sample. This is referred to as the stable end point direction. Typically only the highest three demagnetization steps are used in the average, unless the mean of these three directions has a dispersion parameter <200, in which case the fourth highest demagnetization step is included. When the dispersion parameter is <200, we also use an iterative search to find and remove the direction that is the largest outlier. Stable end point parameters, in addition to the mean direction (inclination and declination), are k = the Fisherian dispersion parameter and N = the number of directions from the three highest demagnetization steps that were averaged. Angular distance = the angular distance between the PCA direction and the stable end point direction. Only a portion of this table appears here. The complete table is available in [ASCII format](#).

**Table T16.** Correlation of the logging depth scale with the mbsf and mcd scales, Hole 1095B.

Depth			
Logging	Core (mbsf)	Core (mcd)	Offset (m)
116.82	110.80	105.30	6.02
123.78	118.78	113.28	5.00
130.52	124.48	118.98	6.04
133.54	127.62	122.12	5.92
139.82	134.82	129.32	5.00
147.94	143.28	137.78	4.66
152.10	148.04	142.54	4.06
156.32	150.76	145.26	5.56
158.82	153.10	147.60	5.72
161.02	156.12	150.62	4.90
164.20	159.62	154.12	4.58
169.14	163.76	158.26	5.38
174.74	169.70	164.20	5.04
175.94	171.50	166.00	4.44
186.48	182.52	177.02	3.96
190.46	187.16	181.66	3.30
200.44	196.82	191.32	3.62
202.12	197.42	191.92	4.70
204.96	200.42	194.92	4.54
220.26	214.84	209.34	5.42
221.08	215.50	210.00	5.58
240.84	235.86	230.36	4.98
255.96	250.44	244.94	5.52
268.88	263.64	258.14	5.24
282.66	277.08	271.58	5.58
312.22	306.80	301.30	5.42
320.84	315.26	309.76	5.58
327.12	320.90	315.40	6.22
356.98	351.30	345.80	5.68
362.16	356.72	351.22	5.44
370.12	365.64	360.14	4.48
374.02	368.84	363.34	5.18
380.88	376.50	371.00	4.38
400.12	395.02	389.52	5.10
404.10	399.70	394.20	4.40*
418.30	412.76	407.26	5.54
423.22	418.28	412.78	4.94
465.06	459.86	454.36	5.20
478.98	474.14	468.64	4.84
492.42	485.74	480.24	6.68*

Notes: Correlation of whole-core susceptibility with susceptibility measured on the second run of the GHMT logging tool was completed using version 1.2 of the program AnalySeries (Paillard et al., 1996). Linear interpolation is used between tie points to convert from one depth scale to another. \* = these tie points are secondary adjustments based on comparing the paleomagnetic inclination data to the remanent anomaly calculated from the second logging run of the GHMT. Offset = logging depth – mbsf depth.